A dilatancy approach to estimating the bearing capacity of shallow foundations on sand
by Craig Robert Madson

A thesis submitted in partial fulfillment of the requirements for the degree of Master of Science in Civil Engineering
Montana State University

Abstract:
Conventional bearing capacity solutions to shallow foundations resting on sand predict that the ultimate bearing capacity increases linearly with footing width and embedment depth. Numerous studies have found this not to be the case. It has been postulated that this observation is due to scale effects arising from non-linear material behavior and progressive failure. The objective of this research was to develop a new design approach to estimate the bearing capacity of sand that 1) accounts for both components of the scale effect and 2) eliminates the need for extensive biaxial testing to establish a material failure envelope. This has been accomplished using dilatancy and strength relationships proposed by Bolton (1986).

In order to evaluate the new approach, results from bearing capacity experiments and shear strength tests were accumulated for 8 study sands. Two of the sands were tested extensively by the author, while data concerning the other 6 sands was collected from previous findings by other researchers. In this thesis, predictions of ultimate bearing capacity using the new approach were compared to the bearing capacity results compiled for each study sand. These predictions were also compared to predictions made using the actual failure envelope of each sand in order to study errors associated with using Bolton's simplified empirical equations.

In general, it was found that using Bolton's empirical equations to estimate the bearing capacity of the study sands did not add an unreasonable amount of error to the predictions. In some cases, using this approach even improved the predictions. These findings are a significant step forward in the estimation of the bearing capacity of sands in that subsurface exploration and material evaluation can be greatly simplified, while at the same time, maintaining reasonable accuracy in bearing capacity predictions.

A DILATANCY APPROACH TO ESTIMATING THE BEARING CAPACITY OF

SHALLOW FOUNDATIONS ON SAND

by

Craig Robert Madson

A thesis submitted in partial fulfillment
of the requirements for the degree

of

Master of Science

in

Civil Engineering

MONTANA STATE UNIVERSITY
Bozeman, Montana

April 1996

APPROVAL

of a thesis submitted by

Craig Robert Madson

This thesis has been read by each member of the thesis committee and has been found to be satisfactory regarding content, English usage, format, citations, bibliographic style, and consistency, and is ready for submission to the College of Graduate Studies.

Dr. Steven W. Perkins — (Signature) — 3-29-96 Date

Approved for the Department of Civil Engineering

Dr. Robert Oakberg — (Signature) — 3/29/96 Date

Approved for the College of Graduate Studies

Dr. Robert Brown — (Signature) — 4/21/96 Date

STATEMENT OF PERMISSION TO USE

In presenting this thesis in partial fulfillment of the requirements for a master's degree at Montana State University-Bozeman, I agree that the Library shall make it available to borrowers under rules of the Library.

If I have indicated my intention to copyright this thesis by including a copyright notice page, copying is allowable for scholarly purposes, consistent with "fair use" as prescribed in the U.S. Copyright law. Requests for permission for extended quotation from or reproduction of this thesis in whole or in parts may be granted only by the copyright holder.

Signature Craig Madsen

Date 3/29/96

Dedicated to the memory of Reverend Greg Kaiser

During the course of preparing this thesis, a very old and dear friend by the name of Greg Kaiser died in an unfortunate accident. Words simply cannot convey the respect and admiration held for this man. Greg approached life with a zest that was unparalleled. Whether he was preaching from the pulpit on a Sunday morning, scouting for elk in the mountains, participating in activities with his friends, or simply spending time with his family his devotion was absolute. He gave of himself freely, never asking for anything in return. Greg was dearly loved by all who knew him, and will be sorely missed. It is in his memory that this thesis is dedicated.

ACKNOWLEDGMENTS

The author would like to express his appreciation to Dr. Steven W. Perkins for his continued guidance and support leading to the completion of this thesis. The author also extends his appreciation to the faculty of the Department of Civil Engineering for their guidance in the academic progress of this student.

Finally, the author would like to express his appreciation to his family and friends for their continued support and patience during the academic career of the author.

TABLE OF CONTENTS

LIST OF TABLES

LIST OF FIGURES

ABSTRACT

Conventional bearing capacity solutions to shallow foundations resting on sand predict that the ultimate bearing capacity increases linearly with footing width and embedment depth. Numerous studies have found this not to be the case. It has been postulated that this observation is due to scale effects arising from non-linear material behavior and progressive failure. The objective of this research was to develop a new design approach to estimate the bearing capacity of sand that 1) accounts for both components of the scale effect and 2) eliminates the need for extensive triaxial testing to establish a material failure envelope. This has been accomplished using dilatancy and strength relationships proposed by Bolton (1986).

In order to evaluate the new approach, results from bearing capacity experiments and shear strength tests were accumulated for 8 study sands. Two of the sands were tested extensively by the author, while data concerning the other 6 sands was collected from previous findings by other researchers. In this thesis, predictions of ultimate bearing capacity using the new approach were compared to the bearing capacity results compiled for each study sand. These predictions were also compared to predictions made using the actual failure envelope of each sand in order to study errors associated with using Bolton's simplified empirical equations.

In general, it was found that using Bolton's empirical equations to estimate the bearing capacity of the study sands did not add an unreasonable amount of error to the predictions. In some cases, using this approach even improved the predictions. These findings are a significant step forward in the estimation of the bearing capacity of sands in that subsurface exploration and material evaluation can be greatly simplified, while at the same time, maintaining reasonable accuracy in bearing capacity predictions.

CHAPTER 1

INTRODUCTION

Background and Problem

In the course of performing a structural design, adequate consideration must be given to the basic support system of the structure, namely, the foundation system. The primary purpose of the foundation is simply to transmit loads to the underlying soil structure. Transmittal of these loads may be done through the use of either footings or rafts. Footings are slabs which provide support to a portion of the structure. Individual footings are often used to support single columns. Footings used to support groups of columns are referred to as combined footings, while load-bearing walls are supported with the use of strip footings. In contrast, a raft footing is a large single slab supporting the entire structure. In cases where the upper layers of soil are incapable of providing sufficient support, piles or drilled piers are often used to transmit the structural loads to suitable soils found at greater depths.

In this thesis, the discussion will be limited to the design of shallow foundations placed on sand. We will not be looking at the design of piles or drilled piers. Perhaps at this point it would be helpful to define the meaning of a shallow foundation. Foundations are considered shallow if the depth, (D_f) of the footing is less than or equal to 3 - 4 times the width (B).

In general, a shallow foundation must meet two requirements. First, any settlement induced by the foundation must be within an acceptable limit. In other words, settlement of the foundation should not cause unacceptable damage or, in anyway, interfere with the basic function of the structure. Secondly, the foundation should be designed in such a manner as not to exceed the ultimate bearing capacity (q_{ult}) of the soil. Here, we are mainly concerned with the possibility of general shear failure resulting in catastrophic damage to the structure. It should be noted that one of these two requirements will often control the design of a foundation. For example, the bearing capacity of the soil may be sufficient to support the structure, yet the settlement associated with the load may be excessive. Therefore, the importance of the function of the structure will play a major role in determining which criteria will control.

Throughout the remainder of this thesis, we will be limiting the discussion to making accurate predictions of bearing capacity, while ignoring any settlement requirements. More specifically, we will be looking at a new technique to make better predictions of the bearing capacity of sands.

In order to better understand discussions throughout the remainder of this thesis, it would perhaps be insightful to provide a definition of the ultimate bearing capacity (q_{ult}). Craig (1992) defines q_{ult} as "the least pressure which would cause shear failure of the supporting soil immediately below and adjacent to a foundation". In general, failure may occur by one of three modes (see Figure 1). General shear failure is associated with the development of a failure surface extending to ground level. Often, general shear failure is accompanied with upheaval of the ground surface immediately adjacent to the structure. In

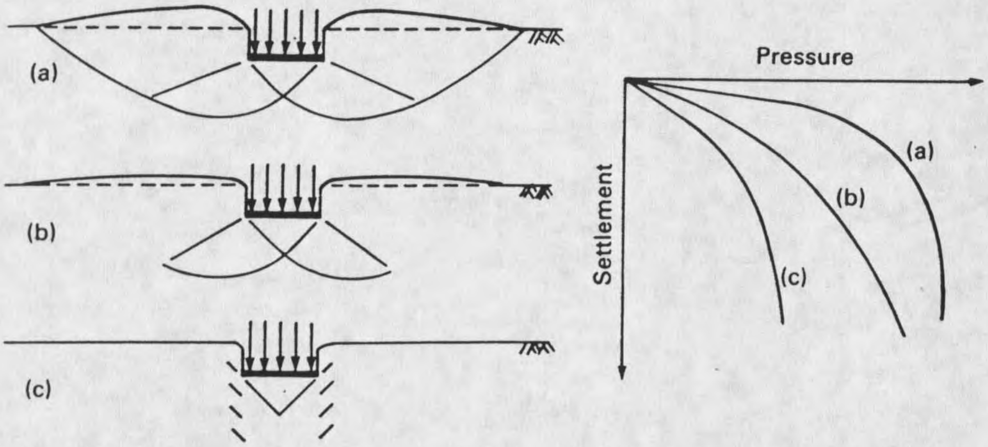

Figure 1. Modes of failure: (a) general shear, (b) local shear, c) punching shear, (from Craig, 1992).

this mode, the ultimate bearing capacity is normally well defined as seen in Figure 1. Failures such as this often occur within dense or stiff soils. In contrast, local shear failure is often associated with only a partial development of a failure surface. Unlike the previous mode, considerable displacement must occur for the failure surface to reach ground surface. The last mode of failure, punching failure, occurs in loose or soft soils and at increased depths of embedment. In this mode, the failure surface does not extend to the ground surface, and the ultimate bearing capacity is often not clearly defined as may be seen in Figure 1. In general, it may be said that the final 2 modes of failure are often associated with excessive settlements of the foundation that ultimately control the design. In contrast, general shear failure is often the failure mode in cases where the ultimate bearing capacity is controlling the design.

In light of the above discussion, the engineer is now left with the problem of making accurate predictions of ultimate bearing capacity in cases where bearing capacity controls.

While conventional solutions exist for bearing capacity problems, in the past, these solutions have been applied with some inherent conservatism, (i.e., relatively large factors of safety). This often may be attributed to the nonhomogeneous conditions that can be found at a particular site. However, in some cases, this conservatism is due to a failure to appreciate the intricacies of soil-structure interaction. Specifically, the following are often not understood.

(a) that a fundamental relationship exists between the dilatancy and strength of a soil, and that the rate of dilation, which is dependent upon the effective stress and density, can be related to appropriate strength parameters. Dilatancy may be defined as the volumetric increase associated with the shearing of a dense sand.

(b) that the scale effect composed of material non-linearity and progressive failure will lower expected bearing capacities, especially at higher mean normal stress levels beneath the footing.

Conventional solutions to bearing capacity problems predict that the ultimate bearing capacity will increase linearly with footing width and embedment depth, and fail to consider scale effects composed of material non-linearity and progressive failure observed in bearing capacity experiments. Material non-linearity may be thought of as the dependence of the peak friction angle on the mean normal stress level (p') beneath the footing. Higher levels of mean normal stress corresponding to increased footing widths and embedment depths are associated with lower peak friction angles. Since conventional solutions assume that the friction angle remains constant with increasing p', they will often over predict the actual bearing capacity at increased footing widths and embedment depths. The second component of the scale effect, progressive failure, is due to the nonuniform distribution of shear strain and thus peak shear resistance along the slip surface. Peak strength has already been reached and exceeded in regions close to the footing, long before the shear strength in regions further away has been mobilized. As a result, the average angle of shearing resistance is decreased and the ultimate bearing capacity is lowered. Radiograph studies by Yamaguchi et al., (1976) indicate that this becomes a greater problem with increasing size and embedment depth of the footing, (i.e., increasing p'). Conventional solutions assume that uniform peak shear resistance is occurring along the entire slip surface.

Scope of Work

The objective of this thesis will be to present a dilatancy approach to the design of vertically loaded shallow foundations resting on sand. Eccentric loadings of shallow foundations are not considered. This approach utilizes dilatancy and strength relationships developed by Bolton (1986). The design methodology separately accounts for both material non-linearity and progressive failure and, at the same time, eliminates the need for extensive shear strength testing in order to define a material failure envelope. In order to evaluate the new design procedure, bearing capacity predictions were compared to results accumulated from bearing capacity experiments performed on 8 study sands. Additionally, predictions made using Bolton's equations were compared to predictions made using the failure envelope of each study sand.

The previous section described, in general terms, the idea of ultimate bearing capacity, and defined some of the problems associated with attempting to evaluate bearing capacity using conventional methods. This section will provide an overview of the different aspects of the study, as well as a brief description of the layout of this thesis.

As noted above, the newly proposed approach to the design of shallow foundations was evaluated using bearing capacity data and shear strength data accumulated for 8 study sands. In all, 61 bearing capacity experiments were used. Bearing capacity tests included both full-scale tests and model experiments using the centrifuge. Shear strength tests included triaxial and plane strain tests. The author performed triaxial tests on two of the study sands (MLS-1 and JSC-1), in conjunction with centrifuge tests performed on these sands by previous researchers. Bearing capacity and shear strength data on the other 6 study sands was accumulated from a variety of sources including papers, research journals, and theses. In some cases, the authors were contacted to acquire further information regarding their research.

The bearing capacity data was analyzed and tabulated for each study sand. Information recorded for each experiment included both the density and relative density of the sand tested, the size and embedment depth of the footing, and the corresponding ultimate bearing capacity. The type of test (full-scale or centrifuge) was also noted in this study, as well as any other experimental factors such as the presence of a groundwater table. In several cases, the load displacement curves demonstrated strain hardening characteristics, (i.e., no peak load). Therefore, the peak load had to be chosen to correspond to a particular normalized settlement (S/B) of the footing, where S and B are the settlement and footing width, respectively.

Shear strength data provided with each study sand was also evaluated by the author. Using the data, peak strength envelopes were developed in p'-q stress space for each study sand. This was done for two reasons. First, Bolton's equations use empirical constants to describe the strength characteristics of a particular sand. The error associated with using these empirical constants was studied by comparing the strength envelope they predict, with the strength envelope developed for each study sand. Second, bearing capacity predictions using the proposed method were compared to predictions using the actual peak strength envelope. This necessitated the development of a peak strength envelope for each study sand. The strength data was also analyzed to find an appropriate constant volume friction angle (ϕ'_{cv}) for each sand. The constant volume friction angle is simply the friction angle associated with the critical state, (i.e., the point at which shearing takes place without any change in volume). As will be shown in later chapters, the constant volume friction angle is primarily dependent upon the mineralogy of the sand. Bolton's relationships incorporate the use of the constant volume friction angle, and for this reason, an appropriate constant volume friction angle had to be chosen for each study sand.

In order to use Bolton's equations, the level of mean normal stress (p') appropriate to the footing has to be found. This required the development of an expression relating the mean normal stress (p') and resulting ultimate bearing capacity (q_{ult}), to an appropriate friction angle. Perkins (1995a) demonstrated that the ratio of mean normal stress to ultimate bearing capacity (p'/q_{ult}) is primarily a function of the friction angle (ϕ'). Using a non-linear limit plasticity solution, an expression was found that related p'/q_{ult} to ϕ'. This equation is given in Chapter 4.

The next chapter of this thesis will begin with an overview of the behavior of sands. This chapter includes an in-depth discussion of the friction angle, including factors that will influence the friction angle of a given sand. Dilatancy characteristics of sand will also be presented, followed by a brief discussion of stress-dilatancy theory by Rowe (1962). Rowe's theories lay the groundwork for Bolton's empirical equations relating dilatancy and strength of sand presented later in the chapter. Also discussed will be several analytical solutions proposed by other researchers to bearing capacity problems on sand. The last section of the chapter will be devoted to a presentation of the scale effect, composed of material non-linearity and progressive failure. The scale effect has been noted by numerous researchers and was briefly described earlier.

Chapter 3 will present the experimental work performed by the author on two of the study sands (MLS-1 and JSC-1). In addition, material properties, bearing capacity results, and shear strength data for the other 6 study sands will be given. Included within this section will be a brief narrative on the testing procedure used in performing bearing capacity and shear strength experiments on each of the study sands.

Chapter 4 presents a detailed description of the proposed design procedure for estimating the bearing capacity of sands. This procedure will separately account for material non-linearity and progressive failure, and will utilize dilatancy-strength relationships proposed by Bolton (1986). The predictions made using Bolton's equations will be compared to the bearing capacity results, as well as to predictions made using the actual strength envelope of each sand.

The last chapter will be devoted to conclusions and recommendations for further work. Also discussed will be simple tests that may be used to establish the material parameters required in Bolton's equations.

CHAPTER 2

LITERATURE REVIEW

Introduction

The literature review in this chapter consists of three sections: strength and dilatancy behavior of sands, overview of the general bearing capacity equation, and a discussion of scale effects which influence the response of shallow foundations.

In section one, the strength and dilatancy properties of sands are discussed in detail. This section provides much of the background required to study the bearing capacity problem. Section two discusses several approaches used to solve bearing capacity problems. These approaches form the basis for the analysis techniques discussed in Chapter 4. The last section presents a discussion of scale effects composed of material non-linearity and progressive failure, and observed in shallow foundation experiments.

Strength and Dilatancy Behavior of Sands

Friction Angle

The resistance of a soil to shear is governed by the soil's shear strength. In order to solve soil stability problems such as bearing capacity problems, a knowledge of the shear strength parameters is required. Coulomb originally expressed the shear strength at failure

(τ_f) as a linear function of the normal stress (σ_f).

$$\tau_f = c + \sigma_f \tan\phi \tag{1}$$

This equation is known as the Mohr-Coloumb failure criteria, and is more properly expressed as a function of effective normal stress as

$$\tau_f = c' + \sigma_f' \tan\phi' \tag{2}$$

where c' and ϕ' are shear strength parameters describing the effective cohesion intercept and the effective angle of shearing resistance or friction angle. Failure of a soil mass will therefore occur on a particular plane at any point where a critical combination of effective normal and shear stress develops.

In practice, the cohesion term in granular soils such as sands is often assumed to be zero resulting in the simplified Mohr-Coloumb failure criteria presented as

$$\tau_f = \sigma_f' \tan\phi' \tag{3}$$

where the shear strength of the sand is simply expressed as a function of ϕ'.

The friction angle of a sand is normally considered to consist of three components. These components are:

1. Mineral to mineral sliding or grain sliding (ϕ_u)

2. Particle interlocking, dilation (geometric effect) (θ)

3. Rolling friction (ϕ_r)

Rowe (1962) found that the grain sliding component (ϕ_u) is generally dependent upon several variables including:

(1) Mineral Composition

(2) Microscopic surface roughness

(3) Testing technique

(4) Particle size

(5) Surface conditions

ϕ_u has, in reality, been shown to be principally a function of mineralogy. For example, the grain sliding component (ϕ_u) of feldspar, a common mineral found in sands, can be as high as 37 degrees, while silica quartz sands have been found to be as low as 26 degrees, (Mitchell, 1976).

The second component of the friction angle (particle interlocking) is associated with the work required to lift particles over one another leading to volume expansion or dilation of the sample. This component may be better understood by consideration of Figure 2.

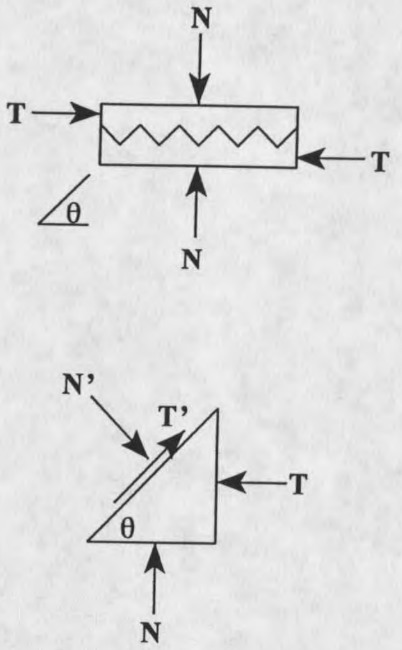

Figure 2. Analogy of particle interlock.

By requiring static equilibrium, the following expressions may be developed:

$$T' = T\cos\theta - N\sin\theta \tag{4}$$

$$N' = T\sin\theta - N\cos\theta \tag{5}$$

The law of friction can be used to relate N' to T' by

$$T' = N'\tan\phi_u \tag{6}$$

Substituting equations 4 and 5 into 6 and simplifying will result in the following expression

$$T = N \tan(\phi_u + \theta) \tag{7}$$

where ϕ_u is the mineral to mineral sliding component of the friction angle and θ is the component due to dilation.

The third component of the friction angle, rolling friction (ϕ_r), is associated with particles rolling past one another and rearranging while the entire mass remains at a constant volume. The rolling friction component is most prevalent in sands at or close to the critical void ratio (CVR), where the critical void ratio is defined as the void ratio in the material such that when the sample is sheared there is no change in volume. As the relative density of the material increases, the contribution to the friction angle by the rolling friction becomes less significant. Eventually, as the minimum void ratio is reached corresponding to 100% relative density, the rolling friction component will become negligible and the friction angle will simply be composed of the first two components. Figure 3 demonstrates the interaction of these 3 components.

As seen in Figure 3, the grain sliding component (ϕ_u) is constant for all relative densities. However, the dilational effect and rolling friction are dependent upon the relative density. It should also be noted that at high relative densities and large confining stresses, particle crushing takes place, effectively reducing the dilational component of the friction angle, (i.e., the magnitude of the values on this diagram are mean normal stress dependent). In subsequent sections, we will be discussing the using of peak and constant volume friction

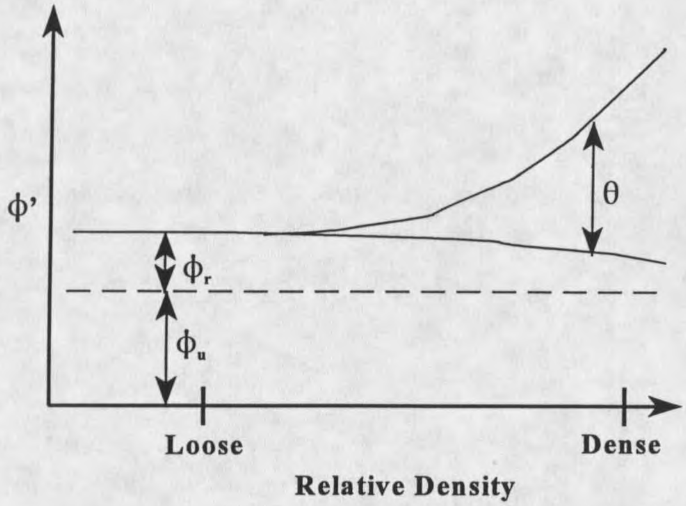

Figure 3. Interaction of the 3 components of the friction angle.

angles, (ϕ'_{peak} and ϕ'_{cv}) within bearing capacity solutions. In reference to Figure 3, the constant volume friction angle is composed mainly of the grain sliding component (ϕ_u) and to a much lesser extent, the rolling friction component (ϕ_r). In contrast, the peak friction angle is composed primarily of the grain sliding (ϕ_u) and dilational (θ) components.

Several factors will influence the peak friction angle of a particular sand. In general, these factors are

1. Relative density of the sand
2. Strain conditions
3. Stress conditions
4. Particle size and gradation

The relative density of the sand will have a significant impact on the friction angle. The relative density is defined by the following

$$I_D = \frac{e_{max} - e}{e_{max} - e_{min}} \tag{8}$$

where e_{max} and e_{min} are the maximum and minimum void ratios for a given sand, and e is the void ratio at which I_D is being defined. In general, studies have shown that as the relative density of a sand increases, the friction angle also increases. Figure 4 from Hilf (1975) presents a graph of the friction angle versus relative density for a number of sands. As can be seen, the friction angle is increasing with increasing relative density. In addition, the friction angle is also increasing with angularity of the sand. This is likely due to the particle interlocking or dilational component of the friction angle. As angularity increases, the particles become more interlocked and require greater work to move over one another, resulting in an increased friction angle.

Strain conditions can also have a significant effect on the friction angle. To understand this, consider the strain conditions present under a strip footing (Fig. 5). The soil underneath the strip footing in Figure 5 may be considered to be in a condition of plane strain. Under these conditions the strain in the intermediate direction (ε_2) is equal to zero. As such, the soil particles can override one another only in the two directions of the plane to which ε_2 is perpendicular. This increases the work necessary for the material to dilate, effectively increasing the friction angle. In contrast, strain in the intermediate direction (ε_2) is not equal to zero under a square or circular footing. In these cases, more of an axisymmetric condition is present. Soil particles may override one another in all three of the

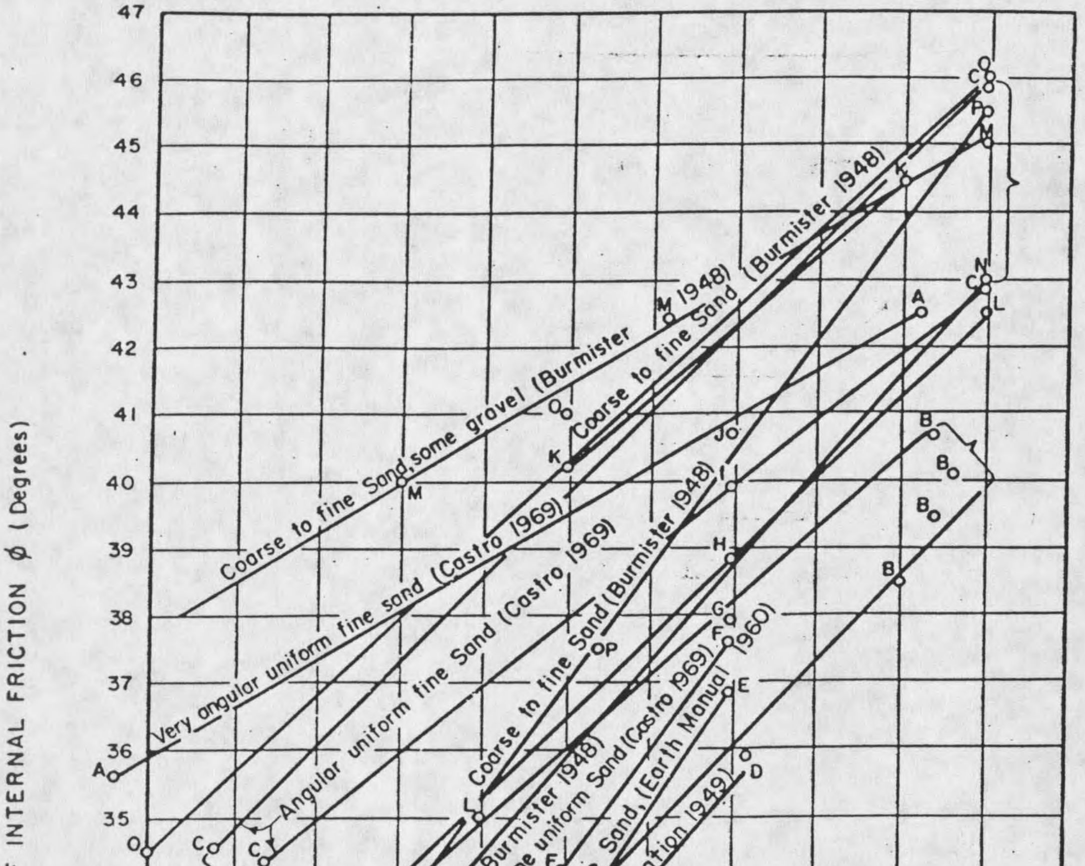

Figure 4. Friction Angle vs Relative Density for a number of sands (from Hilf, 1975).

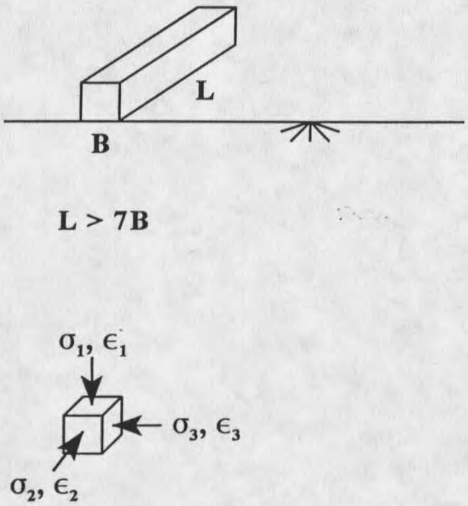

Figure 5. Strain conditions under a strip footing.

principal directions, thereby reducing the friction angle. Wroth (1984) attempted to show that plane strain friction angles are typically 10% higher than triaxial compression friction angles. While this simplification is valid, it will be demonstrated later that the amount by which the plane strain friction angle is greater than the triaxial friction angle is also dependent on the relative density and the level of mean normal effective stress confinement (p').

It has also been shown that the mean normal effective stress (p') equal to the average of the principal stresses (σ'_1, σ'_2 & σ'_3) can affect the friction angle. In general, the greater the mean effective stress in a dense angular sand, the lower the friction angle mobilized. This behavior is often referred to as material non-linearity, and is one of the components responsible for scale effects in foundation experiments to be discussed in a later section.

The particle size and gradation can also have a significant impact on the mobilized friction angle of the sand. It has been shown for example, that changes in the friction angle with confining pressure (σ_3') are much more apparent for soils with larger particle sizes such as gravels. This is most likely due to particle crushing taking place at higher confinements. In contrast, Bolton (1986) found that certain uniform, rounded sands were little affected by confinements up to 1000 kPa. In addition, it was demonstrated that significant particle crushing did not take place in one such sand (Ottawa sand) up to confinements of 4000 kPa.

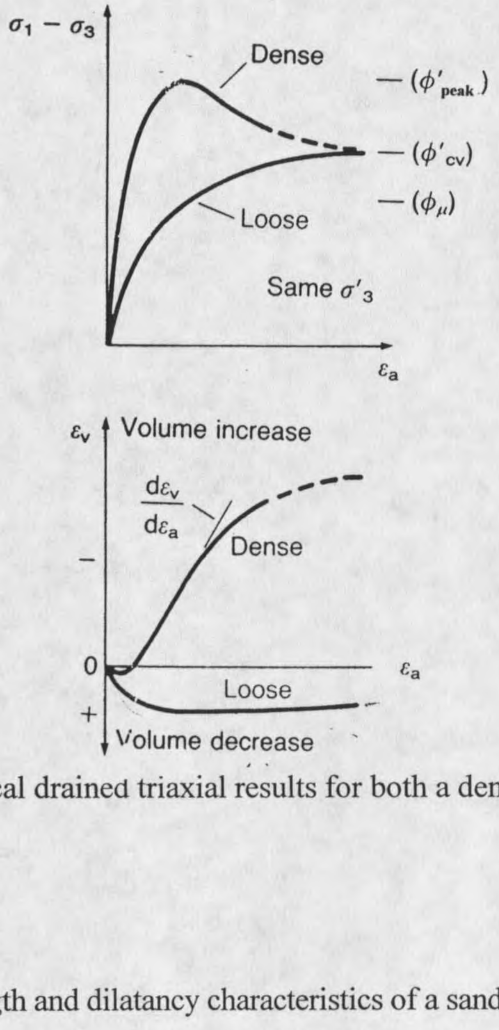

Figure 6. Typical drained triaxial results for both a dense and loose sand.

Dilatancy

Shear strength and dilatancy characteristics of a sand may be found by either drained triaxial compression tests (CTC) or direct shear tests. Typical drained triaxial results for both a loose and dense sand are presented in Figure 6. In these plots, both the axial strain vs principal stress difference and axial strain vs volumetric strain have been plotted. As seen in Figure 6, there is a significant difference in the behavior of a dense versus a loose sample. Dense samples tend to demonstrate significant strain-softening characteristics with peak stress at relatively low strain. In addition, dense samples will first tend to decrease in volume, followed by volumetric expansion or dilation defined as the increase in volume of a sand during shearing. The rate of dilation is defined as $-(d\epsilon_v/d\epsilon_a)$ with compression defined as positive. The maximum rate of dilation, $-(d\epsilon_v/d\epsilon_a)_{max}$, is then associated with peak strength.

Dilatancy may be better understood by considering the high degree of particle interlocking present in a very dense, well-graded sand with angular particles. Before shear failure can occur, particle interlocking and friction resistance of the particles must be overcome. In order to overcome this interlocking, particles will be forced to move over and around neighboring particles leading to dilation of the sample.

In contrast to a dense sand, a loose sand will tend to exhibit little particle interlocking. Therefore, as shearing takes place, the sample will simply continue to decrease in volume, eventually reaching the critical void ratio as defined earlier. In addition, the sample will not demonstrate the strain-softening characteristics associated with dense sands. The principal stress difference will simply increase to an ultimate value.

One further observation may be made in reference to Figure 6. In the axial strain vs principal stress difference plot, both the dense and loose samples are tending towards the same critical state where shearing takes place at a constant volume. The angle of shearing resistance at the critical state is known as the constant volume or critical state friction angle. This observed behavior has importance in later discussions. Throughout the remainder of this thesis, the friction angle associated with the critical state will simply be referred to as the constant volume friction angle (ϕ'_{cv})

Stress-Dilatancy Theory. Rowe (1962) performed much of the original work in relating the shear strength of a sand to both the rate of dilatancy and principal stress ratio at the critical state. His work may be summarized by the following stress-dilatancy relation for plane strain

$$\frac{\sigma_1'}{\sigma_3'} = (\sigma_1'/\sigma_3')_{cv}(1 - d\epsilon_v/d\epsilon_1) \tag{9}$$

where (σ'_1/σ'_3) and $(\sigma'_1/\sigma'_3)_{cv}$ are the principal stress ratios at any point on the stress-strain curve and at the critical state, respectively. $(d\epsilon_v/d\epsilon_1)$ is the dilatancy rate at (σ'_1/σ'_3) with compression defined as positive. This equation was derived strictly from theoretical considerations. Since the principal stress ratio in the ultimate state (i.e., at failure) is a measure of the soil's friction angle, this expression indicates that the friction angle at peak strength (ϕ'_{peak}) is equal to the constant volume friction angle (ϕ'_{cv}) for loose sands where the rate of dilatancy at peak is zero. However, for dense sands, the positive rate of dilatancy implies that the friction angle at peak will exceed the constant volume friction angle. As the confinement increases, the rate of dilatancy will tend to decrease, decreasing the difference between ϕ'_{peak} and ϕ'_{cv}. In addition, the rate of dilatancy is dependent upon the strain boundary conditions, with the rate typically being greater for plane strain as opposed to axisymmetric strain conditions. Thus, the difference between ϕ'_{peak} and ϕ'_{cv} depends on the soil's relative density, mean normal stress confinement, and strain boundary condition. This equation would allow for the peak friction angle to be determined for particular conditions of relative density, mean normal stress, and strain conditions provided the rate of dilatancy could be found. From a practical standpoint, this would be a difficult task.

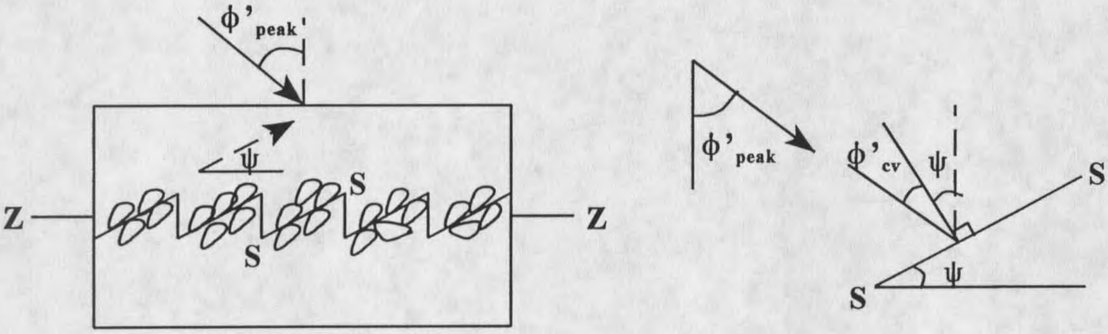

Figure 7. Saw blade model of dilatancy.

Bolton (1986) employed a similar, but less rigorous approach to the development of an equation to estimate the peak friction angle (ϕ'_{peak}), knowing ϕ'_{cv} and the dilatancy angle (ψ). Consider the saw blade model of dilatancy shown in Figure 7. The friction angle, ϕ'_{cv} describes the observed friction angle for soil in its critical state where ψ is equal to zero, and the two halves of the block slide past one another without any vertical component of motion. When the rate of dilation is positive the upper block has a component of displacement in the vertical direction with the block's motion given by the dilatancy angle (ψ). For this case, the observed friction angle of the soil is given by equation 10 below.

$$\phi'_{peak} = \phi'_{cv} + \psi \tag{10}$$

It should be noted that equation 10 provides the same information as the equation developed by Rowe (eq. 9) since the principal stress ratio (σ'_1/σ'_3) and $(\sigma'_1/\sigma'_3)_{cv}$ utilized in Rowe's equation can be expressed in terms of ϕ'_{peak} and ϕ'_{cv}, respectively. The rate of dilation $(1 - d\epsilon_v/d\epsilon_1)$ can also be expressed in terms of the dilatancy angle (ψ). Making these substitutions, it is therefore possible to express Rowe's equation in the form

$$\phi'_{peak} = f(\phi'_{cv}, \psi) \tag{11}$$

The resulting equation is non-linear and algebraically complicated.

Bolton compared equation 9 to equation 10 by plotting ϕ'_{peak} against ψ for an assumed value of ϕ'_{cv}. In his paper, Bolton showed that equation 10 overestimated equation 9 by approximately 20 percent (see Fig. 8). Bolton empirically adjusted his equation to account for this discrepancy, developing the following expression

$$\phi'_{peak} = \phi'_{cv} + 0.8\psi \tag{12}$$

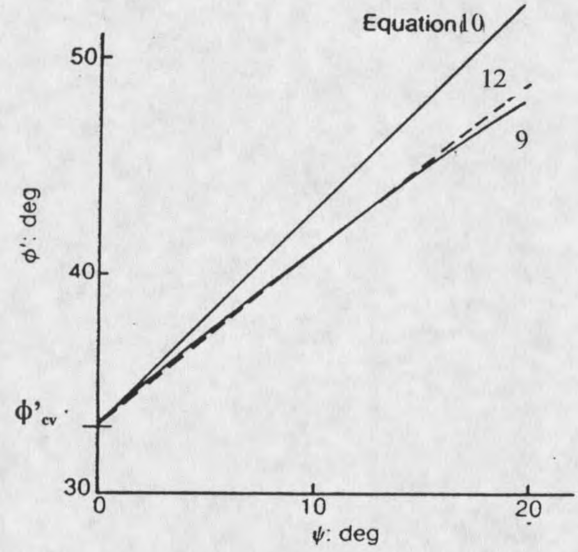

Figure 8. Stress-dilatancy relations from Bolton (1986).

The advantage of equation 12 is that the angle of shearing (ϕ'_{peak}) in excess of the friction angle at constant volume (ϕ'_{cv}), is due solely to the volumetric expansion or dilation of the sand, and is operationally no different than equation 9.

If one were now to assume that the soil particles were perfectly strong and rigid, dilation would simply be a function of relative density since overriding of particles would take place no matter the confinement. However, at elevated confining pressures, particle crushing, asperity breakage, and possible particle yielding occurs which will decrease the peak angles of dilation and shearing (ψ_{peak} and ϕ'_{peak}). This in turn suggests an empirical relationship relating ϕ'_{peak} or ψ_{peak} to both the density and confining pressure.

Bolton developed an empirical expression to relate the dilatancy angle to the relative density and mean effective stress (p'). Making the observation that changes in ϕ'_{peak} were linear with the logarithm of stress (p'), the following expression was proposed

$$\psi_{peak} = A\, I_D \ln\left(\frac{p_{crit}}{p'}\right) \tag{13}$$

where A is a constant, I_D is the relative density of the soil, p' is the mean effective stress at failure, and p'_{crit} is the mean effective stress just sufficient to prevent all dilation.

Due to the lack of data in the literature pertaining to ψ_{peak} and the difficulty associated with defining ψ_{peak} in axisymmetric triaxial tests, an alternative expression to equation 13 was proposed. This equation is given as

$$\psi_{peak} = A\,[I_D(Q - \ln p') - R] \tag{14}$$

where A, Q, and R are constants. The term $(I_D(Q\text{-}\ln p')\text{-}R)$ was termed a relative dilatancy index (I_R) such that

$$I_R = I_D(Q - \ln p') - R \tag{15}$$

which was useful since it could be forced to return a zero value when $p' = p'_{crit}$. Equation 15 could then be substituted into equation 12 to yield

$$\phi'_{peak} = \phi'_{cv} + A\,[I_D(Q - \ln p') - R] \tag{16}$$

or

$$\phi'_{peak} - \phi'_{cv} = A\,I_R \tag{17}$$

where A contains the 0.8 multiplier and whose value will be dependent upon strain boundary conditions. Equation 17 was evaluated using published results of plane strain and triaxial compression tests on 17 sands with I_D ranging from 0.2 to 1.0 and ϕ'_{cv} ranging from 30 to 37 degrees. For conditions of triaxial compression, the following expression was obtained

$$\phi'_{peak} - \phi'_{cv} = 3I_R \tag{18}$$

while for plane strain conditions

$$\phi'_{peak} - \phi'_{cv} = 5I_R \tag{19}$$

For the majority of soils studied, the parameters Q and R were found to provide a good fit to the data when Q = 10, R = 1, giving

$$I_R = I_D(10 - \ln p') - 1 \tag{20}$$

where p' is in units of kPa. It should be noted that Q and R can be adjusted to provide a better fit to the data.

Due to the unavailability of good low stress data for any of the test sands, Bolton set an upper limit of 4 for the relative dilatancy index (I_R). It is noted that this does not indicate equation 20 is invalid for I_R values greater than 4. Bolton (1986) further comments that the dilatancy behavior of certain uniform, rounded sands such as Ottawa sands are not well predicted by these empirical relationships. This is thought to be due to the particle strength possessed by these sands. Due to this particle strength, significant particle crushing does not take place until relatively high stress ranges are reached. As a result, the relative dilatancy index (I_R) is underestimated for these sands.

Utilizing equations 18 and 19, one further observation can be made. Dividing equation 19 by equation 18 results in the following

$$\frac{\phi'_{ps}}{\phi'_{tc}} = \frac{\phi'_{cv} + 5\,I_R}{\phi'_{cv} + 3\,I_R} \qquad (21)$$

where ϕ'_{ps}/ϕ'_{tc} is the ratio of the plane strain friction angle to the triaxial compression friction angle. Looking at equation 21, it becomes apparent that this ratio increases as I_R increases and ϕ'_{cv} decreases. Therefore, it appears that this ratio will not always be 1.1 as Wroth (1984) attempted to show. One may also observe that as I_R approaches zero for loose sands, this ratio approaches 1, which suggests in these cases that the plane strain and triaxial compression friction angles are equal to one another and to ϕ'_{cv}. Therefore, at the critical state, there is no difference between plane strain and axisymmetric conditions.

The practical applications of using equations 18 - 20 in a bearing capacity solution are great. By knowing the relative density of the material in question, and assuming a mean normal effective stress (p') beneath the footing, the engineer is able to calculate an appropriate relative dilatancy index (I_R) using equation 20. Next, knowing the strain restraint condition present underneath the footing and assuming an appropriate constant volume friction angle (ϕ'_{cv}) for the soil in question, the engineer can determine a peak friction angle (ϕ'_{peak}) for use in the bearing capacity solution. This approach would eliminate the need for extensive triaxial testing of undisturbed samples to define a material failure envelope.

The obvious drawbacks to this method are simply not knowing ϕ'_{cv} and the mean normal effective stress (p') beneath the footing. ϕ'_{cv} has been shown to be principally a function of mineralogy and may be determined experimentally using reconstituted samples, or estimated knowing the predominant sand mineral type. However, the mean normal effective stress (p') is not as easily found simply because p' is dependent both on the footing size and the depth of embedment. In the following chapters, a design solution using Bolton's equations will be proposed in conjunction with a procedure to determine p'.

Overview of the General Bearing Capacity Equation

The ultimate bearing capacity (q_{ult}) of a shallow foundation under a static, vertical, central load may be expressed by the following equation suggested by Meyerhof (1963)

$$q_{ult}=cN_cF_{cs}F_{cd} + qN_qF_{qs}F_{qd} + \frac{1}{2}\gamma BN_\gamma F_{\gamma s}F_{\gamma d} \tag{22}$$

where c = cohesion of the soil

q = surcharge pressure at the bottom of the footing

γ = unit weight of the soil

B = width or diameter of the footing

N_c, N_q, N_γ = bearing capacity factors which are functions of ϕ'

F_{cs}, F_{qs}, $F_{\gamma s}$ = shape factors

F_{cd}, F_{qd}, $F_{\gamma d}$ = depth factors

Vesic (1973) and Chen (1975) developed the following expressions for N_c and N_q given as

$$N_c = (N_q - 1)\cot\phi \tag{23}$$

$$N_q = \tan^2(\pi/4 + \phi/2)e^{\pi\tan\phi} \tag{24}$$

At this time, there is still on-going controversy concerning an appropriate expression for the bearing capacity factor $N\gamma$. One possible expression developed from limit plasticity theory by Chen (1975) is given as

$$N_\gamma = \frac{1}{2}\tan\xi[\tan\xi e^{\frac{3\pi}{2}\tan\phi} - 1] + \frac{3\sin\phi\cos\phi}{2(1 + 8\sin^2\phi)(1 - \sin\phi)}$$
$$[[\tan\xi - \frac{\cot\phi}{3}]e^{\frac{3\pi}{2}\tan\phi} + \tan\xi\frac{\cot\phi}{3} + 1] \tag{25}$$

where

$$\xi = \pi/4 + \phi/2$$

The shape factors F_{cs}, F_{qs}, and F_{γ_s} are used to account for non-plane strain conditions and may be expressed by the following equations, (De Beer 1970).

$$F_{cs} = 1 + \frac{B}{L}\frac{N_q}{N_c} \tag{26}$$

$$F_{qs} = 1 + \frac{B}{L}\tan\phi \tag{27}$$

$$F_{\gamma s} = 1 - 0.4\frac{B}{L} \tag{28}$$

The shape factors are empirical relations based on laboratory tests.

The depth factors F_{cd}, F_{qd}, and $F\gamma_d$ are used to account for shear resistance of the soil above the base of the footing. These factors, developed by Hansen (1970), are given by:

Condition(a): $D_f/B <= 1$

$$F_{cd} = 1 + 0.4\frac{D_f}{B} \tag{29}$$

$$F_{qd} = 1 + 2\tan\phi(1 - \sin\phi)^2\frac{D_f}{B} \tag{30}$$

$$F_{\gamma d} = 1 \tag{31}$$

Condition(b): $D_f/B > 1$

$$F_{cd} = 1 + 0.4 \tan^{-1} \frac{D_f}{B} \tag{32}$$

$$F_{qd} = 1 + 2 \tan\phi (1 - \sin\phi)^2 \tan^{-1} \frac{D_f}{B} \tag{33}$$

$$F_{\gamma d} = 1 \tag{34}$$

It should be pointed out that the bearing capacity equation assumes that the groundwater table is located at a depth no less than one footing width below the bottom of the footing, and the depth of the footing (D_f) is less than four times the width of the footing.

In order to solve a bearing capacity problem on a sand, it is important to choose an appropriate friction angle for use in the bearing capacity equation. This has led to numerous problems for engineers. As discussed previously, many sands demonstrate significant variation in the friction angle over a range of mean normal effective stress (p'). This has been termed material non-linearity. For example, the secant friction angle of one of the sands used in this study (MLS-1) varies from 47 to 58 degrees over a mean normal effective stress (p') confinement range of 2300 kPa. The question therefore arises as to an appropriate friction angle for use in the bearing capacity equation. In addition, bearing capacity predictions using friction angles over 50 degrees will become abnormally elevated for relatively small footing widths since the bearing capacity factors are exponential functions of the friction angle.

These problems associated with material non-linearity have therefore led to further analysis by numerous researchers. Following are brief overviews of several techniques proposed to take this material non-linearity into account.

Methods to account for material non-linearity

Kutter et al., (1988) published the results of a number of bearing capacity tests on Monterey Sand. In their study, they compared the bearing capacity results to predicted results using methods proposed by De Beer (1967) and Meyerhof (1948) to account for material non-linearity, as well as their own proposed method.

Meyerhof (1948) in his paper assumed that the average normal stress (σ'_{avg}) developed along the failure surface would be 1/10th of the ultimate bearing capacity. Using a Mohr-Coulomb diagram, the practitioner would then choose a secant friction angle corresponding to the secant slope connecting the origin to this point on the failure envelope. The cohesion is assumed to be equal to zero. This method therefore requires an iterative procedure to find an appropriate friction angle (ϕ'_{peak}), since the choice of σ'_{avg} is dictated by q_{ult} and q_{ult} is governed by the value of ϕ'_{peak}.

Using Meyerhof's idea, De Beer (1967) developed a semi-empirical equation for the average normal effective stress (σ'_{avg}) along the failure surface. His equation is expressed by

$$\sigma'_{avg} = \frac{q_{ult} + 3\gamma d}{4}(1 - \sin\phi'_{peak}) \tag{35}$$

where γ = unit weight of the soil, d = depth of the footing, and q_{ult} is the ultimate bearing capacity of the footing. A review of De Beer's paper revealed little on the exact development of equation 35. As with Meyerhof's solution, this method requires an iterative procedure to find the appropriate ϕ'_{peak}, where one first assumes a value of average normal stress at failure (σ'_{avg}), and determines the peak secant friction angle (ϕ'_{peak}) corresponding to this point on the failure envelope. Next, q_{ult} is computed using ϕ'_{peak}. The values of q_{ult} and ϕ'_{peak} are then used inside equation 35 to determine σ'_{avg} and compared to the assumed σ'_{avg}. A new value of average normal stress (σ'_{avg}) is then assumed and the process repeated until the two values of average normal stress converge.

In his paper, Kutter et al., (1988) compares the above two methods with a more conventional approach utilizing a constant c' and ϕ' from a least-squares fit of the triaxial data in the range of interest for dense Monterey sand. It is interesting to note that an apparent cohesion "c" is used in this proposed method even though sand does not possess a true cohesion. Apparently, it was felt that using a c' parameter provided a better approximation of the curved failure envelope then assuming a cohesion equal to zero.

In their study, they found that De Beer's method and the proposed least squares method both predicted bearing capacities close to the experimental bearing capacities. However, it is maintained by the author that the use of an average friction angle and cohesion is not an appropriate method for selection of shear strength parameters for certain sands demonstrating material non-linearity beyond that of Monterey sand. For example, Kusakabe et al., (1992) found that Scoria sand possesses friction angles that range from 36 to 64 degrees at the lowest confinements. In this case, using an average value for the friction angle and cohesion could lead to some problems, even if one were to narrow this range by assuming an appropriate level of stress under the footing in question. This point is further validated by Perkins (1995a). In his study, he found that using average strength values dramatically overestimated the bearing capacity of another sand (MLS-1) possessing substantial material non-linearity. In addition to the problem of material non-linearity, using average strength parameters does not account for possible progressive failure effects, which become an increasing problem with larger footing widths and greater embedment depths. This phenomenon will be discussed in the next section.

De Beer's method utilizes a friction angle based upon the average normal effective stress under the footing, and is therefore more attractive then using the least-squares approach. In addition, De Beer's method takes into account the increase in σ'_{avg} with depth of embedment of the footing. However, little is available on the exact development of De Beer's expression as well as the equation proposed by Meyerhof, making them a little less attractive for use in a bearing capacity analysis.

Perkins (1995a) developed an expression using the slip line solution relating the ratio of the mean normal effective stress to the ultimate bearing capacity (p'/q_{ult}) for different combinations of footing width, surcharge, and material properties including unit weight, friction angle, and cohesion. It was determined in his study that the ratio of p'/q_{ult} is primarily dependent upon ϕ' for friction angles greater than 30 degrees. His expression is given as

$$\frac{p'}{q_{ult}} = -\frac{4.09}{\sin\phi^3} + \frac{19.06}{\sin\phi^2} + \frac{0.71}{\sin\phi} - 19.73 \tag{36}$$

where p'/q_{ult} is the ratio of mean normal effective stress to ultimate bearing capacity for different values of the friction angle. This expression was found to be valid for plastic materials whose friction angles fall in the range of 20 to 60 degrees. Perkins (1995a) provides further details on the development of equation 36. The plot of equation 36 is found in Figure 9.

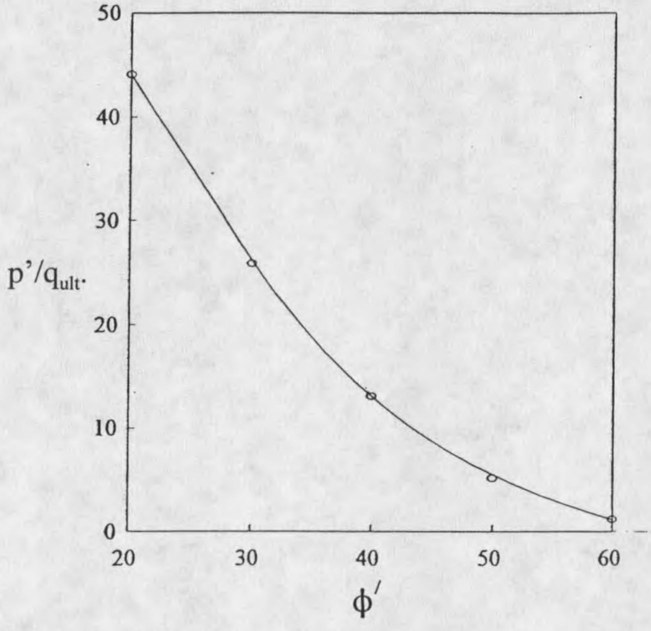

Figure 9. Ratio of p'/q_{ult} vs ϕ (from Perkins, 1995a).

Using equation 36, Perkins (1995a) performed a bearing capacity analysis in the following manner. A particular level of mean normal stress (p') was assumed, from which a secant friction angle (ϕ'_{peak}) could be determined using the strength envelope of the material. Next, the ultimate bearing capacity (q_{ult}) was solved using a conventional bearing capacity solution with the computed friction angle, ϕ'_{peak}. The ratio of p'/q_{ult} was then determined using the assumed value of p', and compared to the ratio given by equation 36 using the value of ϕ'_{peak} computed from the assumed p'. This process was then repeated for a new value of p' until the two calculated p'/q_{ult} ratios converged.

The advantage of using equation 36 is that we have now indirectly accounted for material non-linearity (i.e., the curvature of the failure envelope). This has been accomplished using an iterative procedure to find the appropriate level of mean normal stress (p') beneath the footing, and corresponding ϕ'_{peak} to use in the bearing capacity analysis. Perkins (1995a) found that, on the average, accounting for material non-linearity in this manner still led to large over predictions of experimental results. It was maintained that this was likely due to the phenomenon of progressive failure.

The expression developed by Perkins (1995a) will not be used in further analysis here simply due to the numerical instabilities arising at friction angles greater than 60 degrees. As seen in Figure 9, at friction angles greater than 60 degrees the ratio of p'/q_{ult} goes to the negative side leading to the instabilities. For this reason, a new expression for p'/q_{ult} has been developed and will be presented in Chapter 4.

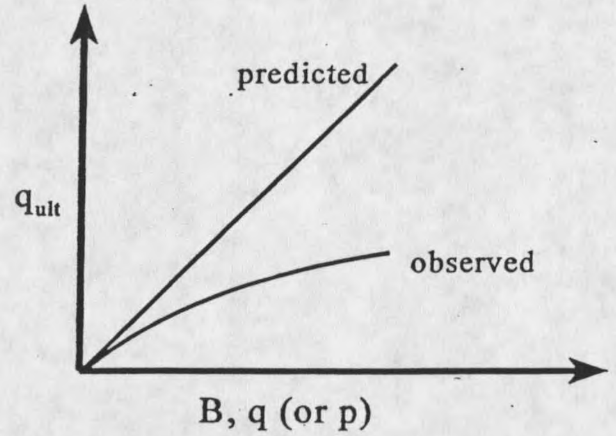

Figure 10. Non-linear dependence of q_{ult} on B, q, or p.

Scale Effects

Numerous bearing capacity studies performed on sands have demonstrated that the ultimate bearing capacity (q_{ult}) does not increase linearly with either footing width (B) or surcharge pressure (q), contrary to that predicted by existing classical solutions. This is illustrated in Figure 10. This observation has been called a scale effect and was recognized as far back as Golder (1941). As far as the author knows, this scale effect was not widely recognized until a paper by De Beer (1963). Since that time, the scale effect has been studied by numerous researchers including Kimura et al., (1985), Kusakabe et al., (1991), and Perkins (1995a) who have confirmed the existence of this scale effect.

One may further observe this scale effect by considering the results of shallow foundation experiments performed on a dense sand (JSC-1) by Perkins and Madson (1996). In Figure 11, the normalized bearing capacity ($N\gamma_q$) is plotted against the footing width (B). The normalized bearing capacity is expressed by

$$N_{\gamma q} = 2\frac{q_{ult}}{B\gamma} \tag{37}$$

where q_{ult} is the bearing capacity measured in each experiment, B is the footing width, and γ is the unit weight of the sand. As seen in Figure 11, the normalized bearing capacity is decreasing with increasing footing width. This phenomenon is due to the decreased angle of shearing resistance associated with larger footing widths and increased embedment depths, and is a consequence of the scale effect.

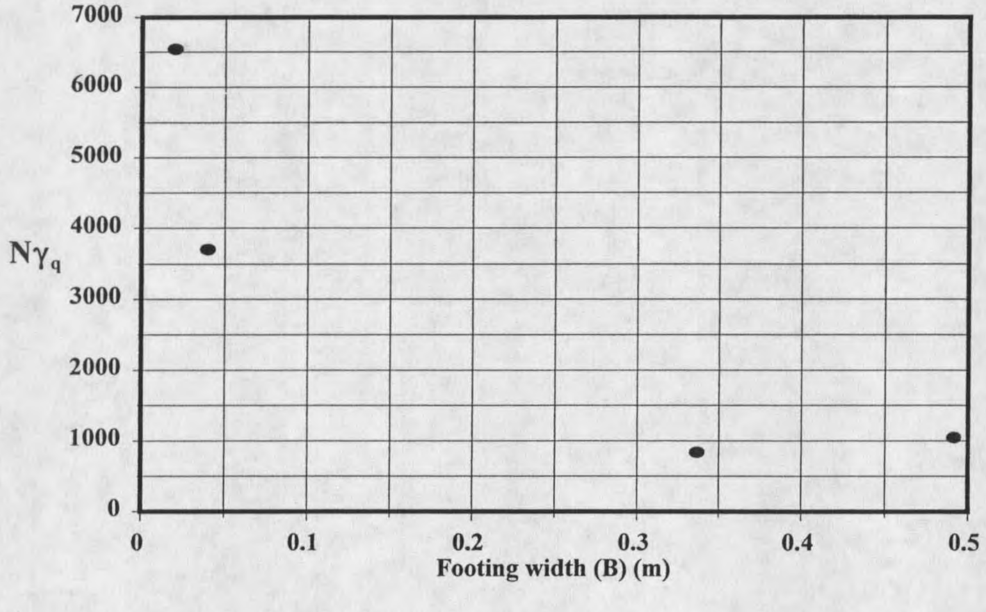

Figure 11. Normalized bearing capacity ($N\gamma_q$) plotted against footing width (B) for JSC-1, (from Perkins and Madson, 1996).

The scale effect may be thought to be made up of two components. The first component is due to the non-linear material behavior observed in many dense sands. This material non-linearity was discussed earlier and may simply be described as the dependence of the friction angle on the mean normal effective stress (p') within the failure zone of the soil. Higher mean normal stresses are associated with lower peak friction angles. It has been speculated that material non-linearity is due primarily to the particle crushing taking place at the higher levels of mean normal stress. Higher mean normal stresses develop whenever the footing width (B), surcharge (q), or a combination of the two increase. As a result of this increase in mean normal stress, the peak friction angle mobilized is decreased and q_{ult} does not increase linearly as expected.

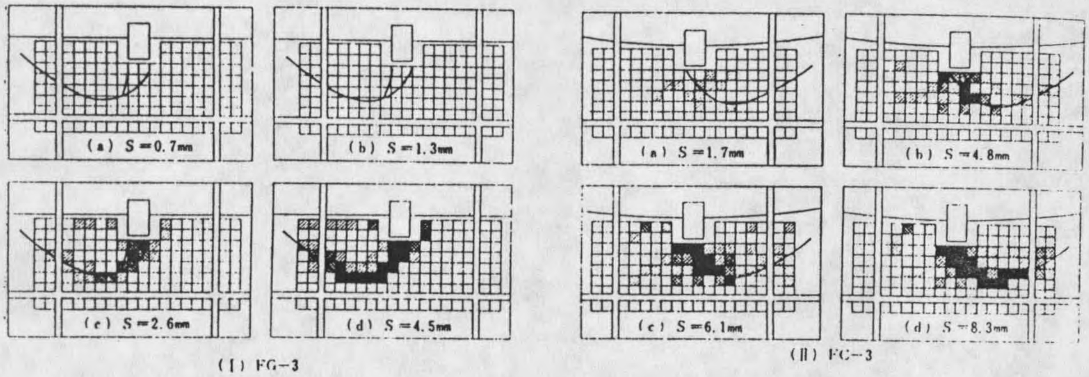

Figure 12. Radiograph studies - propagation of shear strains through Toyoura sand at different load steps for small (FG-3) and large (FC-3) scale footings (from Yamaguchi et al., 1976).

The second component of the scale effect is due to progressive failure within the soil beneath the footing and was first suggested by Muhs (1963). The mechanism of progressive failure may be best understood by considering the results of radiograph studies by Yamaguchi et al., (1976). Figure 12 presents the observed distribution of shear strains taking place in a dense Toyoura sand at different loading steps for both a small-scale surface footing (FG-3), and a large-scale surface footing (FC-3). As observed, the shear strains developed under the small-scale footing at peak capacity (Fig. 12 I(b)) are nearly constant along the slip mechanism. It is therefore reasonable to assume that the angle of shearing resistance averaged over the entire mechanism at peak load is similar to the peak angle of shearing resistance (ϕ'_{peak}). Since this is the case, it is expected that the use of ϕ'_{peak} in the general bearing capacity equation will lead to reasonable estimations of the bearing capacity for smaller surface footings. In general, this is not true for larger footings. As seen in Figure 12 II(b), the shear strains developed at peak capacity under the large-scale footing show considerable variation along the slip line, with the largest strains occurring at the bottom of the footing, and progressively decreasing strains as one moves away from the footing. Yamaguchi et al., (1976) demonstrated that the magnitude of the shear strains near the footing exceeded peak shear strains and corresponded closely to a residual state, where the actual angle of shearing resistance was closer to the critical state or constant volume friction angle (ϕ'_{cv}). In other words, in the region near the bottom of the footing, peak strength had already been reached and exceeded long before the strength in regions further away had been mobilized. Therefore, the assumption of constant shear strain and thus, peak shear resistance along the entire slip mechanism is unacceptable for large footing widths. In these cases, the use of ϕ'_{peak} in a bearing capacity solution has the potential to overestimate the bearing capacity significantly.

It is expected that progressive failure within the soil will also become more pronounced with increasing surcharge (q). Higher mean normal stresses developed as a result of surcharge pressure would likely exceed peak shear strains near the footing, leading to progressive failure.

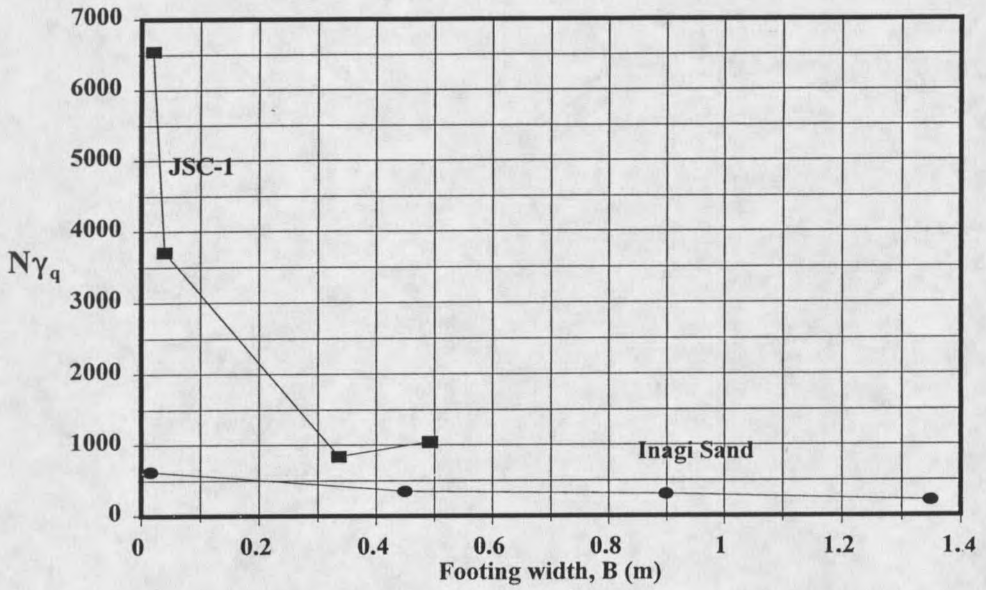

Figure 13. Comparison of the scale effect for JSC-1 and Inagi sand (from Perkins and Madson, 1996 and Kusakabe et al., 1991).

One observation that may be made of the scale effect is that this effect is different for various materials. This may be seen by comparing shallow foundation experiments performed with Inagi sand by Kusakabe et al., (1991), with results from shallow foundation experiments performed with JSC-1 by Perkins and Madson (1996). This is done in Figure 13 where the normalized bearing capacity, $N\gamma_q$ has been plotted against the footing width, B for both the Inagi sand and JSC-1. As seen in Figure 13, JSC-1 exhibits a much greater decrease in $N\gamma_q$ with increasing footing width than the Inagi sand. Material properties therefore, have a significant impact on the magnitude of the scale effect.

As shown in this section, the scale effect composed of material non-linearity and progressive failure can have serious repercussions in regards to the actual bearing capacity of a given sand. Conventional bearing capacity solutions suffer in that they do not account for either component of the scale effect. Material non-linearity may be taken into account indirectly by choosing shear strength parameters appropriate to the stress-strain conditions present under the footing. However, progressive failure cannot be adequately accounted for within conventional solutions, resulting in possible overestimations of bearing capacity. This uncertainty has led to the use of large factors of safety. As discussed earlier, in many cases, these large factors of safety have led to very conservative designs and hence, larger construction costs. In Chapter 4, a new design methodology will be presented to take into account both material non-linearity and progressive failure.

CHAPTER 3

MATERIAL PROPERTIES OF STUDY SANDS

Introduction

The purpose of this chapter is to present the experimental work performed by the author on two sands, as well as to present the material properties and bearing capacity results accumulated for six other study sands. These results will be used in Chapter 4 to calibrate the new approach to bearing capacity analysis proposed in this thesis. In this chapter, only results of experiments performed on the study sands are presented. Predictions of material strength properties using Bolton's equations, as well as predictions of bearing capacity will be presented in Chapter 4. A total of eight study sands were used and are designated as follows:

1. MLS-1
2. JSC-1
3. Toyoura Sand
4. Inagi Sand
5. Texas Sand
6. Ottawa Sand
7. Monterey Sand

8. Scoria Sand

As part of this work, the author conducted experimental work consisting of a series of triaxial tests performed on sands 1 and 2 (MLS-1 and JSC-1) in order to define the strength and deformation properties of each. This work complemented data from centrifuge bearing capacity experiments performed on each sand. It should be noted that all centrifuge test results to be summarized were from concentric, vertical loadings (i.e., no eccentric loads).

Experimental Work

Grain Size Distributions

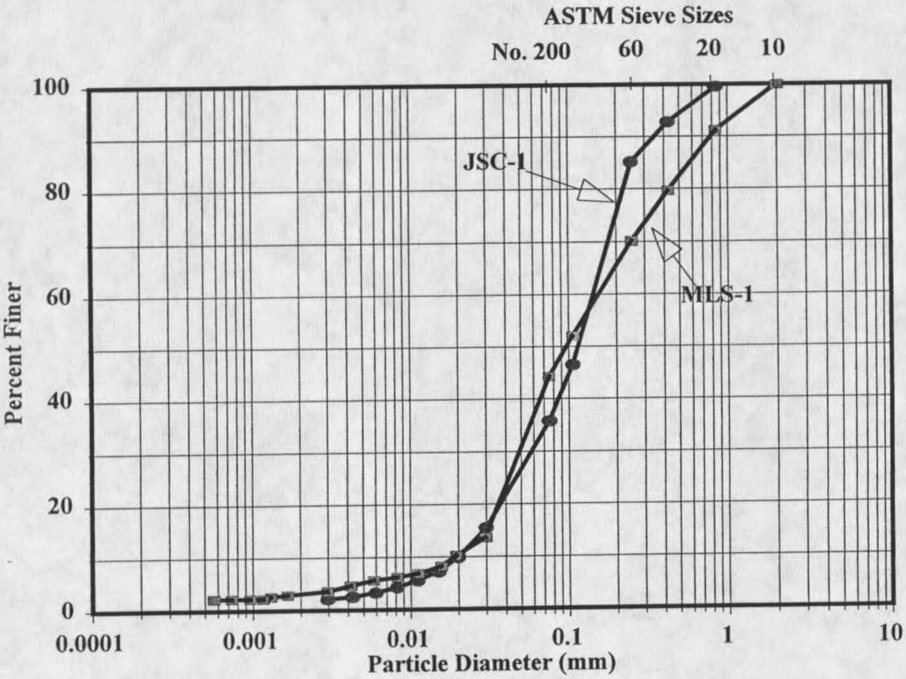

Figure 14. Particle Distributions - MLS-1 & JSC-1, (from Perkins and Madson, 1996).

Grain size distributions of the MLS-1 and JSC-1 are shown in Figure 14. The sieve analysis conformed to ASTM D (421 and 422). As may be observed in Figure 14, both sands are quite comparable with respect to their grain size distribution with the exception of the fines content. Approximately 43% of the MLS-1 passes the number 200 sieve, as compared to 36% for the JSC-1. The coefficient of uniformity of the MLS-1 is 16, while the coefficient of curvature is 1.1. The coefficient of uniformity and coefficient of curvature for the JSC-1 are 7.5 and 1.12, respectively. Both are classified as highly angular, silty sand with non plastic fines.

Conventional Triaxial Compression Tests (CTC)

In order to define the strength and deformation properties of the MLS-1 and JSC-1, a series of isotropically consolidated, drained conventional triaxial compression (CTC) experiments were performed. These tests were conducted using samples prepared in a dry state. The triaxial apparatus consisted of a triaxial chamber with a submersible load cell, volume transducer, axial displacement transducer, and data acquisition unit. The submersible load cell was used to eliminate shaft friction from axial force measurements on the sample during testing. Changes in sample volume during shear were measured using a volume transducer. The transducer operates by measuring the volume of cell water entering or leaving the triaxial chamber as the specimen shears and changes volume. Cell water entering or leaving the cell is collected in a cylindrical reservoir consisting of two chambers separated by a sealed piston. The LVDT (Linear Variable Differential Transducer) attached to the piston measures the displacement and corresponding volume change as the test proceeds. An axial displacement transducer is used to monitor axial strains in the sample during testing. Measurements from the electronic transducers are recorded using a data acquisition unit (DAS).

The consolidated drained (CD) triaxial test consists of two stages, a consolidation stage and a shearing stage. During stage one, the sample is subjected to an all-around confining pressure (σ'_3). The level of confinement is normally consistent with that expected in the field. Once consolidation is complete, the specimen is sheared. This is done by subjecting the specimen to an increasing axial load (σ'_1). During this stage all drainage ports are left open to satisfy the drained criterion. The results of these tests may be plotted on a Mohr-Coulomb diagram and a failure envelope constructed. Alternatively, strength envelopes may be developed in terms of stress invariants p' and q' given by:

$$p' = \frac{1}{3}(\sigma'_1 + 2\sigma'_3) \tag{38}$$

$$q = \sigma'_1 - \sigma'_3 \tag{39}$$

The normal stresses are all effective stresses.

Samples approximately 70 mm in diameter by 135 mm in height with fixed, non-lubricated end platens were used for the CTC experiments. The specimens were prepared inside a latex membrane stretched over a rigid mold. The material was placed in four equal lifts, with each lift compacted to the appropriate density with a small hand vibrator. A vacuum was used to maintain sample rigidity while the mold was removed. The vacuum was maintained until the appropriate confining pressure was applied inside the cell.

CTC experiments were performed with the MLS-1 at levels of confining pressure ranging from 1.7 to 649 kPa. In order to study the effect of different densities on the stress-strain properties of the MLS-1, CTC experiments were performed at the following densities: 1.70, 1.90, and 2.20 g/cm^3. The highest density (2.20 g/cm^3) corresponds to a relative density of 100% for this material. It should be noted that the author only performed tests on the MLS-1 at the highest density (2.20 g/cm^3). Perkins (1991) performed a series of CTC experiments with MLS-1 at densities of 1.70 and 1.90 g/cm^3, corresponding to relative densities of 28% and 61.5%, respectively. In Appendix A are found the axial strain vs principal stress difference and axial strain vs volumetric strain response from CTC tests performed on the MLS-1 at all three densities, where positive volumetric strains are taken as compression. The highest density tested (2.20 g/cm^3) corresponds to the density of the specimens used for bearing capacity experiments discussed later. As may be observed from the CTC results performed at 100% relative density, the MLS-1 is quite dilative and demonstrates significant strain softening for all levels of confinement.

Using the CTC results conducted at the highest relative density, strength envelopes corresponding to peak and residual strength were constructed in p'-q stress space and are presented in Figure 15. As seen, the best-fit envelope for peak strength demonstrates significant curvature over a relatively small range in mean normal effective stress (p'). Secant friction angles at peak strength range from 48 to as much as 58 degrees, with the higher confinements associated with the lower friction angles. These results demonstrate a

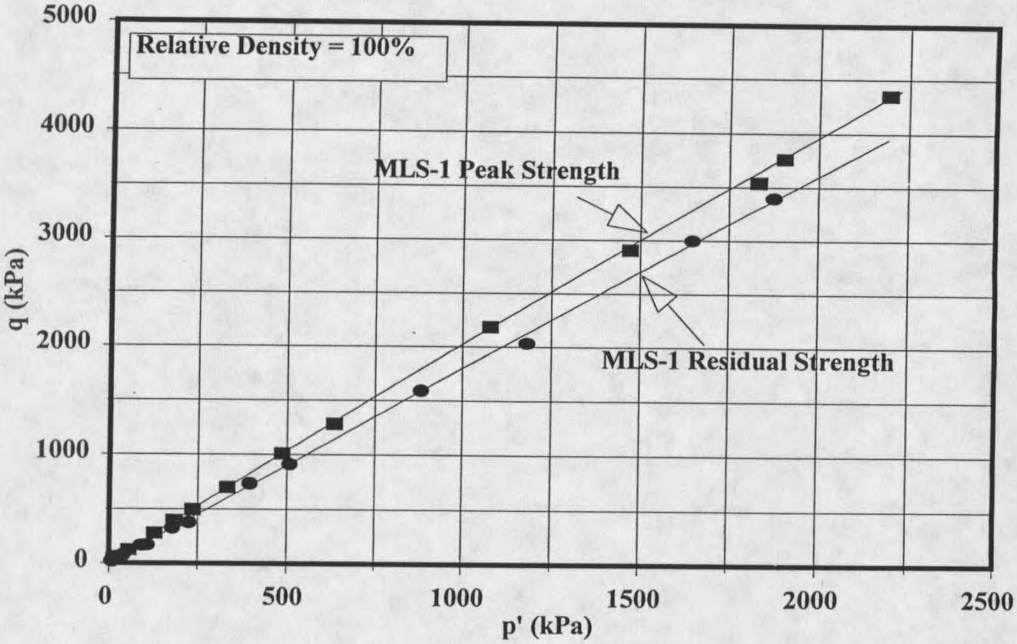

Figure 15. MLS-1 - Peak and residual strength envelopes plotted in p'-q stress space (from specimens compacted to 100% relative density).

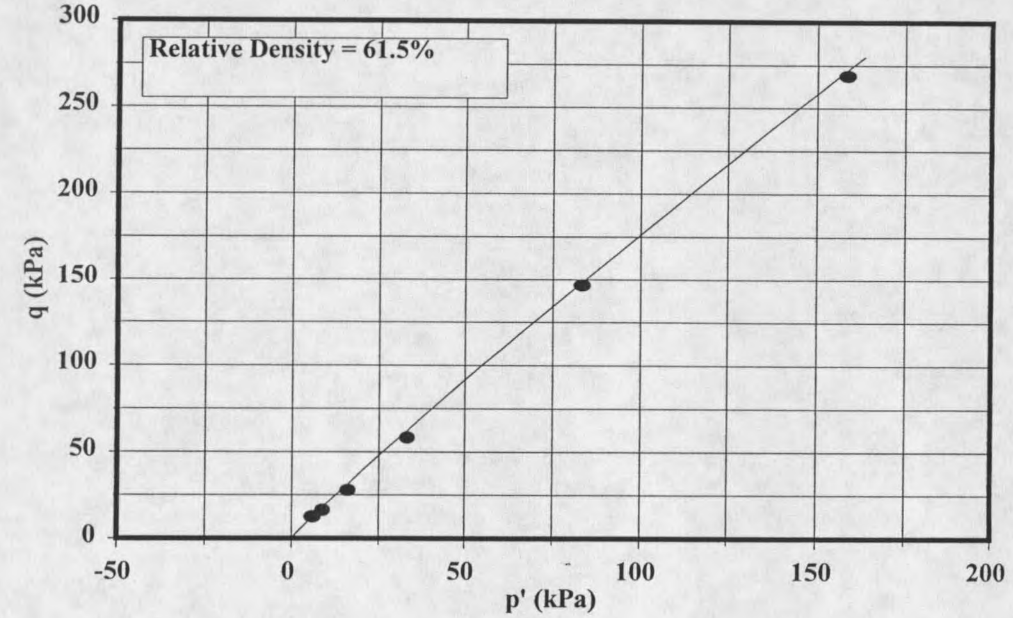

Figure 16. MLS-1 - Peak strength envelope plotted in p'-q stress space (from specimens compacted to 61.5% relative density).

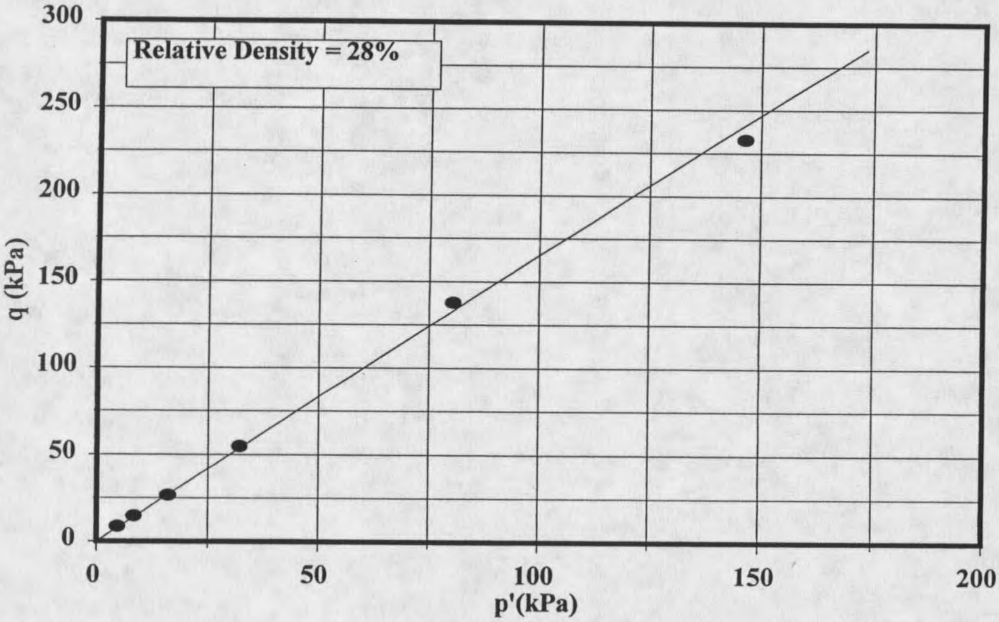

Figure 17. MLS-1 - Peak strength envelope plotted in p'-q stress space (from specimens compacted to 28% relative density).

significant material non-linearity, with the majority of the non-linearity occurring at the lower mean normal stress levels. These findings are summarized in Table 1, where the secant friction angles computed from the best-fit failure envelope have been tabulated with the corresponding mean normal stress at peak strength. As noted in Chapter 2, material non-linearity is one of the major components of the scale effect and causes significant problems in terms of finding appropriate strength parameters for use in conventional bearing capacity solutions. This is compounded by the problem that at elevated friction angles, changes as small as 1 degree can dramatically change design parameters.

Table 1. Secant friction angles at various levels of p' for MLS-1 & JSC-1 compacted to 100% relative density.

Mean Normal Stress (p')	Secant friction angle (ϕ') MLS-1	Secant friction angle (ϕ') JSC-1
10	58	64
40	55	59
625	50	51
1,175	49	50
2,200	48	48

In Figure 15, the residual strength envelope of the MLS-1 has also been plotted using the residual strength levels (i.e., where the curve flattens beyond peak strength) from the stress-strain curves. As observed in Figure 15, the residual strength envelope is quite linear with a friction angle of between 42 and 44 degrees. This general trend is consistent with findings of other studies on sand. These studies have noted that sands will, regardless of confinement or initial relative density, tend toward the same critical state or constant volume friction angle (ϕ'_{cv}). This phenomenon was discussed in detail in Chapter 2. It was further stated in Chapter 2 that the constant volume friction angle is principally a function of the mineralogy of the sand in question. This has significance in later discussions.

Figures 16 and 17 present the peak strength envelopes constructed from CTC tests conducted with MLS-1 at the lower relative densities. While material non-linearity is not as apparent as with the previous results, there is still some curvature in the failure envelopes.

CTC experiments were also performed on the JSC-1 at nine different levels of confinement ranging from 21 to 700 kPa. The samples were prepared in the same manner as the MLS-1, with the exception that this material was compacted to a density of 1.78 g/cm^3.

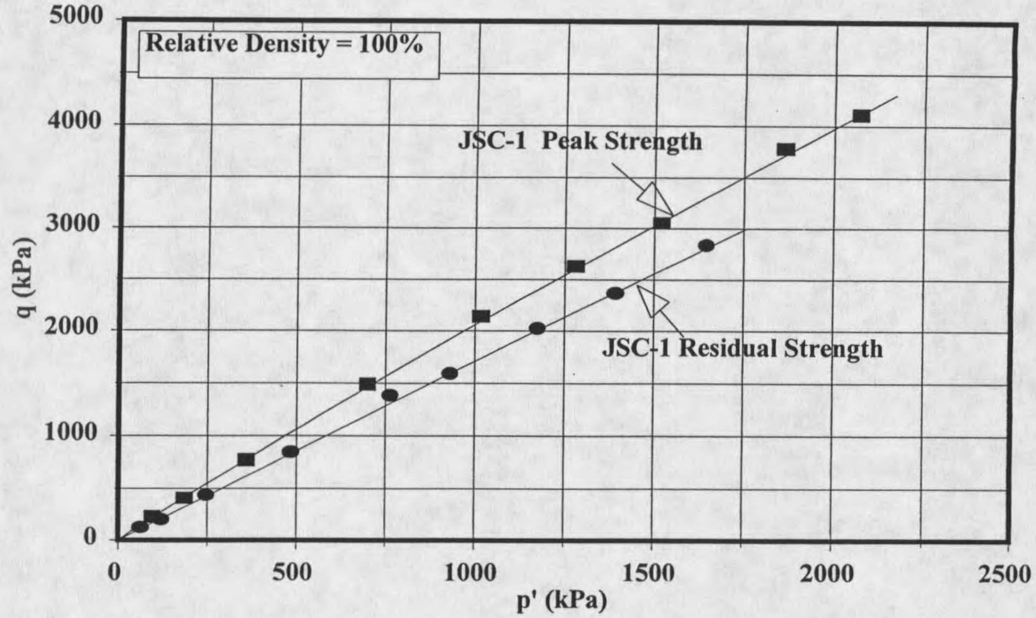

Figure 18. JSC-1 - Peak and residual strength envelopes plotted in p'-q stress space (from specimens compacted to 100% relative density).

This density corresponds to a relative density of 100% for this material. In Appendix A are found the axial strain vs principal stress difference and axial strain vs volumetric strain response for the JSC-1. Again, many of the same trends seen at 100% relative density with the MLS-1 are observed with the JSC-1. At higher confining pressures, the JSC-1 exhibits slightly more dilation during shear compared to the MLS-1. Strain softening is also apparent for all levels of confinement.

The secant friction angles at peak strength range from 48 to 64 degrees as determined from the best-fit envelope, demonstrating again a significant material non-linearity, (Table 1). Figure 18 presents the failure envelope developed for the JSC-1. From Table 1, it is apparent that the secant friction angles at moderate to high values of mean normal stress are quite comparable between the two sands. As with the MLS-1, the residual strength envelope of the JSC-1 is also quite linear with a friction angle of 42 to 44 degrees.

The peak secant friction angles of the JSC-1 differ somewhat from those reported by Willman et al., (1995). Willman et al., (1995) reported that the friction angle of JSC-1 was 45 degrees. However, this value was developed from CTC tests on samples with considerably lower mass densities (1.50 - 1.65 g/cm^3). It should also be noted that this was a tangent friction angle where a cohesion intercept of 1 kPa was assumed. The results provided by Willman et al. (1995) also demonstrate little change in the friction angle with changes in confinement, contrary to the findings discussed here. This trend continued even at the higher densities (1.60 - 1.65 g/cm^3). It is speculated that this is simply due to the fact that the samples were prepared close to the density corresponding to the critical void ratio. As noted by Bolton (1986) and discussed in Chapter 2, samples prepared at or above the critical void ratio tend toward the same critical state or constant volume friction angle (ϕ'_{cv}). Stress-strain curves from the CTC tests performed by Willman et al., (1995) were not available to confirm this statement.

Centrifuge Bearing Capacity Experiments

In conjunction with the previously described triaxial tests on the MLS-1 and JSC-1, a series of bearing capacity experiments were performed on these sands using the centrifuge. While the author did not perform these tests, the data accumulated is pertinent to later discussions and is therefore presented here. These experiments are further described by Gui (1995), Perkins (1995a), and Perkins and Madson (1996).

Briefly, the bearing capacity experiments were performed using the 400 g-ton centrifuge located at the University of Colorado at Boulder. The centrifuge consists of an unsymmetrical rotor arm with a counterweight on one end and a swing platform on the other. The swing platform carries the test payload and is capable of carrying test loads up to 1.22 m by 1.22 m by 0.91 m in size and 2,000 kg in mass.

Scaling Relationships. Scaling relationships for the centrifuge have been shown to be valid through both dimensional analysis (Gui, 1995) and by modeling-of-models studies (Kutter, et al., 1988). Therefore, an in-depth discussion will not be provided here. However, the basic premise of centrifuge tests is that a large scale or prototype foundation width may be modeled by subjecting a model footing to an increased gravity environment. The size of the prototype foundation width is simply the model foundation width multiplied by the acceleration level to which the model is subjected using the centrifuge. For example, if the model footing width is 10 mm and is accelerated to a gravity level of 30g, the prototype footing width will be 300 mm. Often, centrifuge tests are performed in-lieu of full-scale bearing capacity tests simply due to the cost involved with full-scale tests. For this reason, centrifuge tests have become quite popular over the last 20 years.

Experimental Set-up. The model foundation experiments performed on the MLS-1 and JSC-1 were done under plane strain conditions such that a strip footing was modeled. In order to maintain plane strain conditions, the foundation was constructed in five segments. The three interior segments were of sufficient length (two times the foundation width) such that a plane strain condition existed under the three interior segments. Together, the foundation had a length to width ratio (L/B) of 7. Model foundation widths of 10, 20, and

40 mm were used for different experiments. Rotation was allowed for each individual foundation segment. All experiments were performed with rough foundations. This was accomplished by gluing sand to the bottom surface of each foundation segment.

The foundation system was loaded through a hydraulic actuator such that load control experiments were performed. Load was measured for the three interior foundation segments by placing load cells between the segments and the supporting cross-arm, while displacement was measured by an LVDT for the entire foundation assembly. The experimental configuration has been described in greater detail by Perkins (1995a).

Specimen Preparation. Both the MLS-1 and JSC-1 were prepared in the same manner with the exception of the density to which they were compacted. The MLS-1 and JSC-1 were compacted in a dry state to a density of 2.20g/cm^3 and 1.78 g/cm^3, respectively. These densities match those used in the triaxial experiments and correspond to relative densities of 100%. A pneumatically driven ball vibrator attached to a 150 mm square steel plate was used in compacting each specimen. A uniform density was achieved by first placing the material in a uniform state by gently vibrating the material through a sieve covering the entire specimen container. The lift was then compacted to the appropriate density by compacting the layer to a lift height line scribed on the sides of the container. This process was then repeated for each additional lift. Additional details are provided by Perkins (1995a).

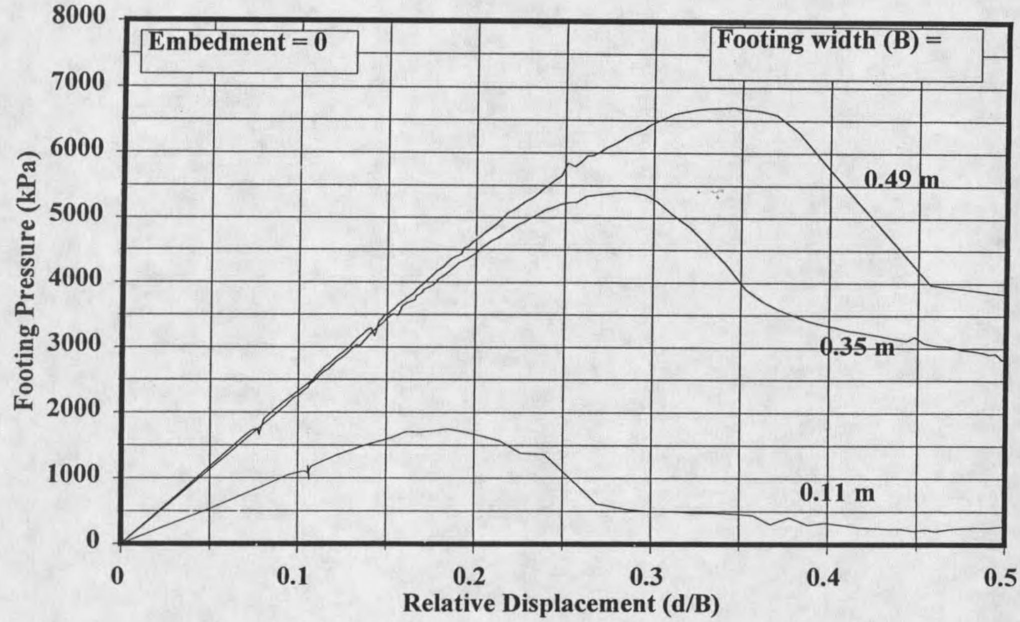

Figure 19. MLS-1 - Bearing capacity results; D = 0.

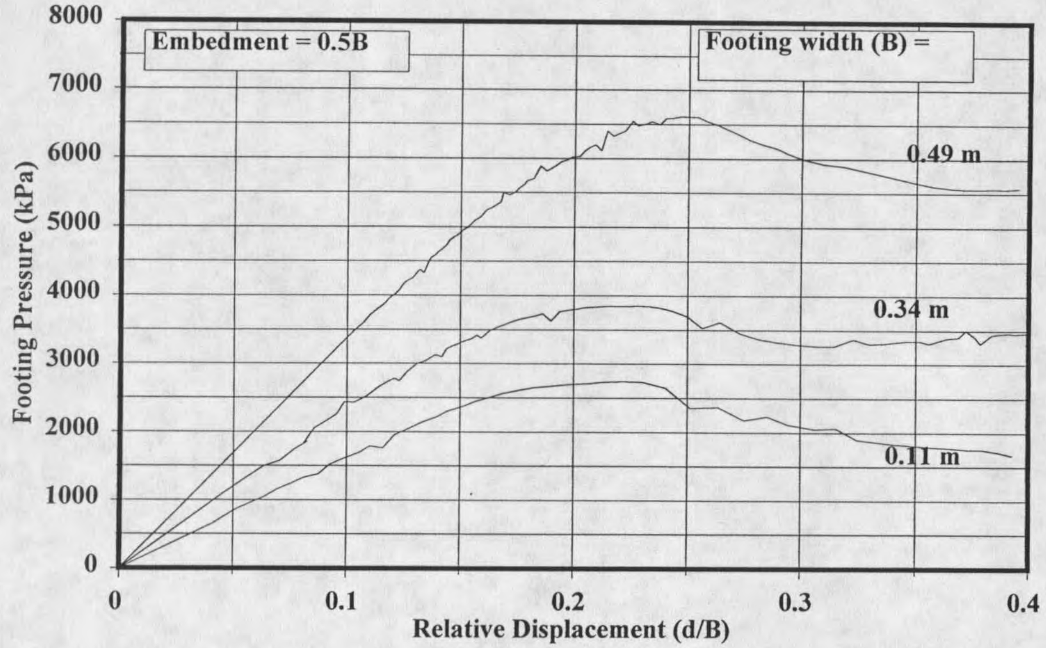

Figure 20. MLS-1 - Bearing capacity results; D = 0.5B.

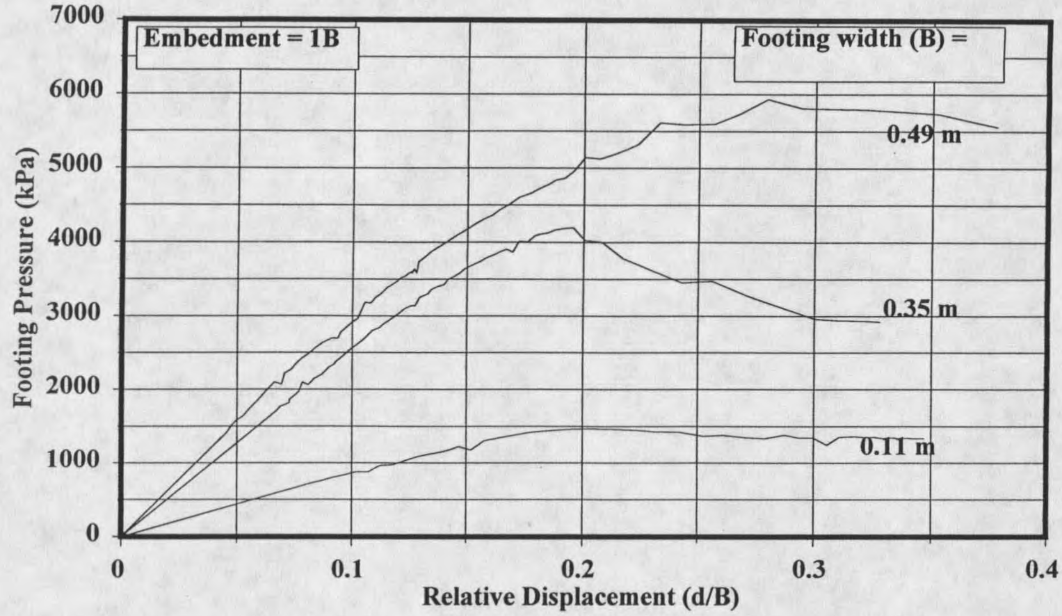

Figure 21. MLS-1 - Bearing capacity results; D = 1B.

Experimental Results. A total of nine model foundation experiments were performed on the MLS-1 at different gravity levels to model various footing widths. The model footing width for all the centrifuge experiments performed with the MLS-1 was 20 mm. In order to study the effect of surcharge, three depths of embedment were modeled, namely D=0, D=0.5B, and D=1B where B is the footing width. The results of these experiments are presented in Figures 19 - 21. In each figure, the footing displacement (d) is normalized by the footing width (B) and is plotted against the vertical stress under the central footing segment, (i.e., the segment considered to be in a condition of plane strain).

As expected, the peak footing pressure and subgrade stiffness increase with increasing footing width. However, Perkins (1995a) showed that this increase is less than that predicted using conventional bearing capacity theories employing a constant friction angle. In other words, the bearing capacity factor, $N\gamma_q$ exhibits a significant scale effect. This observation is a manifestation of the decreasing friction angle with increasing mean normal stress confinement (i.e., increasing footing width and footing pressure) and has been noted in other centrifuge studies (Yamaguchi et al., 1976; and Kutter et al., 1988), as well as in full-scale foundation studies (Kusakabe et al., 1992). This effect was discussed in detail within Chapter 2. Alternative forms of conventional/bearing capacity theories have been presented by Perkins (1995a) to capture the effect of material non-linearity. Another method to capture the effect of non-linear material behavior will be presented in Chapter 4.

As seen in the figures, the peak bearing capacity for the MLS-1 generally increases only moderately at increased depths of embedment and even decreases in some cases. In conventional bearing capacity theory, the bearing capacity is assumed to linearly increase with increasing depth of embedment due to surcharge effects. Again, this apparent lack of increase in the bearing capacity may be attributed to the scale effects discussed previously. One further observation of the results may be made. It appears that as the depth of embedment increases, the difference between the peak and residual strength becomes less for all footing widths. In other words, strain-softening is not nearly as apparent. This may be attributed to material non-linearity where higher mean normal stresses are associated with lower peak friction angles. Therefore, as the mean normal stress increases with depth of embedment, the peak friction angle is tending towards the critical state. As a result, strain hardening becomes more pronounced as the depth of embedment increases. It is expected that at higher depths of embedment there would be no difference between peak and residual strength.

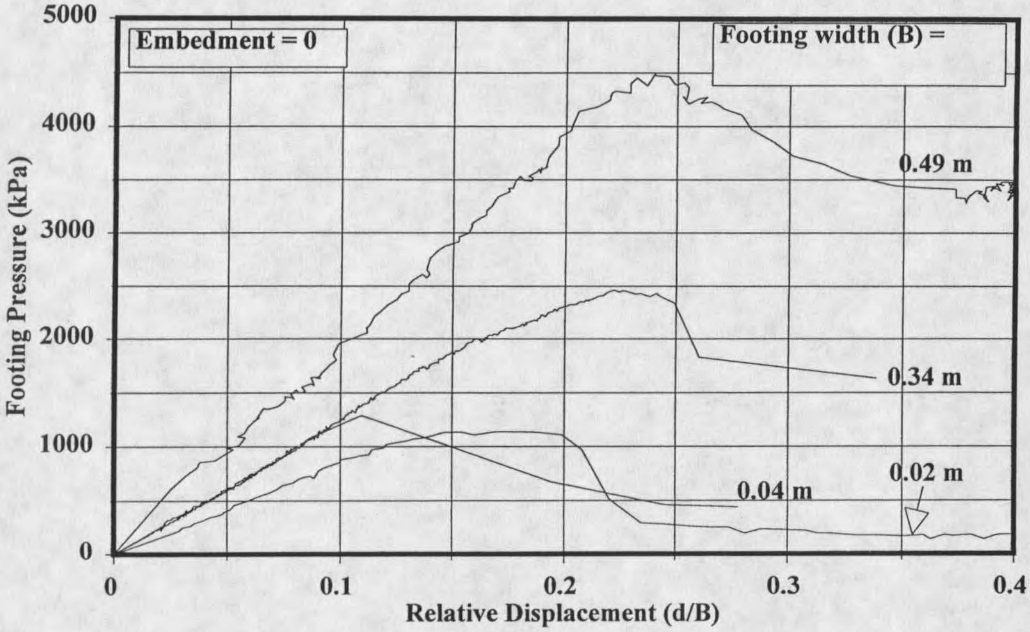

Figure 22. JSC-1 - Bearing capacity results; D = 0.

A total of twelve bearing capacity experiments were performed on the JSC-1 at various gravity levels and model footing widths. Only surface bearing capacity experiments were performed with this material. Four footing widths were modeled. These widths were: B=0.02 m, B=0.04 m, B=0.34 m, and B=0.49 m. The first two tests were simply small-scale experiments performed in the 1-g environment. Figure 22 presents the experimental results. Similar to the results with the MLS-1, the bearing capacity and subgrade stiffness of this material increase with footing width. It can also be shown that the bearing capacity results with the JSC-1 is less than that predicted using conventional bearing capacity theory. Again, this may be attributed to scale effects discussed earlier.

A summary of the results of the centrifuge tests performed on the MLS-1 and JSC-1 are presented in Table 2.

Table 2. Bearing Capacity Results - MLS-1 & JSC-1.

Sand	Prototype Footing Width (m)	Normalized Embedment Depth (D/B)	q_{ult} (kPa)
MLS-1	0.494	0	6700
MLS-1	0.348	0	5400
MLS-1	0.109	0	1750
MLS-1	0.492	0.5	6620
MLS-1	0.349	0.5	3850
MLS-1	0.108	0.5	2740
MLS-1	0.494	1.0	5810
MLS-1	0.352	1.0	4190
MLS-1	0.107	1.0	1470
JSC-1	0.492	0	4487
JSC-1	0.337	0	2468
JSC-1	0.04	0	1292
JSC-1	0.02	0	1140

Summary of Study Sands

The remainder of Chapter 3 will be devoted to summarizing shear strength data and bearing capacity results (both centrifuge and full-scale bearing capacity tests) performed by different researchers on the other six study sands. This discussion will include material properties and other pertinent information.

Toyoura Sand

Kimura et al., (1985) used the centrifuge to study the bearing capacity of Toyoura sand. In their experiments rough foundations were modeled. Model foundation widths used were 20, 30, and 40 mm. All tests were conducted under plane strain conditions such that strip footings were modeled. Prototype footing widths modeled varied from 0.03 m to 1.60 m with normalized depths of embedment (D/B) ranging from 0 to 1.0.

The material (Toyoura Sand) was compacted in 10 mm lifts using a vibrator. Each lift was vibrated for one minute. The resulting dry unit weight of this material was 15.9 kN/m^3. The dry unit weight of this material corresponds to a relative density of approximately 87%.

The results of the bearing capacity tests are found in Appendix B. In the plots, the bearing capacity factor ($N\gamma_q$) has been plotted against another normalizing factor ($\gamma B_N/E_q$), where E_q is Young's modulus of the parent rock of the Toyoura sand and B_N is the prototype width of the footing. E_q is taken to be 98 kN/m^2. Due to the complexity of accurately back calculating the actual bearing capacity for each footing width, Kimura (1995) was kind enough to provide the load settlement curves for each of the tests. These plots are also found in Appendix B. In the plots, the settlement (s) has been plotted against the corresponding load intensity (q), where B is the model footing width and g is the gravity level to which the model was subjected. Using the plots, Table 3 was assembled summarizing the results.

Table 3. Bearing Capacity Results - Toyoura Sand.

Prototype Footing Width (m)	Normalized Embedment Depth (D/B)	q_{ult} (kPa)
0.03	0	133
0.60	0	1727
1.20	0	2188
0.03	0.5	235
1.20	0.5	3924
0.03	1.0	387
0.04	1.0	442
0.80	1.0	3689
1.20	1.0	3630
1.60	1.0	4660

Fukushima and Tatsuoka (1984) performed a series of triaxial tests on the Toyoura sand at relative densities of approximately 34 and 75 percent. The results of these tests are found in Appendix A and are presented as smooth curves with the friction angle at peak strength plotted against the effective minor principal stress. Fukushima and Tatsuoka (1984) provide a detailed explanation of the test procedure followed. Using the plot, p'-q diagrams for both relative densities were constructed and are shown in Figures 23 and 24.

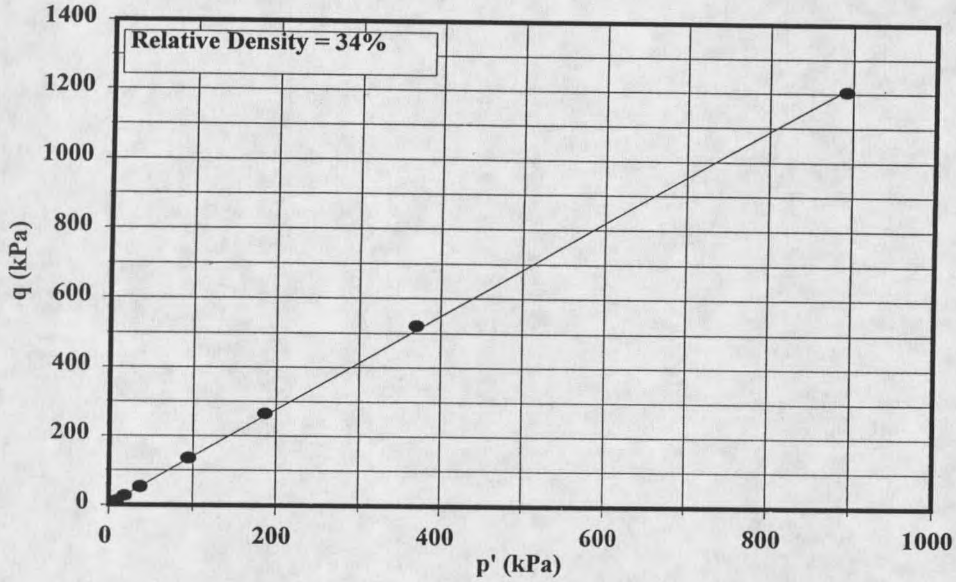

Figure 23. Toyoura sand - Peak strength envelope plotted in p'-q stress space (from triaxial tests conducted at 34% relative density).

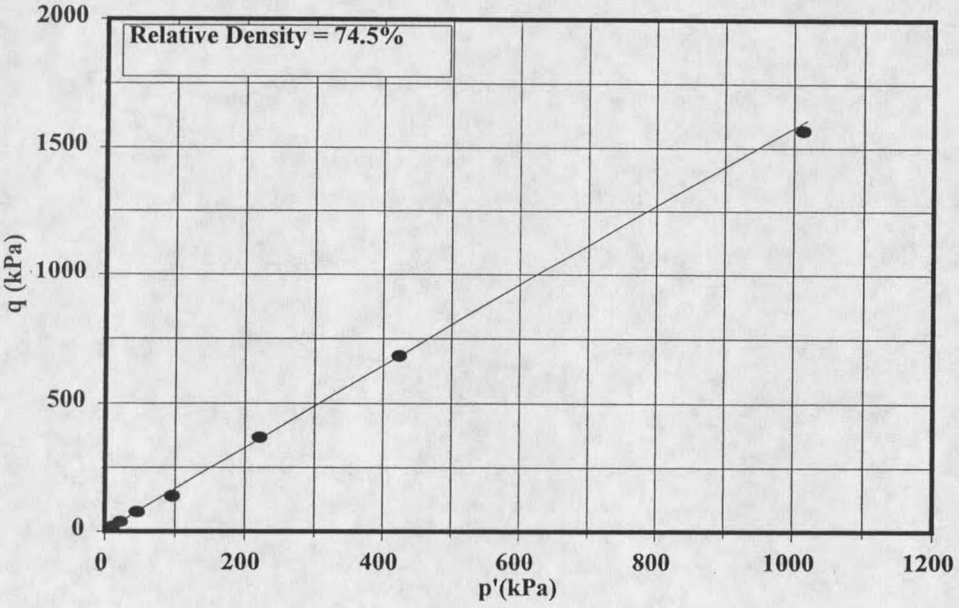

Figure 24. Toyoura sand - Peak strength envelope plotted in p'-q stress space (from triaxial tests conducted at 75% relative density).

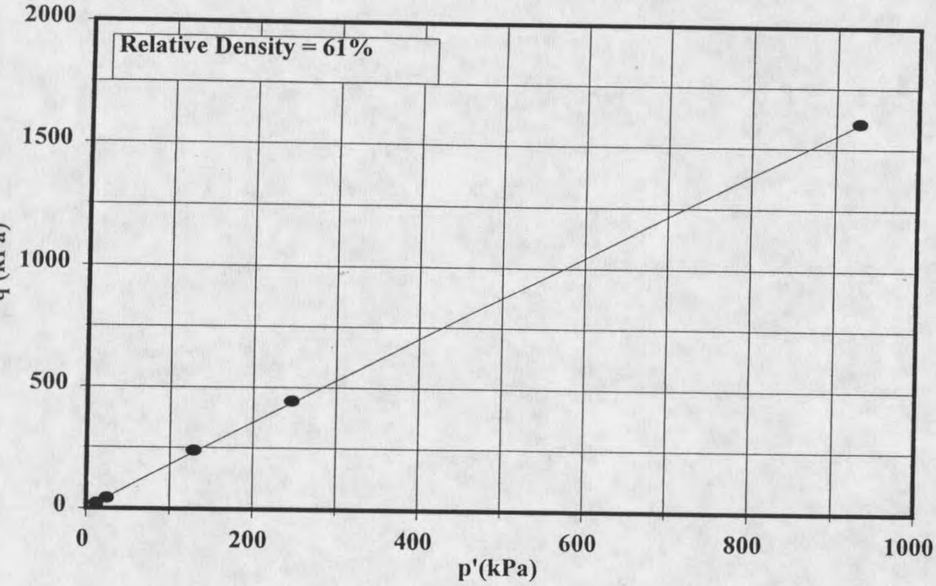

Figure 25. Toyoura sand - Peak strength envelope plotted in p'-q stress space (from plane strain tests conducted at 61% relative density).

In addition to the triaxial results, Tatsuoka et al., (1986) performed a series of plane strain compression tests with Toyoura sand compacted to a relative density of 61%. The results of these tests are presented in Appendix A, where the principal stress ratio has been plotted against the axial strain. Tatsuoka et al., (1986) provide details on the procedure followed in performing these tests. Using the plane strain data, a third failure envelope was developed and is shown in Figure 25.

Inagi Sand

Kusakabe et al., (1991) performed a series of bearing capacity tests using the centrifuge with a dry Inagi sand. In their experiments both circular and rectangular footings were modeled. The width of the rectangular footings modeled ranged from 0.03 to 2.70 m, with aspect ratios (L/B) of 3 and 7, respectively. Only surface footings were modeled. The following model footings were used in these experiments:

circular footing
30 mm diameter (L/B=1)

rectangular footings
30 mm wide x 90 mm long (L/B=3)
15 mm wide x 105 mm long (L/B=7)

Rough footings were modeled by gluing sand particles to the base of the footings. During the course of the tests the footings were allowed to both rotate and move horizontally.

The material was prepared by allowing the sand to freely drop 0.8 meters into a rectangular box. Preparation in this manner resulted in an average unit weight of 16.474 kN/m^3 corresponding to an average relative density of 81.8%. Kusakabe et al., (1991) provide a detailed description of the test procedure.

The results of the centrifuge tests with the Inagi Sand are shown in Appendix B. In each graph, the normalized load intensity ($N\gamma$) has been plotted against the normalized settlement (S/B), where S is the settlement and B is the footing width. Aspect ratios of 1, 3 and 7 were modeled. The curves in each graph represent the gravity level to which the model footing was subjected. It should be noted that an aspect ratio of 1 corresponded to the circular footings. Using the plots, Table 4 was assembled summarizing the results.

Table 4. Bearing Capacity Results - Inagi Sand.

Prototype Footing Width or Diameter (m)	Aspect Ratio L/B	Normalized Embedment Depth (D/B)	q_{ult} (kPa)
0.03	1	0	67
0.90	1	0	1149
1.80	1	0	1705
2.70	1	0	2223
0.03	3	0	91
0.90	3	0	1705
1.80	3	0	2520
2.70	3	0	3558
0.015	7	0	77
0.45	7	0	1297
0.90	7	0	2298
1.35	7	0	2446

Kusakabe et al., (1991) also performed a series of drained triaxial compressions tests on the Inagi sand. These tests were conducted at confinements ranging from 49 to 686 kPa. The resulting secant friction angle at failure assuming zero cohesion was plotted against the mean principal stress at failure (p'_f) for a relative density of 80%. This is shown in Appendix A. A regression curve was then fit to the data to describe the change in friction angle with mean principal stress at failure. This expression is given as

$$\phi = 41.8 - 2.5 \log(\frac{p_f}{p_o}) \tag{40}$$

where p_o = 98 kPa and ϕ is in degrees.

Using this data, Figure 26 was constructed for the Inagi sand.

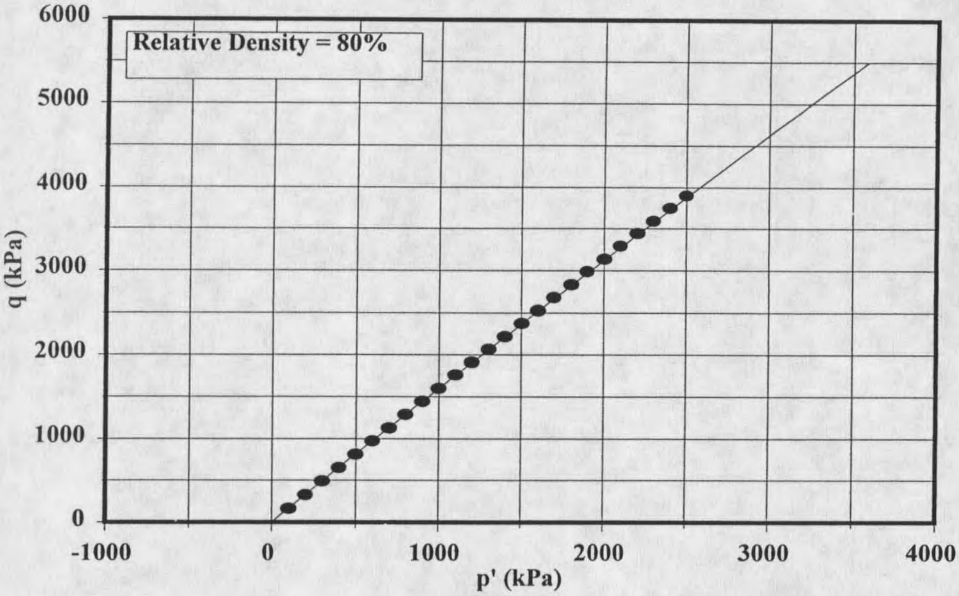

Figure 26. Inagi sand - Peak strength envelope plotted in p'-q stress space (from triaxial tests conducted at 80% relative density).

Texas Sand

Briaud and Gibbens (1994) presented the results of a series of full-scale load tests performed on a sandy soil which, for the remainder of this thesis, will be referred to as Texas sand. The results were part of a Prediction Symposium sponsored by the Federal Highway Administration at the Settlement '94 ASCE Conference held at Texas A&M University. The symposium was established in order to evaluate different design approaches for spread footings placed on granular soils. Data on the sand, as well as the full-scale spread footings to be tested was made available to all interested parties as a part of the Prediction Symposium. The data was used to predict the behavior of the footings on the Texas sand. These predictions were then compared to the measured behavior from load tests. Data made available from the symposium has also been used in this research.

Five full-scale spread footings were load tested for this symposium. The spread footings ranged in size from approximately 1x1 m to 3x3 m and were load tested to 150 mm of vertical displacement. The normalized embedment depths (D/B) of the spread footings ranged from 0.25 to 0.72. Briaud and Gibbens (1994) provide a detailed description of the procedure used for loading the footings.

In order to characterize the properties of the sand deposit, a detailed site investigation was conducted. Testing performed included CPT, pressuremeter, and triaxial tests. The site investigation revealed a predominate sand layer from 0 to 11 meters, below which a clay layer existed to a depth of approximately 33 meters. Groundwater was located at a depth of 4.9 meters. The average moist unit weight of the sand was 15.4 kN/m^3, and the average in-situ relative density was approximately 55%. The relative density was estimated from CPT values and SPT data.

Results from the full-scale load tests performed on the sand are included in Appendix B. In each curve, the load has been plotted against the settlement (S). Since all five footings demonstrated strain hardening characteristics, (i.e., no peak load), a value for the peak bearing capacity had to be chosen at some level of settlement. Rather then choosing the load at the final displacement of 150 mm for all the footings, it was felt that a more logical choice would be to use the load associated with a constant normalized settlement (S/B). Since a displacement of 150 mm corresponded to a normalized settlement (S/B) of 0.05 for the largest footings, this value was chosen as the normalized settlement associated with peak strength for all the footings. Table 5 summarizes the bearing capacity data for the Texas sand.

Table 5. Bearing Capacity Results - Texas Sand.

Footing No.	Length x Width (m)	Normalized Embedment Depth (D/B)	q_{ult} (kPa)
1 N. Footing	3.004 x 3.004	0.25	1136
2	1.505 x 1.492	0.51	1069
3 S. Footing	3.023 x 3.016	0.29	973
4	2.489 x 2.496	0.31	1062
5	0.991 x 0.991	0.72	1120

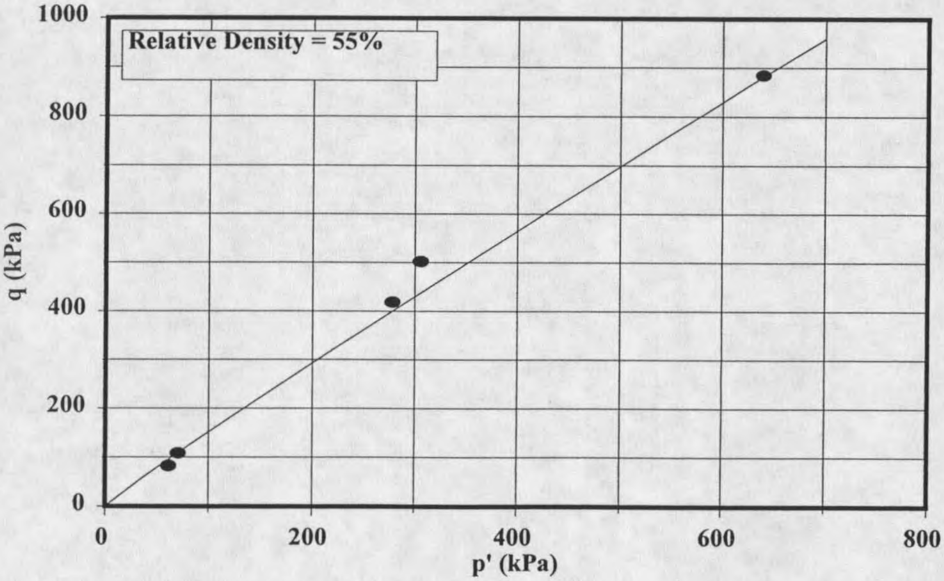

Figure 27. Texas sand - Peak strength envelope plotted in p'-q stress space (from triaxial tests conducted on reconstituted samples at 55% relative density).

In order to characterize the shear strength of the sand, consolidated drained triaxial tests were performed on reconstituted samples. The samples were reconstituted in such a manner as to match the estimated in-situ relative density of 55% and water content of 5%. The samples were prepared by light tamping in small layers. Tests were conducted on samples taken at depths of 0.6 and 3.0 meters. CTC tests were performed at three different confining pressures: 34.5 kPa, 138 kPa, and 345 kPa. The results of the triaxial tests are given in Appendix A, with the p'-q diagrams constructed from these plots presented in Figure 27 above.

Ottawa Sand

Aiban (1991) used the centrifuge to perform a number of bearing capacity experiments on an F-75 series Ottawa sand. In his experiments, a 38 mm wide footing was accelerated to a gravity level of 30-g such that a prototype footing width of 1.14 meters was modeled. Normalized depths of embedment (D/B) of the footing ranging from 0 to 1 were studied. The model footings were constructed of aluminum and consisted of three segments. The outer two segments had lengths of 38 mm each, while the inner segment had a length of 51 mm for a total length to width ratio (L/B) of 3.67. In his thesis, Aiban maintains that the length to width ratio was sufficient to maintain plane strain conditions under the central footing such that a strip footing was modeled. Sand glued to the bottom of the footing simulated a rough footing. Rotation of the footing was allowed during the course of the experiment. Aiban (1991) presents a detailed explanation of the test procedure.

The material was prepared by allowing the sand to freely drop into an aluminum container from a hopper. The drop height was approximately 762 mm. The resulting relative density was approximately 88%, which, according to the thesis, is the maximum density that can be achieved without vibration. The relative density corresponds to a density of approximately 1.80 g/cm^3, estimated from the maximum and minimum void ratios for Ottawa sand.

Table 6. Bearing Capacity Results - Ottawa Sand.

Prototype Footing Width (m)	Normalized Embedment Depth (D/B)	q_{ult} (kPa)
1.14	0	2247
1.14	0	2127
1.14	1/6	2950
1.14	1/3	3280
1.14	½	4040
1.14	2/3	4380
1.14	5/6	4980
1.14	1	5450

The results of the centrifuge tests performed on the Ottawa sand are given in Appendix B. In the graph, the normalized settlement (S/B) has been plotted against the average vertical stress under the central segment for the 1.14 m wide footing, where each curve represents a different embedment depth. Table 6 summarizes the bearing capacity data for the Ottawa sand.

Aiban (1991) also performed a series of conventional triaxial compression (CTC) tests in order to characterize the shear strength of the Ottawa sand. The tests were conducted at confining pressures of 69, 138, and 207 kPa, the results of which are presented in Appendix A. In addition, Schipporeit (1988) also conducted a series of CTC tests on Ottawa sand. His results are also presented in Appendix A. A best-fit failure envelope was fit to the data given by Aiban (1991) and Schipporeit (1988), and is presented in Figure 28.

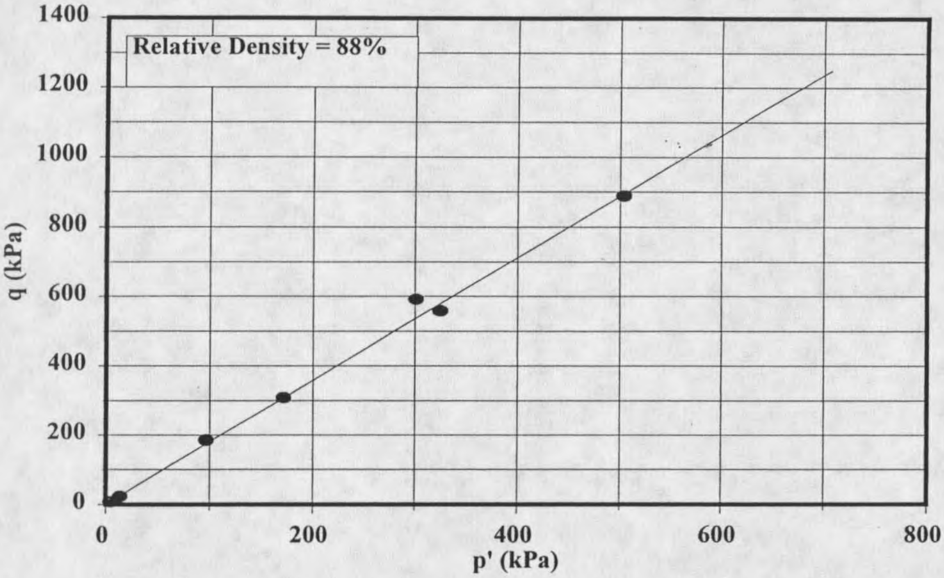

Figure 28. Ottawa sand - Peak strength envelope plotted in p'-q stress space (from triaxial tests conducted at 88% relative density).

Monterey Sand

Kutter et al., (1988) presented the centrifuge test results of concentric loading of circular surface footings on dry, dense Monterey 0/30 sand. In their study, model footing diameters of 50.8 and 38.1 mm were accelerated to levels of 18.75, 25, and 50 g such that prototype footing diameters of 0.96 and 1.90 meters were modeled. Once the appropriate acceleration level was reached, an electric motor was used to push the model footing into the sand at a rate of 2 mm/min. In addition, a small scale test was conducted in the 1-g environment using the 50.8 mm diameter model footing. The model footings consisted of aluminum discs with sand glued to the bottom simulating a rough footing. Rotation of the footing was allowed in only one test (BS-5), while in the remaining tests the foundation was prevented from rotating. Kutter et al., (1988) provides further details on the procedure used.

Kutter provides very little in terms of a description of the procedure used in preparing the material. According to the paper, the relative density of the Monterey sand was between 93 and 95 percent for all the tests conducted, corresponding to void ratios of 0.55 to 0.56. Using data provided in the paper, the dry density was computed to be approximately 1.66 g/cm^3.

The results of the bearing capacity experiments performed on the Monterey sand are given in Appendix B. Using the results, Table 7 was assembled summarizing the bearing capacity results.

Table 7. Bearing Capacity Results - Monterey Sand.

Test	Prototype Footing Diameter (m)	Normalized Embedment Depth (D/B)	q_{ult} (kPa)
BS-1	0.9525	0	2060
BS-2	1.905	0	3045
BS-3	0.9525	0	2012
BS-4	0.0508	0	227
BS-5	1.905	0	3087

Kutter et al., (1988) also provided a plot of the mean normal stress at failure (p') versus the peak friction angle gathered from conventional triaxial compression (CTC) tests performed on dense Monterey sand. This plot, as well as stress-strain curves from the CTC tests performed by Abghari (1987) with the Monterey sand are provided in Appendix A. The density of the sand used in the CTC tests matched that used in the centrifuge tests. Using the data, a peak strength envelope was constructed for the Monterey sand and is presented in Figure 29.

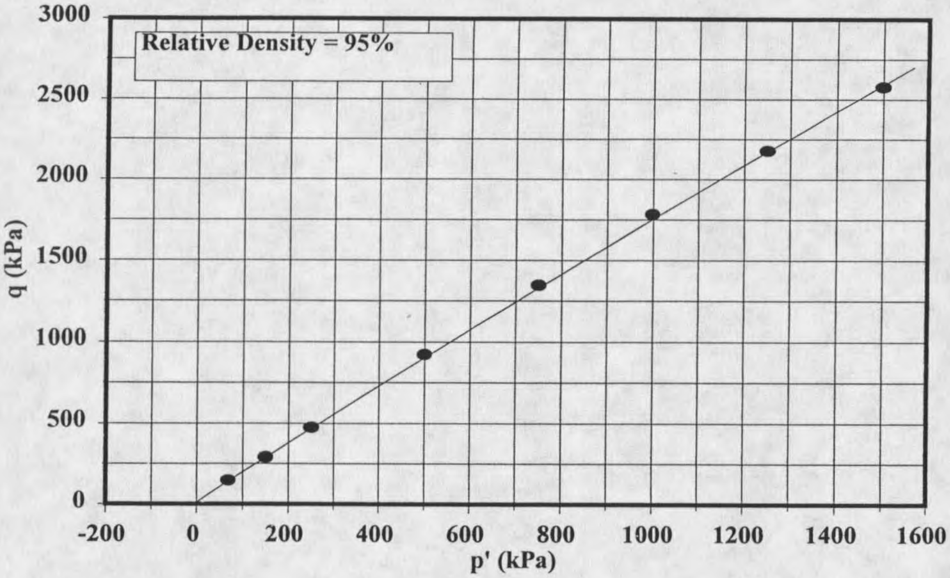

Figure 29. Monterey sand - Peak strength envelope plotted in p'-q stress space (from triaxial tests conducted at 93% - 95% relative density).

Scoria Sand

Kusakabe et al., (1992) presented the results of full-scale loading tests of square and rectangular footings placed on naturally occuring deposits of extremely dense Scoria sand. The deposits were located near Mt. Fuji and Mt. Hakone in Japan. Scoria sand is a granular material normally associated with volcanic activities. All loading tests were performed in the base chamber of a caisson with dimensions of 16 m in diameter by 23 m in height. Loading tests were conducted at levels of 11m, 14m, and 18m below ground surface. These three elevations are referred to as A, B, and C ground in the paper.

The footings were constructed of rigid steel frames placed on the ground level within the caisson. A rough condition at the footing base was simulated by pouring a layer of mortar on the ground surface before placement of the footing. Loading of the footings was accomplished using hydraulic jacks.

During the loading tests, the ground water level was held at the ground surface. Drained conditions during each test were maintained by applying the load in steps, with the applied force held constant for 15 minutes to allow excess pore water pressure to dissipate before application of the next load step. The 15 minute time limit was established by performing permeability tests as well as by using finite element analysis. Kusakabe et al., (1992) provide further details on the procedure used.

In order to characterize the physical properties of the Scoria sand, a series of tests ranging from particle size analysis to relative density were performed at each ground level. The pertinent data from each ground level is summarized in Table 8. It should be noted that the in-situ relative densities are very high (between 120 and 140 percent). This can likely be attributed to the high amount of preloading that may have occurred in the material's geologic past, as well as from cyclic loadings due to earthquakes in this region.

Table 8. Physical Properties of Scoria Sand.
(from Kusakabe et al., 1992).

Ground Level	Relative Density I_D (%)	Saturated Unit Weight γ_{sat} (kN/m^3)
A	137.5	17.75
B	120.8	18.63
C	127.1	17.75

Results from each of the load tests are provided in Appendix B. In the plots, the load

(q) has been plotted against the normalized settlement (S/B). As with the Texas sand, strain hardening is apparent for all the tests. The strain hardening taking place in the load tests is rather unusual. In most cases, very dense samples will exhibit strain softening characteristics when loaded. It is noted that this apparent discrepancy cannot be explained at this time. Since there was not a peak load associated with each test, a value of ultimate bearing capacity had to be chosen. It was felt that choosing the ultimate bearing capacity at normalized settlements (S/B) greater than 0.3 would not be realistic. The ultimate bearing capacity was therefore defined as the load associated with a normalized settlement (S/B) of 0.10. In most cases, the load intensity-settlement curves beyond this point become essentially linear and quite flat, making the choice of 0.10 reasonable. The results of the loading tests are summarized in Table 9.

Table 9. Bearing Capacity Results - Scoria Sand.

Ground Level	Test Case	Length x Width (m)	Normalized Embedment Depth (D/B)	q_{ult} (kPa)
A	VII_s	0.3 x 0.3	0	6667
A	IV	0.7 x 0.7	0	9300
B	VI_s	0.3 x 0.3	0	8400
B	II	0.4 x 1.20	0	7143
B	I	0.4 x 0.4	0	8100
B	III	0.4 x 2.00	0	6500
C	$VIII_s$	0.3 x 0.3	0	7500
C	V	1.30 x 1.30	0	9400

In conjunction with the load tests, Kusakabe et al., (1992) also performed a series of consolidated, isotropically drained (CID), conventional triaxial compression (CTC) tests.

The tests were conducted on undisturbed samples of Scoria sand taken from the test site. Undisturbed samples were taken by first freezing the samples, then cutting out blocks 0.4 m in length by 0.3 m in width by 0.3 m in height using a diamond cutter. The blocks were then brought into the lab for testing.

Triaxial tests were performed at confinements ranging from 19.6 to 4700 kPa. The results of these tests are presented in Appendix A. It should be noted that this material demonstrates a high degree of non-linearity, with secant friction angles ranging from 36 to as high as 64 degrees at the lowest confinements, the most of all the study sands. In addition, there is an appreciable amount of apparent cohesion which can likely be attributed to the high degree of particle interlocking that was observed by the researchers. Using the triaxial results, the following p'-q diagram was constructed (Figure 30).

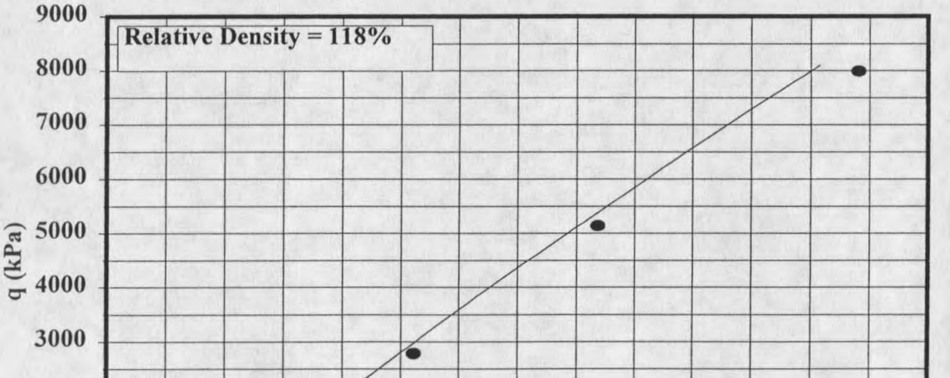

Figure 30. Scoria sand - Peak strength envelope plotted in p'-q stress space (from triaxial tests conducted at approximately 118% relative density).

Conclusion

Using the previously described material properties and bearing capacity results from all eight study sands, a design methodology will be presented in the next chapter for estimating the bearing capacity of sands. The approach will account separately for both components of the scale effect, namely, material non-linearity and progressive failure. The approach will utilize dilatancy and strength relationships proposed by Bolton (1986) and discussed in Chapter 2. This solution will eliminate the need for extensive triaxial testing in order to define peak strength friction angles, making subsurface exploration and ensuing material property evaluation much simpler.

CHAPTER 4

DESIGN PROCEDURE FOR BEARING CAPACITY ANALYSIS

Introduction

The purpose of Chapter 4 is to present a design procedure for estimating the bearing capacity of a sand. As discussed in Chapter 2, conventional solutions to bearing capacity problems predict that the ultimate bearing capacity, q_{ult} will increase linearly with footing width (B) as well as with embedment depth. Perkins and Madson (1996), Kusakabe et al., (1992), and numerous other researchers have demonstrated this not to be true. This observation has been attributed to a so-called scale effect and was first recognized by Golder (1941). A significant portion of Chapter 2 was devoted to the discussion of this phenomenon. The new design methodology to be presented in this chapter will account for this scale effect.

Two components make up the scale effect. The first component is due to material non-linearity, simply described as the dependence of the peak friction angle (ϕ'_{peak}) on the level of mean normal effective stress (p') beneath the footing. Higher levels of p', corresponding to larger footing widths and/or increased embedment depths result in decreased values of the friction angle. Overall, it may be said that the relative density (I_D), mean normal effective stress (p'), and strain restraint condition will affect the magnitude of this scale effect. The second component of the scale effect is due to progressive failure within the material failure zone beneath the footing. As discussed in Chapter 2, progressive failure occurs whenever a non-uniform distribution of shear strain develops within the zone of failure. In general, the degree to which a non-uniform distribution of shear strain develops increases as p' increases, corresponding to larger footing widths and/or increased embedment depths. Larger shear strains occur at points closest to the bottom of the footing, and slowly migrate outwards along the slip surface. As a result, the average angle of shearing resistance changes along the failure surface, with zones closest to the footing tending toward the critical state or constant volume friction angle (ϕ'_{cv}). The combination of material non-linearity and progressive failure results in a reduced bearing capacity when compared to predictions using a given peak friction angle taken at a moderate level of p'.

To account for the first component of the scale effect, material non-linearity, a means of describing ϕ'_{peak} appropriate to the footing configuration to be analyzed is required. This in turn suggests that the level of mean normal effective stress (p') beneath the footing must be known to determine ϕ'_{peak}, as well as a means of correcting ϕ'_{peak} for the particular strain restraint condition of the footing. In cases where axisymmetric or triaxial strain conditions exist beneath the footing, ϕ'_{peak} is simply equal to ϕ'_{tc}, where the subscript *tc* denotes triaxial compression. In contrast, plane strain conditions beneath the footing suggest the use of a plane strain friction angle ϕ'_{ps}, where the subscript *ps* denotes conditions of plane strain. In cases of intermediate strain conditions, the peak friction angle (ϕ'_{peak}) may be taken as being linearly dependent upon the relative distance between triaxial and plane strain conditions. Using ϕ'_{peak} corrected for the strain restraint condition, the ultimate bearing capacity ($q_{ult\text{-}peak}$)

may be determined through the use of the conventional bearing capacity equation. We therefore require a method of finding the peak friction angle. ϕ'_{peak} may be determined by either using the actual failure envelope of the material, or by using relationships developed by Bolton (1986) relating the strength and dilatancy characteristics of sands. These relationships were discussed in Chapter 2.

The essential ingredients in determining ϕ'_{peak} using the actual strength envelope is as follows. The peak strength envelope of the material must first be established. This may be done using results from conventional triaxial compression (CTC) or plane strain tests performed on the material. It is noted that these tests should be performed at the same relative density (I_D) as the soil found at the site. Once the failure envelope has been established, ϕ'_{peak} may be determined knowing the level of mean normal effective stress (p') beneath the footing. Knowing the constant volume friction angle (ϕ'_{cv}), the peak friction angle (ϕ'_{peak}) can then be corrected for the particular strain restraint condition existing beneath the footing. This is accomplished using certain relationships proposed by Bolton (1986). Finally, this corrected peak friction angle is used within the bearing capacity equation to compute the ultimate bearing capacity ($q_{ult\text{-}peak}$).

The above described method to account for material non-linearity can be greatly simplified using expressions developed by Bolton (1986) which relate the strength and dilatancy of sand. These equations were described in Chapter 2. The expressions will allow for the determination of ϕ'_{peak} for use in the bearing capacity equation, given knowledge of the relative density (I_D) and constant volume friction angle (ϕ'_{cv}) of the sand, as well as the strain restraint condition beneath the footing. This will therefore eliminate the need to define the strength envelope of the material in the laboratory.

An abbreviated discussion of these expressions is as follows. The relative dilatancy index (I_R) is computed as

$$I_R = I_D(Q - \ln p') - R \tag{41}$$

where I_R simply describes the dilatancy characteristics of the material, and is dependent upon the relative density (I_D) and mean normal effective stress confinement (p'). Q and R are empirical constants describing the strength properties of the material, and in most cases may be taken as 10 and 1, respectively. The relative dilatancy index (I_R) may be related to the peak friction angle (ϕ'_{peak}) by the following

$$\phi'_{peak} - \phi'_{cv} = A I_R \tag{42}$$

where ϕ'_{cv} is the constant volume friction angle. The constant A ranges from 3 to 5 depending upon the strain restraint condition, with 3 corresponding to conditions of triaxial strain and 5 corresponding to conditions of plane strain. It may therefore be said that I_R also describes the amount by which the peak friction angle exceeds the constant volume friction angle for a particular strain and mean normal stress condition beneath the footing. Using equations 41 and 42, it is therefore possible to determine the peak friction angle (ϕ'_{peak}) for use in the bearing capacity equation.

As suggested by the previously described methods to calculate ultimate bearing capacity, in order to determine a peak strength friction angle (ϕ'_{peak}), a value of p' appropriate to the footing to be analyzed must be computed. In general, it is expected that the average mean normal effective stress (p') beneath a footing will increase with footing width and depth of embedment. As discussed in Chapter 2, Meyerhof (1948) and De Beer (1967) both proposed equations relating the average normal effective stress on the plane of failure (σ'_{avg}) to the ultimate bearing capacity of the footing (q_{ult}). It was further stated in Chapter 2 that these equations would not be used due to the lack of information concerning their development. Also discussed in Chapter 2 was an equation developed by Perkins (1995a) relating the ratio of p'/q_{ult} to the friction angle (ϕ'). This expression was developed strictly from classical plasticity theory using a slip line solution. It was further stated within the section that this equation would not be used due to numerical instabilities at high friction angles. In a later section, a new equation will be presented which uses non-linear limit plasticity to relate p'/q_{ult} to an appropriate peak friction angle (ϕ'_{peak}).

Unfortunately, simply accounting for the scale effect due to material non-linearity using a ϕ'_{peak} appropriate to the footing still results in significant over predictions of ultimate bearing capacity (Perkins 1995a). This may be attributed to the second component of the scale effect, progressive failure. Progressive failure may be accounted for by the development of an index of progressive failure (I_{PF}). The I_{PF} describes the relative distance of the predicted bearing capacity between that associated with peak ($q_{ult-peak}$), and constant volume (q_{ult-cv}), determined using the strength parameters ϕ'_{peak} and ϕ'_{cv}, respectively. For example, if the I_{PF} is equal to 1 then $q_{pred} = q_{ult-peak}$, while $q_{pred} = q_{ult-cv}$ if the I_{PF} is equal to 0. It is postulated that the I_{PF} is simply a function of the relative dilatancy index (I_R), where I_R

describes the state of the soil subject to a certain level of mean normal effective stress (p'). This is maintained since both I_R and progressive failure are functions of footing width and embedment depth, both of which influence p'. Development of a curve describing progressive failure will be performed in a later section.

The balance of Chapter 4 will be devoted to the presentation of a new design methodology to estimate the bearing capacity of shallow foundations on sand, using Bolton's equations to account for material non-linearity, and an index of progressive failure (I_{PF}) to account for progressive failure. The results of this analysis will be compared to predictions made using the actual failure envelope of each material. The purpose of this is to examine any errors introduced through simplifications associated with the use of Bolton's equations.

The Bearing Capacity Equation

A simplified form of the general bearing capacity equation presented in Chapter 2 was used for all predictions of bearing capacity in this chapter. This equation is given as

$$q_{ult} = qN_q + \frac{1}{2}\gamma BN_\gamma \tag{43}$$

where N_q and $N\gamma$ are bearing capacity factors determined using equations presented in Chapter 2 (eqs. 24 and 25). B and q are the footing width and surcharge pressure at the bottom of the footing. γ is the unit weight of the soil. It should be noted that the cohesion term (c') is assumed to be equal to zero and a secant friction angle is used. It is further noted that this solution does not incorporate depth factors (F_{qd} and $F\gamma_d$), which account for extra shearing resistance developed above the base of the footing. Additionally, shape factors are not used in equation 43 since the design approach already utilizes a correction for the strain restraint condition beneath the footing. It should also be noted that the surcharge (q) is computed at the original base of the footing (i.e., no correction is made for additional surcharge as the footing penetrates into the soil).

Modifications are made to account for the reduced bearing capacity in cases where the groundwater is within the influence zone of the footing, as was the case in the full scale tests performed with the Scoria sand. The groundwater level was maintained at the ground surface for these experiments. In cases where the groundwater table is within the zone of influence of the footing, modifications in γ are required to account for the fact that the buoyant unit weight is the only unit weight developing normal effective stresses along the slip plane. The modifications result in a reduced bearing capacity. The methods used to account for the influence of the water table followed those recommended by Das (1990).

Prediction of $q_{ult\text{-}peak}$ using Bolton's Equations

As discussed previously, the design approach proposed using Bolton's equations to evaluate bearing capacity will account for material non-linearity knowing the constant volume friction angle (ϕ'_{cv}) and relative density (I_D) of the sand, and the strain restraint condition existing beneath the footing. The solution process incorporates the following steps.

First, the relative dilatancy index (I_R) is determined using

$$I_R = I_D(Q - \ln p') - R \tag{44}$$

where I_D is the relative density of the material, and p' is the mean normal effective stress level appropriate to the footing. Q and R are empirical constants describing the strength of the material. In lieu of actual strength data, Bolton suggested setting Q and R equal to 10 and 1, respectively. It is noted that p' must be assumed initially and therefore, determination of the ultimate bearing capacity ($q_{ult-peak}$) will be an iterative process.

Once I_R is determined, the peak friction angle (ϕ'_{peak}) for use in the bearing capacity analysis is determined knowing the strain restraint condition beneath the footing. The strain restraint condition is simply based upon the length-to-width ratio of the footing (L/B). For example, an L/B = 1 corresponds to a square or circular footing, while an L/B = 7 corresponds to a strip footing. The equations for determining ϕ'_{peak} are given as

For plane strain conditions (L/B > or = 7)

$$\phi'_{peak} - \phi'_{cv} = 5\, I_R \tag{45}$$

For triaxial conditions (L/B = 1)

$$\phi'_{peak} - \phi'_{cv} = 3\, I_R \tag{46}$$

where ϕ'_{cv} is the constant volume friction angle and may be determined experimentally by a simple triaxial test performed on a loose, reconstituted sample. Alternatively, ϕ'_{cv} may be assumed knowing the predominate sand mineral type since ϕ'_{cv} is primarily a function of mineralogy. For strain conditions between plane and triaxial strain, (i.e., $1 < L/B < 7$), a linear ratio between 3 and 5 is used in the equation to describe the intermediate strain condition present.

Next, the peak bearing capacity ($q_{ult-peak}$) is computed from equation 43 using ϕ'_{peak} determined previously. The bearing capacity factors (N_q and $N\gamma$) used in the bearing capacity equation are determined using equations 24 and 25 from Chapter 2. If appropriate, modifications of the soil's unit weight (γ) should be made here to account for the influence of the water table.

As noted previously, a particular level of mean normal effective stress (p') is initially assumed beneath the footing in order to compute $q_{ult-peak}$. In order to find p' appropriate to the footing being analyzed, an expression is required that relates the ratio of the average mean normal effective stress developed and resulting bearing capacity of the footing (p'/q_{ult}), to the friction angle (ϕ'). A non-linear limit plasticity solution was used to develop such an expression for p'/q_{ult}. The non-linear limit plasticity solution was used to find the normal stress (σ') at various points along an assumed mechanism of collapse. The average normal stress (σ'_{avg}) along the slip line was then found by summing individual contributions (i.e., normal stress multiplied by the contributory length), and dividing by the total length of the slip surface. Next, the average mean normal effective stress (p') beneath the footing was determined by assuming the intermediate stress (σ'_2) was equal to the average of the principal stresses, σ'_1 and σ'_3. Ratios of p'/q_{ult} were then generated for various linear friction angles, with the following best fit curve being obtained

$$\frac{p'}{q_{ult}} = 3.1e^{-0.073\phi'} \tag{47}$$

where ϕ' is in degrees. Perkins (1995b) discusses the use of non-linear limit plasticity theory and its application to bearing capacity predictions.

The next step in the analysis is to compute the ratio of $p'/q_{ult\text{-}peak}$ using the assumed p' and calculated $q_{ult\text{-}peak}$. This value is then compared to that given by equation 47 above using the value of ϕ'_{peak}. A new value of p' is then assumed and the process repeated until the two values of p'/q_{ult} converge. As will be shown later, the predictions of ultimate bearing capacity ($q_{ult\text{-}peak}$) based on peak strength friction angles are, for the most part, in excess of the experimental values. Therefore, the next step in the analysis will be to account for progressive failure.

Once $q_{ult\text{-}peak}$ has been determined, the ultimate bearing capacity associated with the critical state ($q_{ult\text{-}cv}$), is computed using a linear friction angle equal to the constant volume friction angle (ϕ'_{cv}). Knowing $q_{ult\text{-}peak}$ and $q_{ult\text{-}cv}$, the predicted bearing capacity can then be determined using the index of progressive failure (I_{PF}) developed in the next section.

Since an iterative process is involved in determining p' and corresponding ϕ'_{peak} appropriate to the problem, a computer program was written in Fortran to facilitate the solution. This program is presented in Appendix D. In general, one simply inputs the following parameters: Q, R, relative density (I_D), ϕ'_{cv}, and the density of the sand (ρ), as well as the size and embedment depth of the footing. The program then outputs the peak friction angle (ϕ'_{peak}) appropriate to the problem, the bearing capacity associated with ϕ'_{peak} and ϕ'_{cv} ($q_{ult\text{-}peak}$ and $q_{ult\text{-}cv}$), and the relative dilatancy index (I_R).

At this point, little has been said concerning the choice of Q and R for each of the study sands. As mentioned previously, Bolton (1986) suggested setting Q and R equal to 10 and 1, respectively, in the absence of sufficient strength data. For the purposes of this research, it was decided to evaluate the error associated with choosing $Q = 10$ and $R = 1$. In order to study this, strength envelopes developed from Bolton's equations were compared to strength envelopes developed strictly from the triaxial or plane strain data provided for each study sand. The failure envelopes were compared by plotting $\phi'_{peak} - \phi'_{cv}$ against mean normal effective stress (p'). Failure envelopes using Bolton's equations were developed by first computing I_R (eq. 44) over a range of p' for relative densities matching those used in the actual strength tests. The value of $\phi'_{peak} - \phi'_{cv}$ was then computed over the full range of I_R for the assumed ϕ'_{cv}, using either equation 45 or 46 depending upon the type of strength test Bolton's predictions were being compared to (i.e., triaxial or plane strain). The value $\phi'_{peak} - \phi'_{cv}$ was then plotted against the corresponding p'. In order to develop the failure envelope using the actual strength data, the secant friction angle was computed over a range of p' using the p'-q failure envelopes created using strength data provided for each study sand. The p'-q curves were presented in Chapter 3. For the assumed ϕ'_{cv}, the value of $\phi'_{peak} - \phi'_{cv}$ was next determined over the full range of p'. This plot was then compared to the plot generated using Bolton's equations for each of the study sands. These graphs are presented in Appendix C.

Table 10. Assumed material properties of study sands.

Sand	Q	R	ϕ'_{cv}	Mineral Type	I_D (%)	ρ (g/cm^3)
MLS-1	10	1	41	feldspar	100	2.2
JSC-1	10	1	41	feldspar	100	1.775
Scoria sand	11	0	38	NA	Level A - 137.5 Level B - 120.8 Level C - 127.1	Level A - 1.81 Level B - 1.90 Level C - 1.81
Toyoura sand	10	1	34	NA	87	1.62
Inagi sand	10	1	36	NA	81.8	1.68
Monterey sand	10	1	36	NA	95	1.66
Texas sand	10	1	32	NA	55	1.57
Ottawa sand	10	1	33	silica quartz	88	1.80

Table 10 presents the material properties assumed for each of the study sands. For the majority of the study sands, Q = 10 and R = 1 were found to provide a sufficiently accurate fit to the material's strength envelope. However, it was found that choosing Q = 10, R = 1 did not provide a realistic fit to the strength envelope of the Scoria sand. This is believed to be due largely to the extreme material non-linearity possessed by the Scoria sand. It was further determined that choosing Q = 11 and R = 0 provided the best fit to the strength envelope in the lower mean normal effective stress region, (p' < 1500 kPa). Since the footings were not large enough to induce mean normal stresses larger than 1500 kPa, it was felt that simply matching the failure envelope in the lower stress regions would be sufficiently accurate. One further comment should be made in regards to the Ottawa sand. Bolton's predictions fail to sufficiently predict the strength behavior of the Ottawa sand. This may be seen by comparing the actual strength envelope to that predicted by Bolton.

Bolton's equations under predict the actual strength of this material. Again, this is attributed to the particle strength possessed by Ottawa sand and was noted by Bolton (1986).

Constant volume friction angles (ϕ'_{cv}) were chosen in different manners depending upon the data available. If strength data was provided at low relative densities such as with the Texas sand, the secant friction angle associated with peak strength was assumed to be close to ϕ'_{cv}. For strength tests performed at high relative densities where strain softening was apparent, ϕ'_{cv} was often taken to be at or close to that associated with the secant friction angle at the critical state (i.e., where the curve flattens beyond peak strength). Finally, in some cases, the mineralogy was examined in order to define a realistic ϕ'_{cv}, since ϕ'_{cv} is made up primarily of mineral to mineral sliding (ϕ_u), and to a much lesser extent, rolling friction (ϕ_r). This may be seen in the case of the Ottawa sand which is composed primarily of silica quartz sand. The constant volume friction angle (ϕ'_{cv}) of this material was determined to be 33 degrees. Mineral to mineral sliding (ϕ_u) for silica quartz sand is approximately 26 degrees. The rolling friction component (ϕ_r) is therefore only 7 degrees. In the same way, ϕ'_{cv} for the MLS-1 and JSC-1 is composed of a mineral to mineral sliding component (ϕ_u) for feldspar of 37 degrees, as well as a rolling friction component (ϕ_r) of 4 degrees.

Incorporation of the Index of Progressive Failure (I_{PF})

In the previous section, material non-linearity was accounted for using Bolton's expressions relating strength and dilatancy. In general, this method will provide predictions of ultimate bearing capacity ($q_{ult\text{-}peak}$) in excess of experimental results. This is postulated to be due to progressive failure. Within this section, an index of progressive failure (I_{PF}) will be developed that will take this effect into account.

As discussed several times, progressive failure under a footing becomes more significant with both increasing footing size and depth of embedment. The mobilized friction angle associated with larger footings and/or deeper embedment depths is normally closer to the critical state or constant volume friction angle. On the other hand, the average friction angle developed along the slip mechanism for smaller footings and/or shallower embedment depths is typically closer to the peak friction angle. Evidence of this is provided by radiograph studies performed by Yamaguchi et al., (1976) and presented in Chapter 2.

In light of this discussion, an index of progressive failure (I_{PF}) has been developed and is shown in Figure 31, where the I_{PF} has been plotted against I_R Using the results of bearing capacity tests performed on the test sands, the index of progressive failure (I_{PF}) was computed as

$$I_{PF} = \frac{q_{ult-\exp} - q_{ult-cv}}{q_{ult-peak} - q_{ult-cv}} \tag{48}$$

where *exp*, *peak*, and *cv* describe bearing capacity from the experiments and computed from peak and constant volume friction angles, respectively. It is noted that the curve was developed using ϕ'_{peak} determined using Bolton's equations. The index of progressive failure describes the relative position of the experimental results between peak and constant volume capacity, with an I_{PF} equal to 0 when $q_{ult-exp} = q_{ult-cv}$ and an I_{PF} equal to 1 when $q_{ult-exp} = q_{ult-peak}$. In Figure 31, the I_{PF} has been plotted against the corresponding relative dilatancy index (I_R)

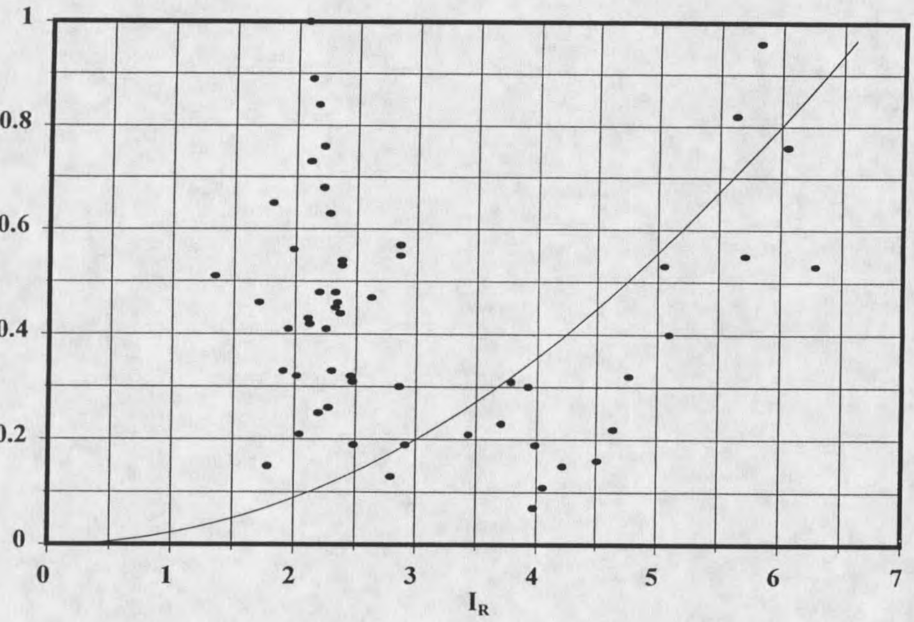

Figure 31. I_{PF} vs I_R - Developed using Bolton's equations.

associated with ϕ'_{peak} for all 61 bearing capacity experiments. The reason the I_{PF} is plotted against I_R rather than the footing width (B) is that I_R describes the state of the soil subject to a certain level of p', effectively combining the effects of footing width and embedment. A curve was then fit to the data.

The rationale behind relating the relative dilatancy index (I_R) to the index of progressive failure (I_{PF}) can be seen by consideration of the following. Consider the situation of a footing placed on a sand. As the footing width and/or embedment depth increase, one would expect a corresponding increase in the level of mean normal effective stress (p') beneath the footing. Based upon Bolton's development of the relative dilatancy index (I_R), one would further expect a lower dilatancy index (I_R) and a lower associated index of progressive failure (I_{PF}). This would indicate that the ultimate bearing capacity is closer to that associated with the constant volume capacity. Alternatively, as the footing width decreases and/or embedment depth decreases, the ultimate bearing capacity will approach that associated with peak capacity. Again, this argument is based on the premise that progressive failure is less for smaller footing widths and/or decreased depths of embedment. This situation would correspond to higher levels of I_R and I_{PF}, respectively. Therefore, since I_R has been shown to be largely dependent upon p', which is a function of footing width and depth of embedment, the argument has been made that I_R can be used to find the I_{PF} for use in the bearing capacity analysis.

Looking at Figure 31, it appears that significant scatter exists at the lower I_R values. However, it will be shown below that this scatter is somewhat minor when one considers that lower values of I_R correspond to situations where peak and constant volume friction angles are approaching one another. As such, the bearing capacities predicted using ϕ'_{peak} and ϕ'_{cv} will be relatively close to one another and the impact of the I_{PF} will be minimal. In addition, since the curve has been drawn through the lower points, one can expect the predictions to be largely conservative in this region.

The scale effect due to progressive failure is accounted for in the following manner. Using the relative dilatancy index (I_R) associated with $q_{ult\text{-}peak}$, a value for the index of progressive failure (I_{PF}) is found using Figure 31. The predicted bearing capacity (q_{pred}) is then given as

$$q_{pred} = (q_{ult\text{-}peak} - q_{ult\text{-}cv}) I_{PF} + q_{ult\text{-}cv} \qquad (49)$$

where $q_{ult\text{-}peak}$ and $q_{ult\text{-}cv}$ correspond to bearing capacities associated with the peak and constant volume friction angles, and the I_{PF} ranges from 0 to 1.

In order to examine the accuracy of predictions of bearing capacity made using Bolton's equations, the normalized bearing capacity ($N\gamma_q$) was plotted against the relative dilatancy index (I_R) for all eight study sands (Figures 32 - 38). $N\gamma_q$ is defined as

$$N_{\gamma q} = 2\frac{q_{ult}}{B\gamma} \tag{50}$$

where q_{ult} corresponds to either the peak, constant volume, experimental, or predicted bearing capacity, B is the footing width, and γ is the unit weight of the sand. In each graph, $N\gamma_q$ corresponding to peak, constant volume, experimental, and predicted capacities has been plotted against the corresponding I_R. As observed, in most instances the predicted bearing capacities are quite close to the experimental results. It is noted that using peak strength parameters, (i.e., only accounting for material non-linearity) results in dramatic over predictions of bearing capacity. One comment should be made concerning the Texas sand in light of the discussion earlier about the scatter observed in the I_{PF}-I_R plot at the lower ranges of I_R. The relative dilatancy index of the Texas sand is quite low (1 to 2), due to the low relative density of this material. For this reason, the constant volume and peak strength friction angles are similar. As such, the scatter in the I_{PF} has little influence on the predicted results for the Texas sand. One further comment should be made concerning the Ottawa sand. In all cases, the predicted results under predict the actual bearing capacity substantially, with the amount of error increasing with increasing depth of embedment. This is understandable in light of the comment made by Bolton (1986) that the dilatancy behavior of Ottawa sand is under predicted, meaning that the actual peak friction angles are substantially higher. This has been attributed to the particle strength possessed by uniform sands such as Ottawa sands (i.e., the resistance to particle crushing leading to little change in the rate of dilatancy with increasing p').

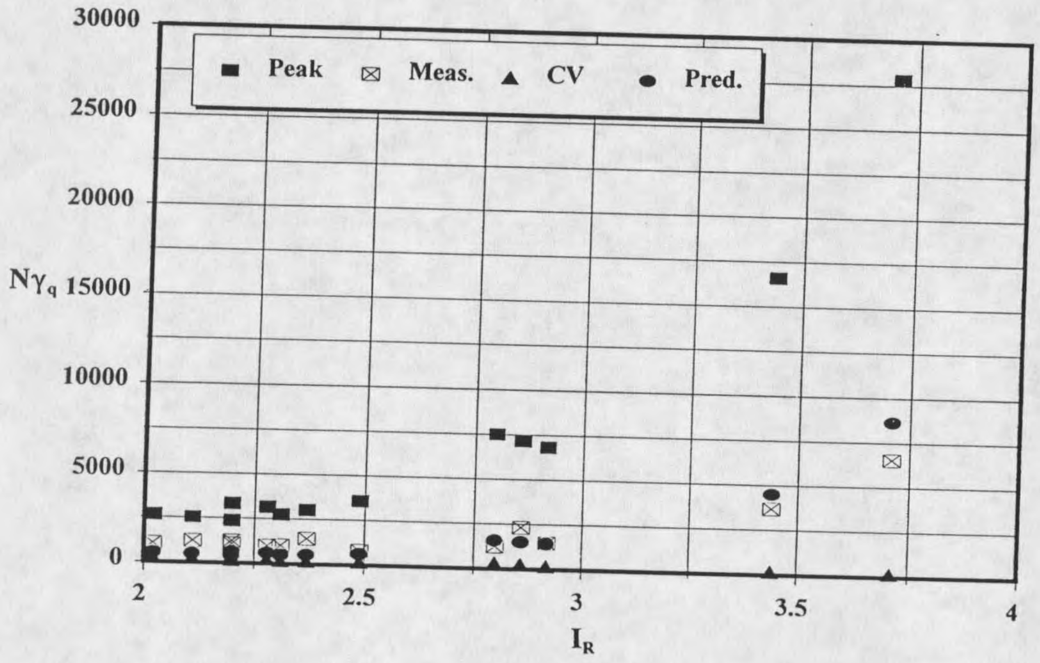

Figure 32. $N\gamma_q$ vs I_R - MLS-1 & JSC-1 - Predicted using Bolton's equations.

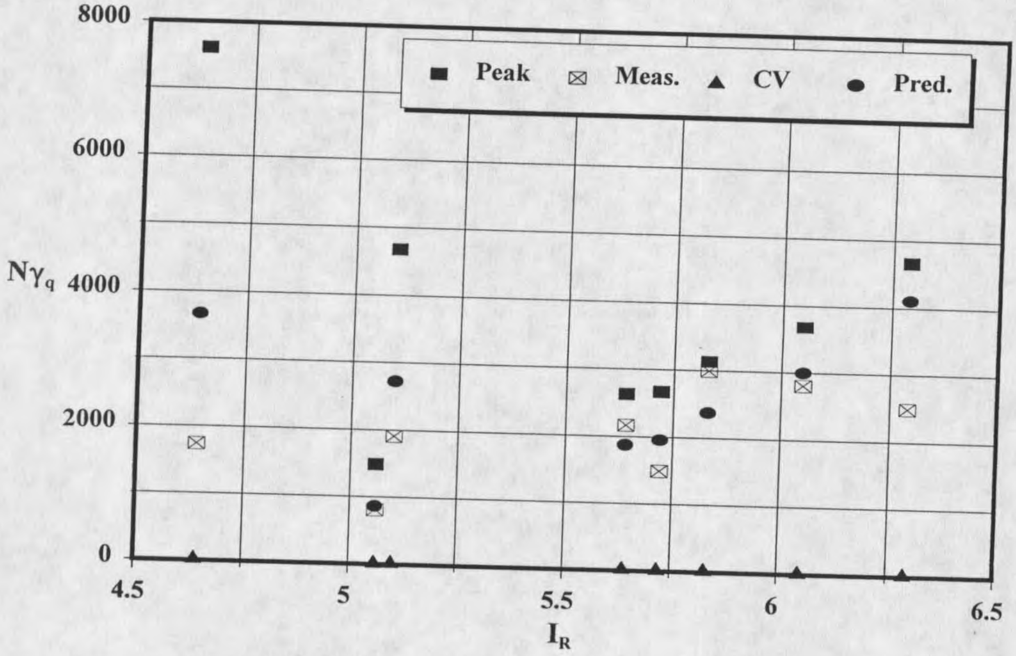

Figure 33. $N\gamma_q$ vs I_R - Scoria Sand - Predicted using Bolton's equations.

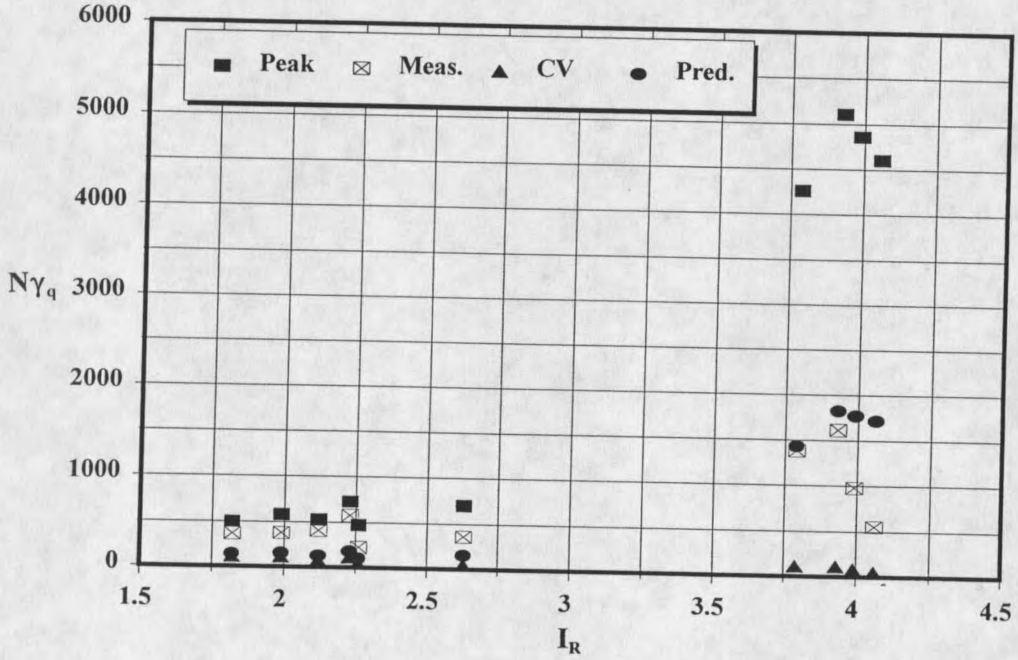

Figure 34. $N\gamma_q$ vs I_R - Toyoura Sand - Predicted using Bolton's equations.

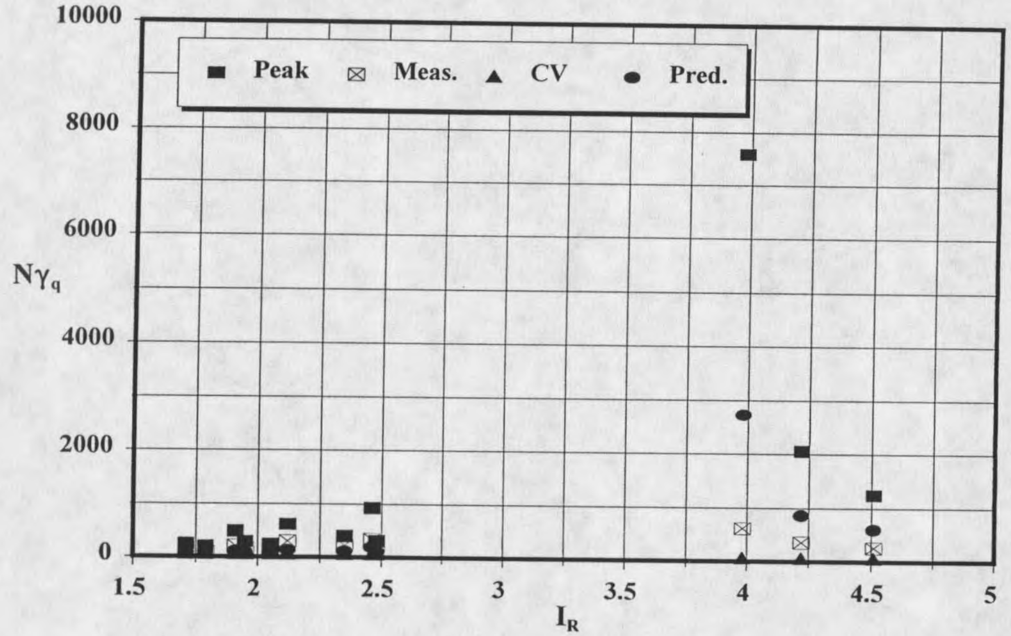

Figure 35. $N\gamma_q$ vs I_R - Inagi Sand - Predicted using Bolton's equations.

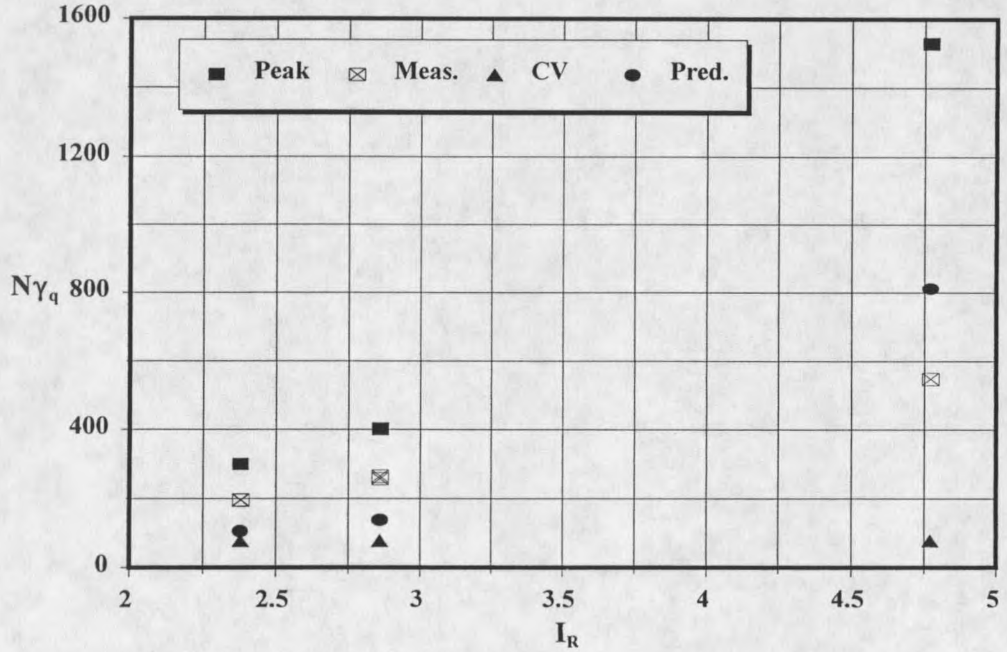

Figure 36. $N\gamma_q$ vs I_R - Monterey Sand - Predicted using Bolton's equations.

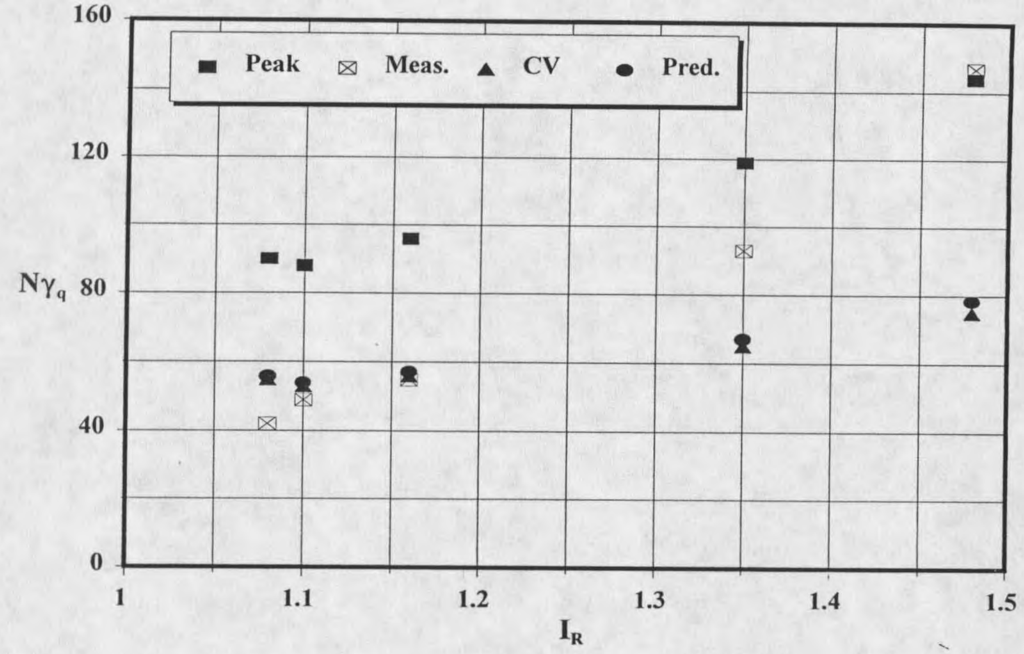

Figure 37. $N\gamma_q$ vs I_R - Texas Sand - Predicted using Bolton's equations.

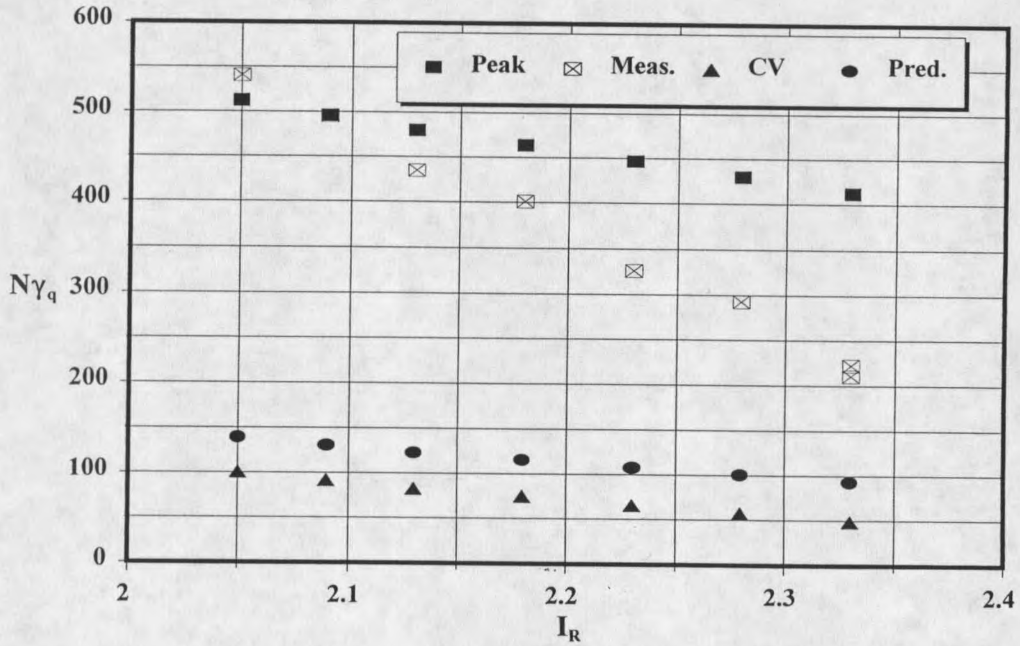

Figure 38. $N\gamma_q$ vs I_R - Ottawa Sand - Predicted using Bolton's equations.

Influence of using Bolton's Equations

In order to fully evaluate the potential of using Bolton's empirical equations to predict bearing capacity, predictions were also made using the actual strength envelope of each sand. As the solution using Bolton's equations did, this approach will account for strain conditions, scale effects due to material non-linearity, and progressive failure.

The first step in the analysis is to describe the peak strength envelope in p'-q stress space. This is done using a function of the yield surface for the constitutive model developed by Sture et al., (1989). The function for the yield surface is given as

$$F = q\left(1 + \frac{q}{q_a}\right)^m - \eta(p - p_c) = 0 \tag{51}$$

where m describes the curvature of the function, η is the steepness of the curve (similar to the friction angle), p_c describes the isotropic tensile strength which is related to the soil's cohesion, q_a is a reference stress normally taken as 1, and q and p are the invariant shear and mean normal stresses. Values of m, η, and p_c describing the shape of the failure surface for each study sand are given in Table 11.

It should be noted that the parameters describing the failure envelope of each sand are from triaxial tests performed at the same relative density as those used in the corresponding bearing capacity experiments with one exception. Triaxial tests with the Toyoura sand were performed at a relative density of 75%, while the bearing capacity experiments were conducted at a relative density of 87%. This significantly impacted the predicted results with the Toyoura sand as will be shown later.

Table 11. Values of m, η, and p_c for each sand.

Sand	m	η	p_c
MLS-1	0.0332	2.61	-0.1
JSC-1	0.05	3.01	-0.1
Scoria sand	0.14	5.6	-18
Toyoura sand	0.025	1.9	0
Inagi sand	0.032	2.02	-0.2
Monterey sand	0.037	2.3	-5
Texas sand	0.055	2	0
Ottawa sand	0.01	1.90	0

As with the previous solution using Bolton's equations, a value of p' appropriate to the footing to be analyzed must be initially assumed. This is therefore an iterative process utilizing the p'/q_{ult} expression developed from non-linear limit plasticity (eq. 47). The approach to calculate ultimate bearing capacity using the actual p'-q strength envelope is given by the following steps.

A value of p' is assumed from which the invariant deviatoric stress (q) is found using the function describing the peak strength envelope, (eq. 51). The secant friction angle (ϕ'_{tc}) is then computed using

$$\sin\phi'_{tc} = \frac{q}{2p' + \frac{q}{3}} \tag{52}$$

where the subscript *tc* denotes that the friction angle pertains to conditions of triaxial compression. Next, ϕ'_{tc} is corrected for the strain restraint condition beneath the footing using the expression

$$\phi'_{peak} = \phi'_{tc} \frac{AI_R + \phi'_{cv}}{3I_R + \phi'_{cv}} \tag{53}$$

where ϕ'_{cv} is the assumed constant volume friction angle of the material. I_R is the relative dilatancy index proposed by Bolton (1986). The value of A ranges from 3 to 5, with A equal to 3 under conditions of triaxial compression, (L/B = 1). Under plane strain conditions, (L/B > or = 7), A is equal to 5. A is interpolated for intermediate strain conditions, ($1 < L/B < 7$).

The relative dilatancy index (I_R) used in equation 53 is given by the following

$$I_R = \frac{\phi'_{tc} - \phi'_{cv}}{3} \tag{54}$$

where I_R describes the amount by which the peak friction angle exceeds the constant volume friction angle for a particular strain restraint condition. As discussed earlier, I_R is a function of the relative density of the sand, as well as the mean normal effective stress condition (p'). It should be noted that as ϕ'_{tc} decreases with increasing p', I_R will also decrease.

Using the previously determined ϕ'_{peak}, the ultimate bearing capacity ($q_{ult\text{-}peak}$) is next calculated using the previously given bearing capacity equation (eq. 43). Finally, the ratio of $p'/q_{ult\text{-}peak}$ is determined using the assumed value of p', and compared to the ratio given by equation 47 using ϕ'_{peak}. A new value of p' is then assumed and the iteration repeated until the two computed p'/q_{ult} ratios converge. Finally, $q_{ult\text{-}cv}$ is determined using a linear friction angle equal to the constant volume friction angle. Therefore, using this approach with the actual strength envelope, the scale effect due to material non-linearity has been taken into account.

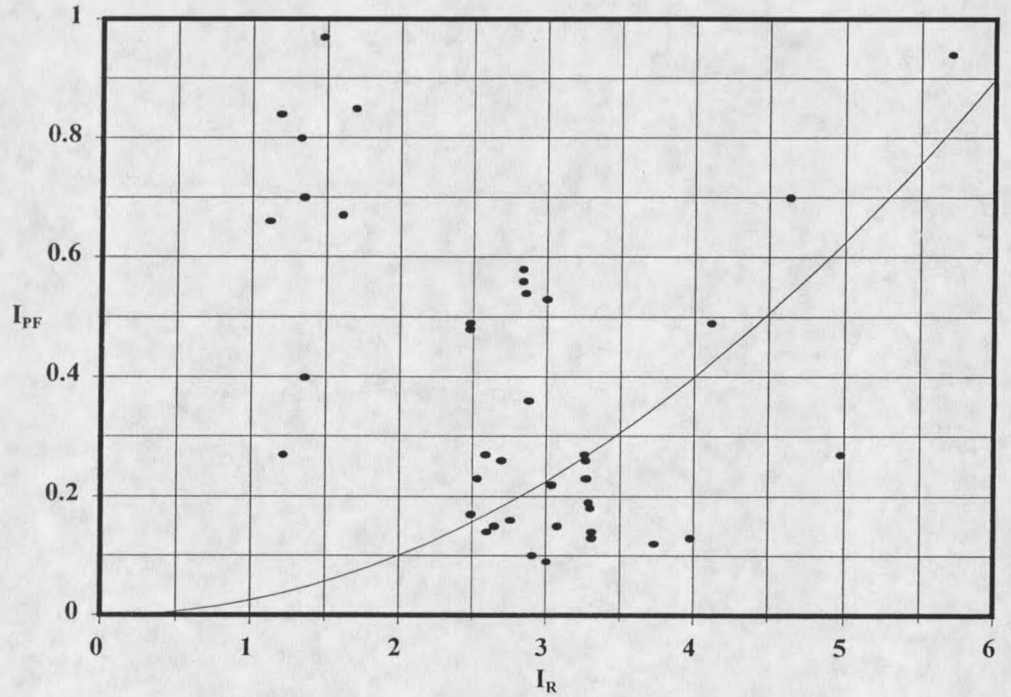

Figure 39. I_{PF} vs I_R - Developed using the actual p'-q strength envelope.

Next, the scale effect due to progressive failure is taken into account. This step is implemented in much the same manner as the previous solution. Figure 39 presents the index of progressive failure (I_{PF}) constructed using $q_{ult\text{-}peak}$ and $q_{ult\text{-}cv}$, determined using the actual material strength envelope of each sand. It is noted that the results using the Toyoura sand were not used in developing Figure 39 since the relative density used in the triaxial tests was substantially lower than that used in the bearing capacity experiments. As such, using these results to develop Figure 39 would have skewed the graph. Using the data, a curve was fit to the points. The curve describing progressive failure was drawn in such a manner as to be largely conservative.

Accounting for progressive failure is done in the same manner as described earlier. Using Figure 39, an index of progressive failure (I_{PF}) is established based upon the relative dilatancy index (I_R). Then, knowing the I_{PF}, a predicted bearing capacity (q_{pred}) is computed using equation 49.

Due to the iterative nature of the solution, a computer program was written in Fortran to determine $q_{ult\text{-}peak}$ and $q_{ult\text{-}cv}$. This program may be found in Appendix D. In general, required input includes the footing width (B), normalized depth of embedment (D/B), the density (ρ) and constant volume friction angle (ϕ'_{cv}) of the sand, as well as m, η, and p_c describing the failure envelope. The program then computes $q_{ult\text{-}peak}$, $q_{ult\text{-}cv}$, and I_R, from which the index of progressive failure (I_{PF}) can be found using Figure 39. Finally, as described earlier, the predicted bearing capacity (q_{pred}) is determined using the index of progressive failure (I_{PF}).

In order to evaluate the predicted bearing capacity results, the normalized bearing capacity ($N\gamma_q$) was plotted against I_R for all eight study sands. These graphs are presented in Figures 40-46. In each graph, $N\gamma_q$ corresponding to peak, constant volume, experimental, and predicted capacities has been plotted against the corresponding I_R. Looking at the figures, it may be seen that the predictions using the strength envelopes are, on average, quite close to the experimental results, with the notable exception of the Toyoura sand. In the case of the Toyoura sand, the predicted results are substantially less than the experimental results. This may be attributed to the lower relative density at which the triaxial tests were conducted as compared to the bearing capacity experiments. As a result, the frictional properties were underestimated, resulting in substantial under prediction. It should be further noted that in the case of the Ottawa sand the predictions are substantially better using the strength envelope versus using Bolton's empirical equations. However, in light of the earlier discussion concerning the dilatancy behavior of Ottawa sand, this is to be expected. One last comment should be made concerning the use of peak strength parameters. Similar to the predictions using Bolton's equations, using peak strength parameters, (i.e., only accounting for material non-linearity), results in rather large over predictions of bearing capacity.

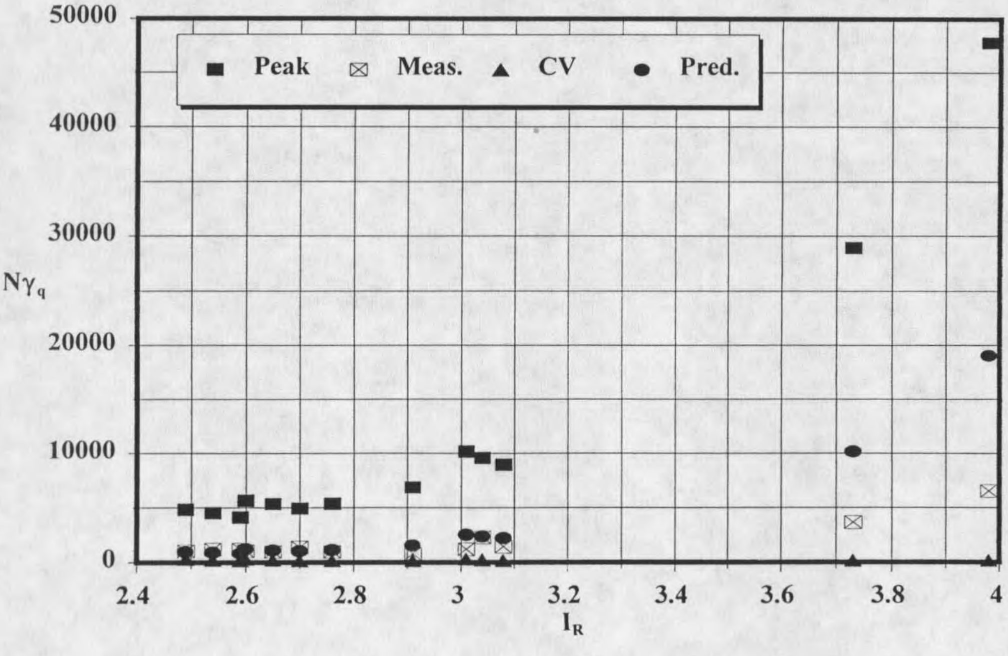

Figure 40. $N\gamma_q$ vs I_R - MLS-1 & JSC-1- Predicted using p'-q strength envelopes.

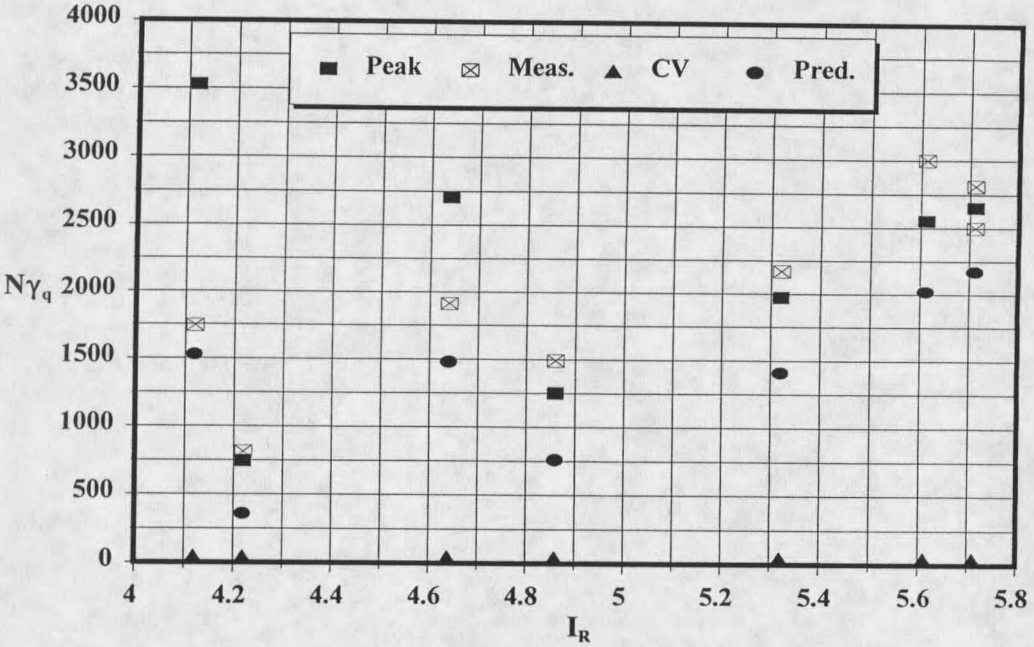

Figure 41. $N\gamma_q$ vs I_R - Scoria Sand - Predicted using p'-q strength envelope.

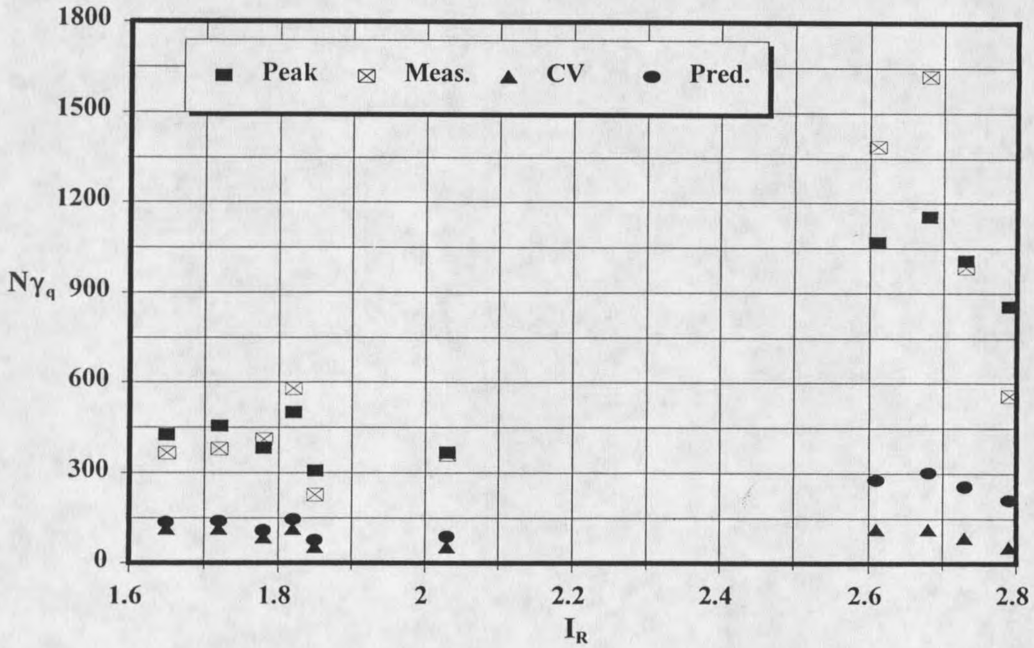

Figure 42. $N\gamma_q$ vs I_R - Toyoura Sand - Predicted using p'-q strength envelope.

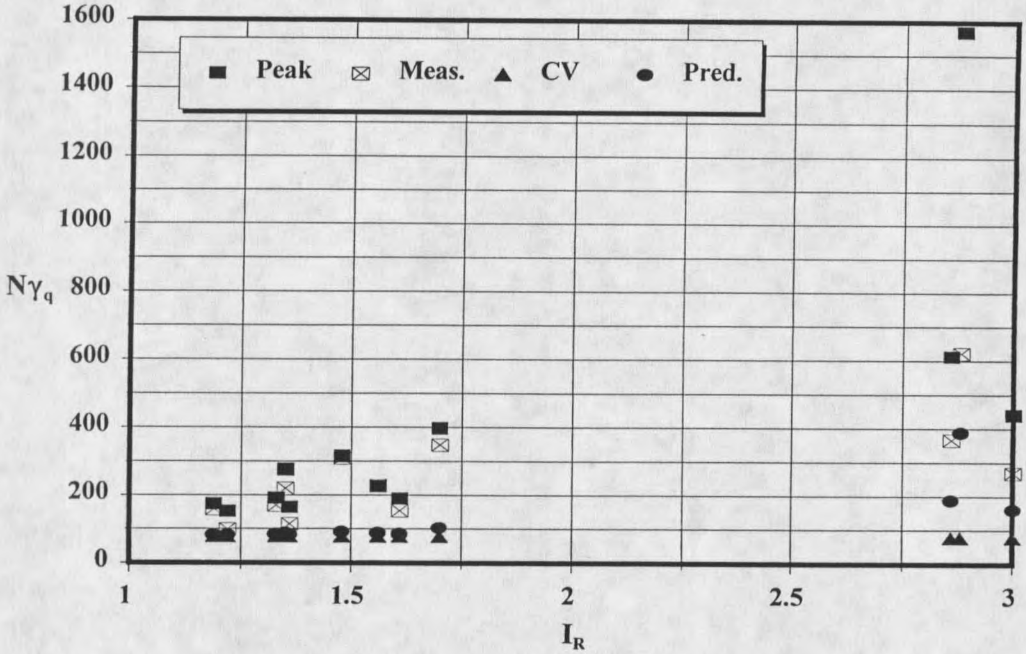

Figure 43. $N\gamma_q$ vs I_R - Inagi Sand - Predicted using p'-q strength envelope.

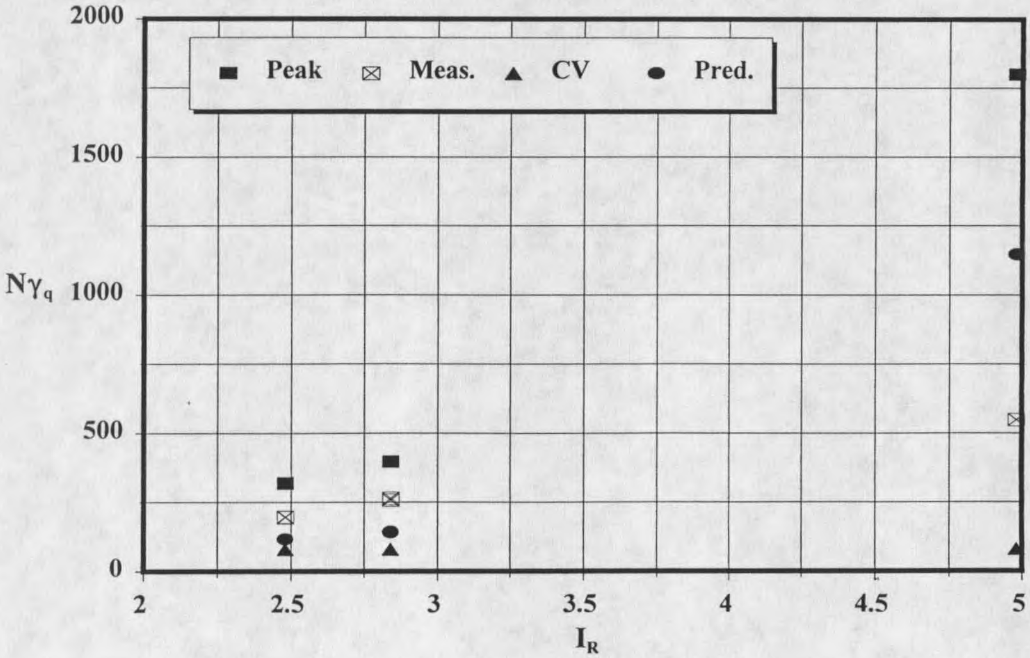

Figure 44. $N\gamma_q$ vs I_R - Monterey Sand - Predicted using p'-q strength envelope.

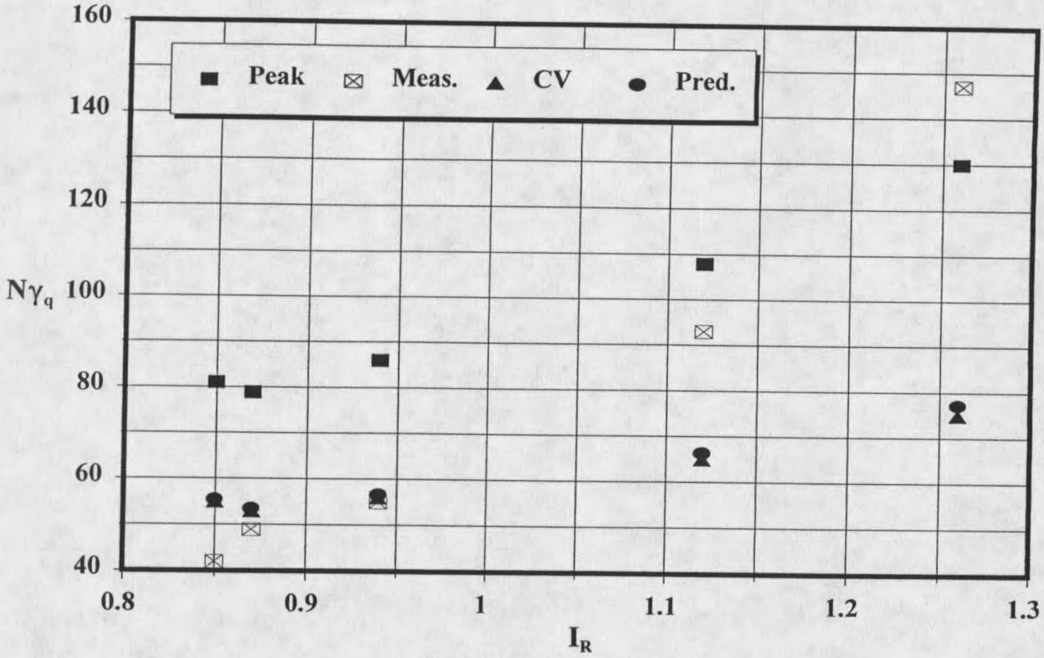

Figure 45. $N\gamma_q$ vs I_R - Texas Sand - Predicted using p'-q strength envelope.

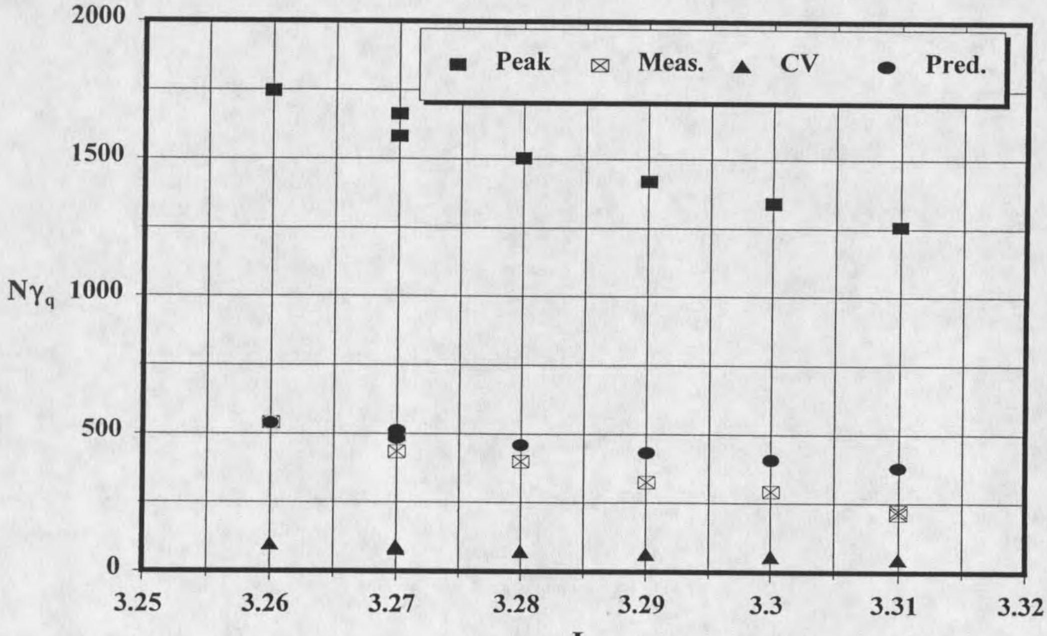

Figure 46. $N\gamma_q$ vs I_R - Ottawa Sand - Predicted using p'-q strength envelope.

Due to the difficulty in comparing Bolton's empirical predictions with predictions using the actual failure envelope, a more quantitative way was required to compare the results. A statistical analysis was therefore performed to quantitatively measure the amount of over/under prediction of bearing capacity for each of the experiments. In Figures 47-60, the amount of over/under prediction has been plotted for each experiment using both Bolton's empirical predictions and predictions made using the actual failure envelope. A value of zero corresponds to situations where the actual and predicted bearing capacities match. The root mean square (RMS) was then computed with each prediction technique for all eight study sands. The root mean square measures the average amount of over/under prediction. Table 12 presents the root mean square determined for each sand using both prediction techniques.

Table 12. Root mean square (RMS) for each study sand.

Sand	RMS Bolton's predictions	RMS p'-q predictions
MLS-1	1.09	0.45
JSC-1	0.59	1.37
Scoria sand	0.50	0.63
Toyoura sand	1.48	2.83
Inagi sand	1.29	1.30
Monterey sand	0.80	0.83
Texas sand	0.46	0.47
Ottawa sand	2.23	0.42

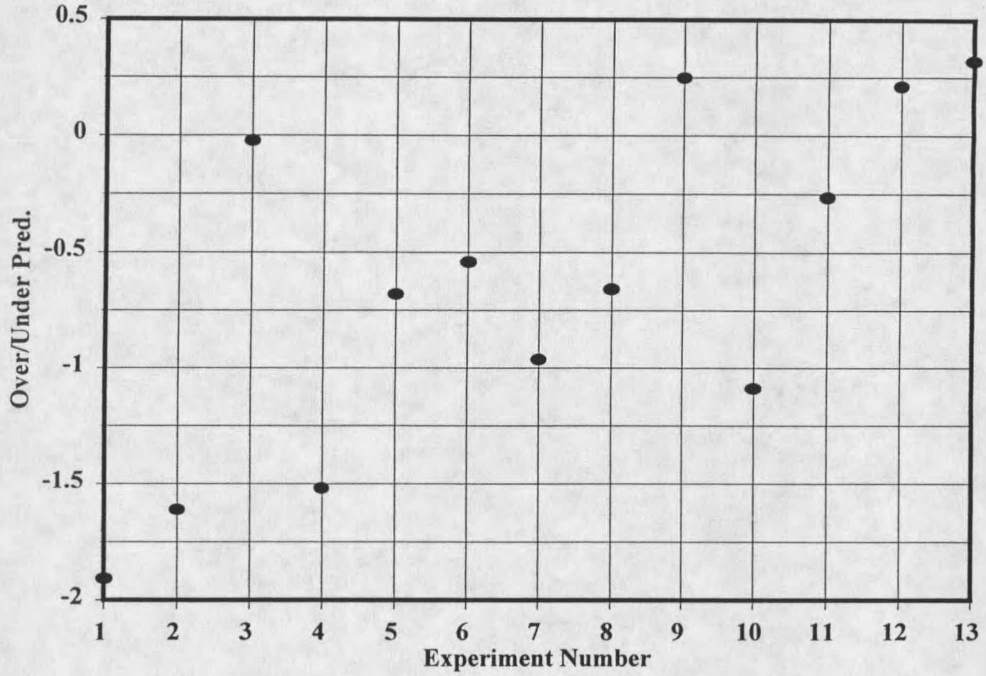

Figure 47. Amount of over/under pred. with MLS-1 & JSC-1 using Bolton's equations.

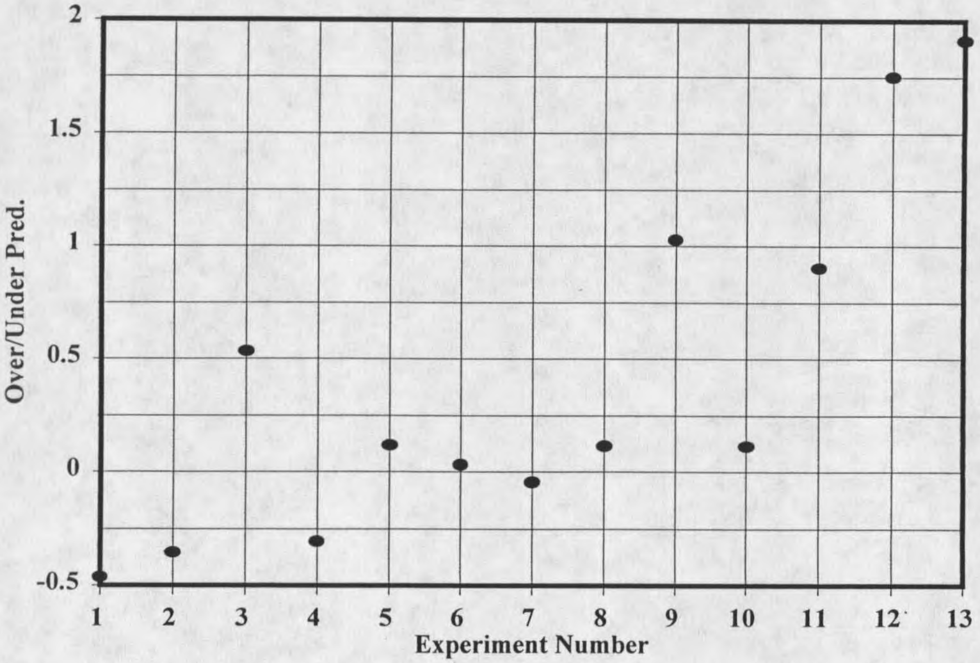

Figure 48. Amount of over/under pred. with MLS-1 & JSC-1 using p'-q strength envelope.

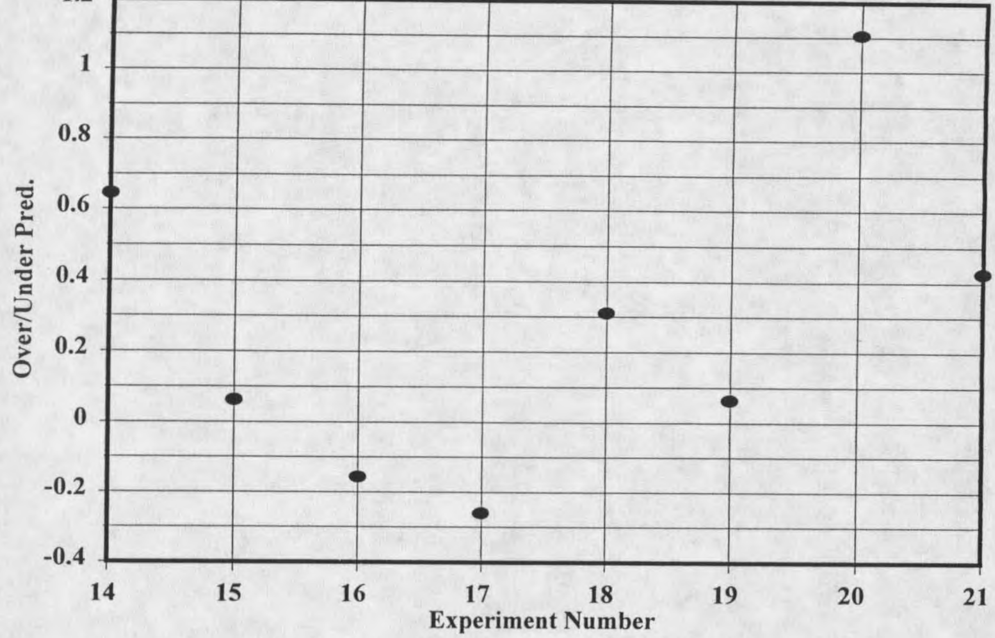

Figure 49. Amount of over/under pred. with Scoria sand using Bolton's equations.

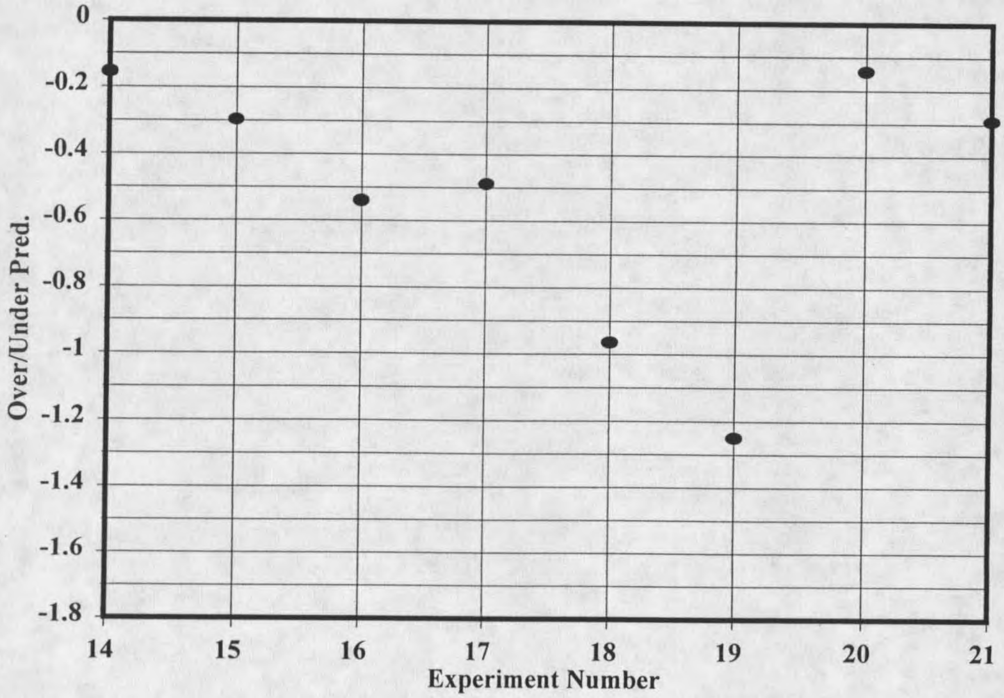

Figure 50. Amount of over/under pred. with Scoria sand using p'-q strength envelope.

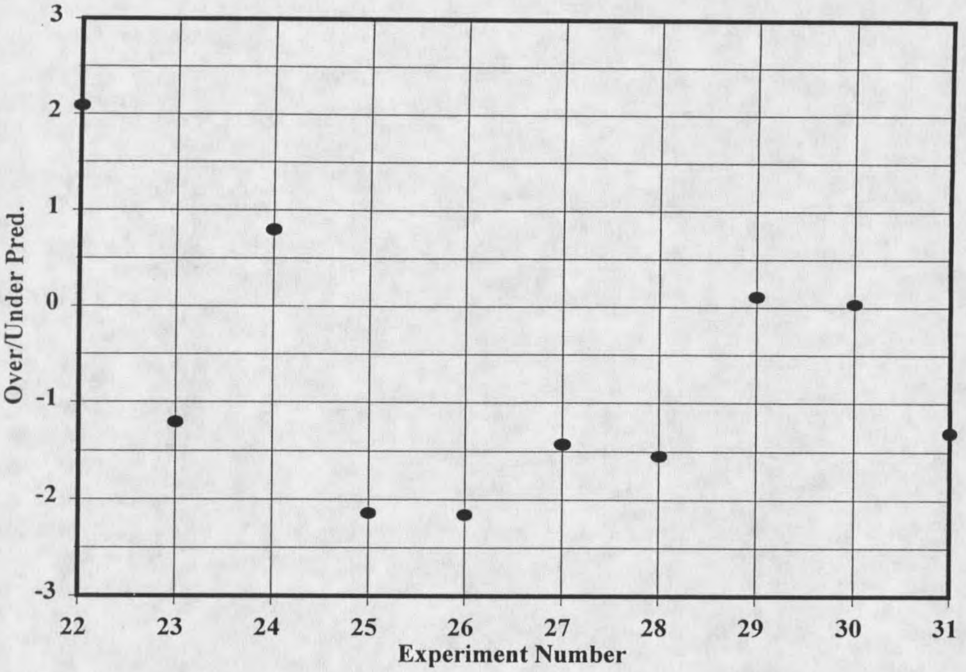

Figure 51. Amount of over/under pred. with Toyoura sand using Bolton's equations.

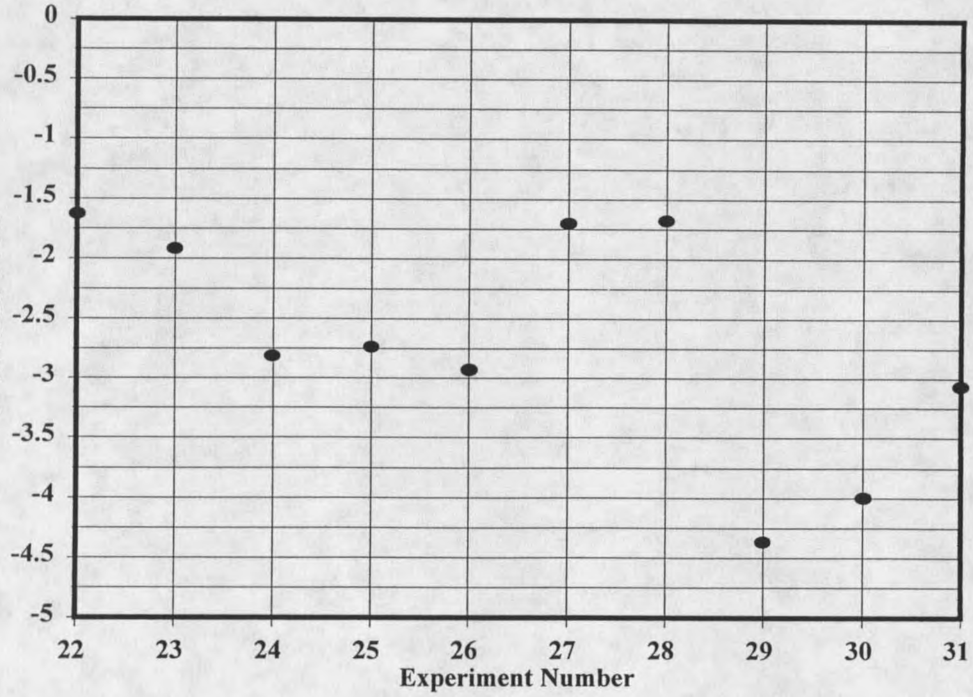

Figure 52. Amount of over/under pred. with Toyoura sand using p'-q strength envelope.

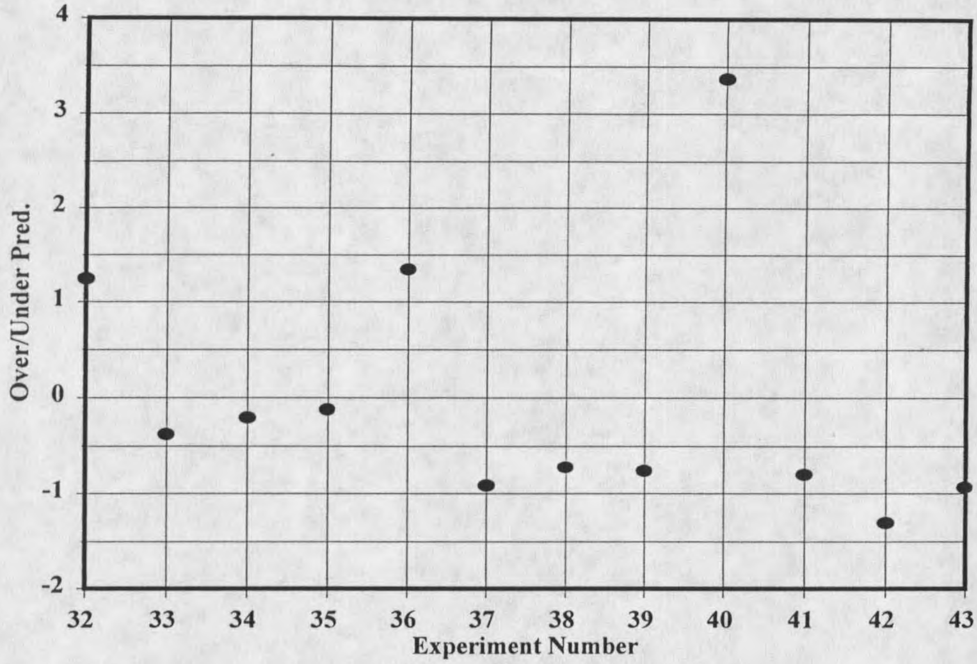

Figure 53. Amount of over/under pred. with Inagi sand using Bolton's equations.

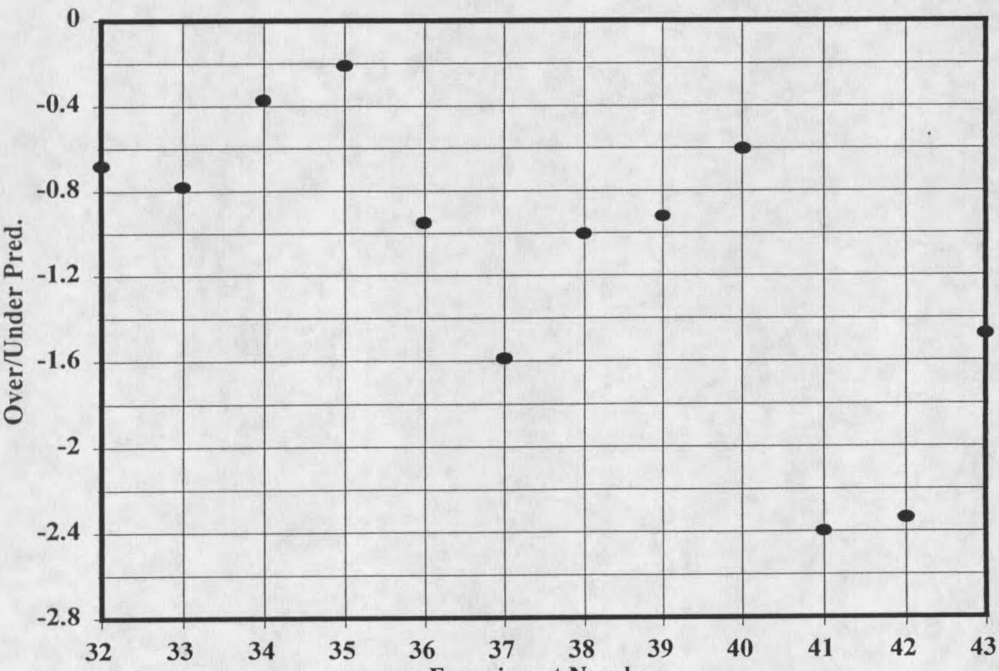

Figure 54. Amount of over/under pred. with Inagi sand using p'-q strength envelope.

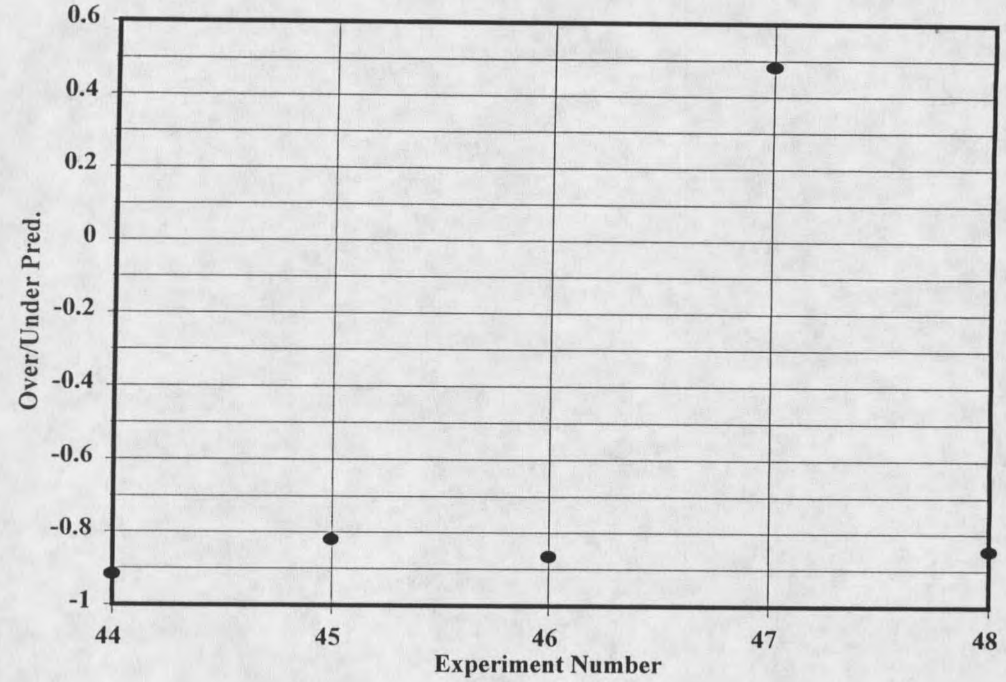

Figure 55. Amount of over/under pred. with Monterey sand using Bolton's equations.

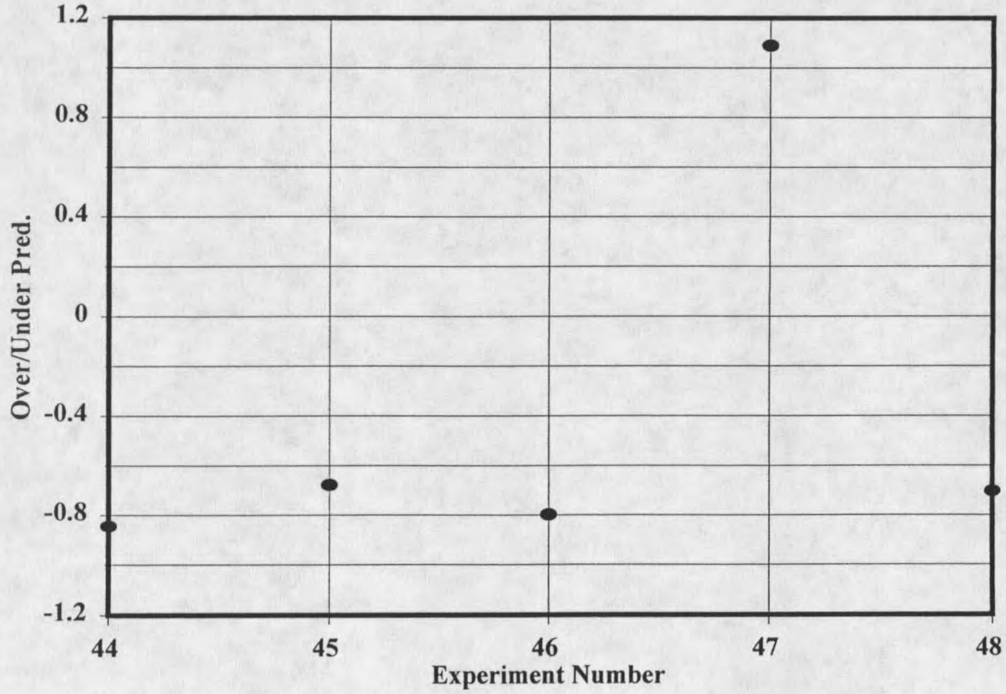

Figure 56. Amount of over/under pred. with Monterey sand using p'-q strength envelope.

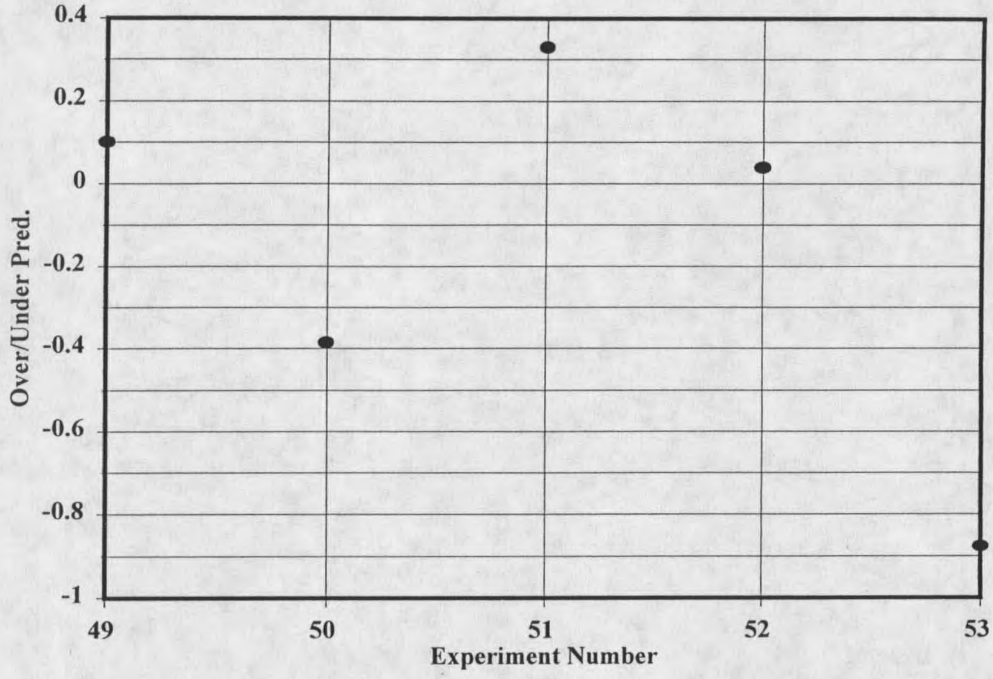

Figure 57. Amount of over/under pred. with Texas sand using Bolton's equations.

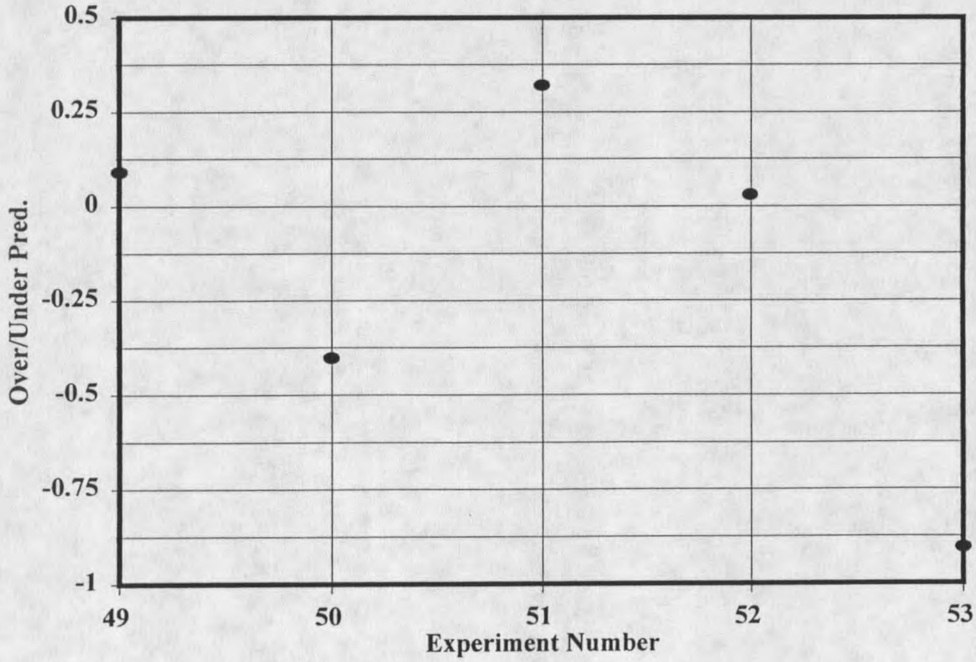

Figure 58. Amount of over/under pred. with Texas sand using p'-q strength envelope.

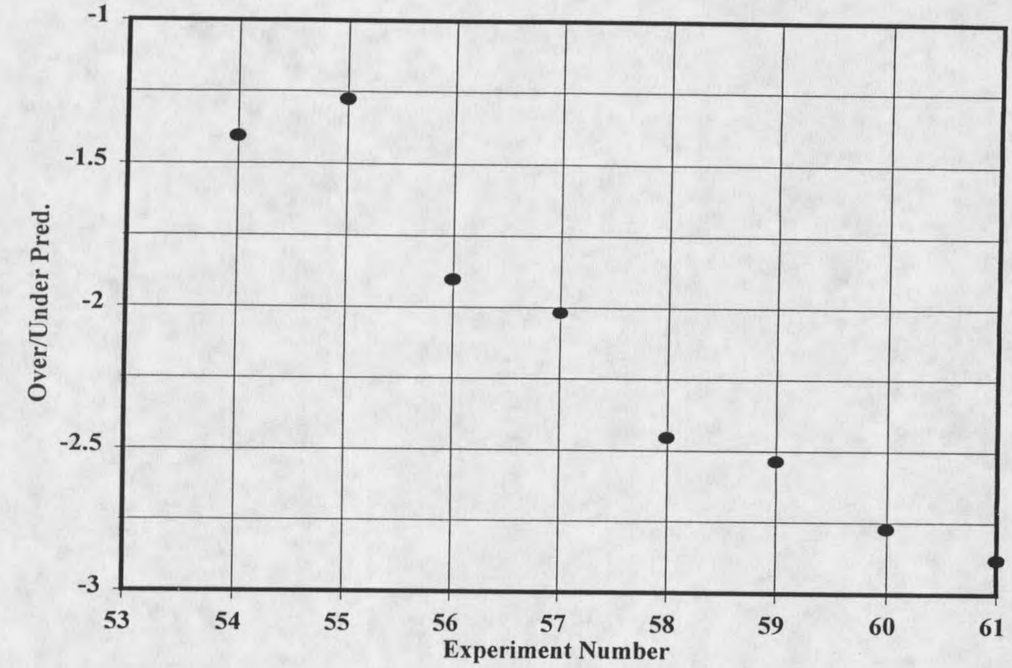

Figure 59. Amount of over/under pred. with Ottawa sand using Bolton's equations.

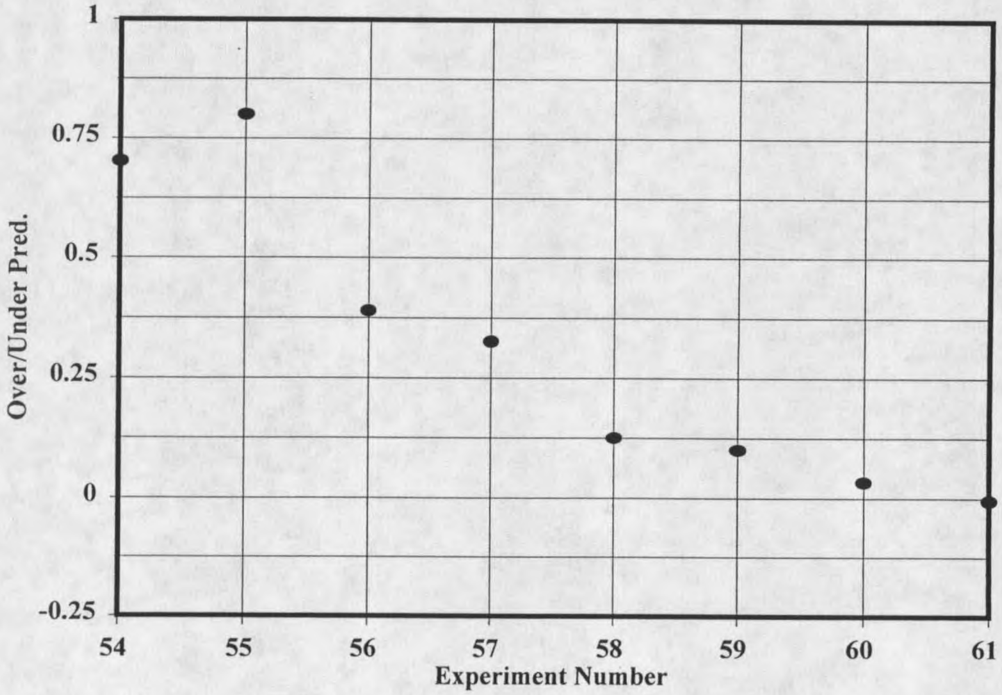

Figure 60. Amount of over/under pred. with Ottawa sand using p'-q strength envelope.

A few comments should be made with reference to Table 12. The results using the actual failure envelope with the Toyoura sand are obviously skewed since the relative densities in the triaxial tests and bearing capacity experiments differed. Therefore, the high RMS is expected. Bolton's predictions do not perform well with the Ottawa sand (RMS = 2.23). As shown previously, Bolton's equations under predict the dilatancy behavior of this material. Taken as a whole, the predictions made using the actual failure envelopes perform better than using Bolton's technique. The overall root mean square using the actual failure envelope excluding the Toyoura sand was 0.87, while the RMS using Bolton's predictions was 1.28. However, if the Ottawa sand results are dropped, the RMS using Bolton's predictions drop to 1.07. It is not unexpected that using the actual failure envelope for each material provides better predictions of bearing capacity. Bolton's equations describing dilatancy and strength are empirically derived and are an approximation of the actual strength envelope. Yet, it has been shown that using Bolton's equations does not introduce an unreasonable amount of error into the solution. It is further expected that Bolton's predictions may be refined by choosing appropriate empirical constants (Q and R), rather then simply assuming 10 and 1 are valid.

One last comment should be made in regards to the shear strength test results. Often, some of the strength data provided was rather sparse and open to interpretation. In other cases, the test results looked a little suspect. As a result, some of the failure envelopes may be slightly inaccurate, leading to inaccuracies in predicting bearing capacity. However, given the data available, it is felt that the failure envelopes are of sufficient accuracy for comparison purposes.

Conclusion

The purpose of this chapter has been to present a new design methodology for predicting the bearing capacity of sands. The solution takes into account both components of the scale effect, namely, material non-linearity and progressive failure. Material non-linearity was accounted for using strength and dilatancy relationships developed by Bolton (1986). Progressive failure was accounted for by the development of an index of progressive failure (I_{PF}), which describes the relative position of the predicted bearing capacity between peak and constant volume capacities, given the relative dilatancy index (I_R).

Predictions using Bolton's equations were compared to those using the actual strength envelope of the material. This was done by plotting the amount of over/under prediction with both solution techniques and comparing the two. It was determined, on the average, that the use of the actual failure envelope resulted in better predictions of bearing capacity. However, given that Bolton's equations use empirical equations relating dilatancy and strength, the error introduced is rather small.

It is noted that the use of Bolton's strength and dilatancy expressions require a knowledge of the relative density (I_D) and the constant volume friction angle (ϕ'_{cv}) of the material. In addition, this approach requires an assumption that the empirical constants (Q = 10 and R = 1) can be used to provide a sufficient match between Bolton's equations and data provided by strength tests. In most cases, this was found to be sufficiently accurate. The notable exception was in the case of the Scoria sand where the extreme material non-linearity required that new values of Q and R be chosen.

The development of this bearing capacity solution has great application to the engineer in that material property evaluation is greatly simplified, while maintaining an acceptable degree of accuracy in bearing capacity predictions. However, this approach will require the determination of the constant volume friction angle and relative density of the sand, as well as the empirical constants Q and R. Possible methods to determine these parameters will be discussed in the final chapter.

CHAPTER 5

SUMMARY, CONCLUSIONS AND RECOMMENDATIONS FOR FURTHER WORK

Summary

In order to adequately design a shallow foundation resting on a sand, proper consideration must be given to the load carrying capacity of the sand. Traditionally, this is done by conducting shear strength tests on the material in question in order to determine an appropriate friction angle. This friction angle is then used within the conventional bearing capacity solution, with appropriate modifications for such items as the influence of the groundwater table, strain restraint condition beneath the footing, and increased shear resistance due to embedment depth. The conventional bearing capacity solution predicts that the ultimate bearing capacity will increase linearly with footing width and embedment depth. However, numerous researchers including Kusakabe et al., (1992) and Perkins and Madson (1996) have shown this not to be true. This phenomenon is called the scale effect and has been discussed extensively throughout this thesis. The objective of this research has been to develop a simpler method to estimate bearing capacity which eliminates the need for extensive triaxial testing, and, at the same time, accounts for material non-linearity and progressive failure, both components of the scale effect.

A new design approach was proposed using strength and dilatancy relationships developed by Bolton (1986). Using these empirical relationships, a peak friction angle (ϕ'_{peak}) could be determined knowing the soil's relative density (I_D), strain restraint condition for the footing, and the soil's constant volume friction angle (ϕ'_{cv}), as well as the level of mean normal effective stress (p') beneath the footing. Finding ϕ'_{peak} in this manner accounts for material non-linearity (i.e., dependence of ϕ'_{peak} on p'). The approach assumes that certain empirical constants (Q and R) describing the strength of the sand are reasonable.

Since a value of p' appropriate to the footing problem had to be determined, an expression relating p'/q_{ult} to ϕ' was also developed using non-linear limit plasticity theory. The solution process therefore required an iterative procedure in order to find the appropriate p' and corresponding ϕ'_{peak} to use in the general bearing capacity equation.

In this thesis, it was shown that using peak strength parameters resulted in large over predictions of bearing capacity. This was attributed to progressive failure, the second component of the scale effect. To account for progressive failure, an index of progressive failure (I_{PF}) was developed in Chapter 4. This index described the relative position of the predicted bearing capacity (q_{pred}), between that associated with peak and constant volume capacities, ($q_{ult\text{-}peak}$ and $q_{ult\text{-}cv}$). The degree of progressive failure was shown to be largely dependent upon the relative dilatancy index (I_R), which is in turn dependent upon p'. Using the I_{PF}, a predicted bearing capacity (q_{pred}) could be computed.

Bolton's empirical expressions were used to make predictions of bearing capacity for 8 study sands. These predictions were then compared to results from bearing capacity experiments performed on each study sand. In order to study the error associated with using this simplified approach, predictions were also made using the actual material failure envelope developed from shear strength tests conducted on each sand. A statistical analysis was then performed to evaluate the error introduced in using Bolton's empirical equations.

Conclusions

It was found in Chapter 4 that using Bolton's equations did not introduce a significant amount of error into bearing capacity predictions. This conclusion was based on a statistical analysis of the average amount of over/under prediction for each of the study sands. However, it was noted in Chapter 4 that Bolton's equations did not perform well with the Ottawa sand, especially at increased embedment depths. Bolton's equations predict a non-linear material response in that the peak friction angle will decrease with increasing p', corresponding to greater embedment depths. However, in the case of Ottawa sand, it has been shown that the friction angle remains quite constant, even at elevated values of mean normal stress. This is attributed to the unusually high particle strength of Ottawa sand. As a result, at increased depths of embedment the predicted ϕ'_{peak} is substantially less than the actual ϕ'_{peak}, leading to gross under predictions of bearing capacity.

It was also noted in Chapter 4 that some scatter existed in the I_{PF} - I_R plot at lower values of I_R. It was further pointed out that since ϕ'_{peak} and ϕ'_{cv} are approaching one another at low values of I_R, the impact of the index of progressive failure is minimal. In addition, since low values of I_R correspond to situations where the material's relative density is low, the ultimate bearing capacity often will not be the determining factor in the design. In these situations, settlement considerations often dictate the design. In general, the ultimate bearing capacity controls in situations where large settlements will not affect the function or purpose of the structure. Examples of such structures include railway bridges, warehouses, retaining walls, silos, and blast furnaces. In contrast, settlement considerations will often control for structures such as office buildings, residential structures, and manufacturing facilities.

Using Bolton's equations require values for the relative density (I_D) and constant volume friction angle (ϕ'_{cv}) of the sand. The relative density (I_D) may be determined directly using in-situ tests such as the standard penetration test (SPT) and cone penetration test (CPT). The constant volume friction angle (ϕ'_{cv}) may be determined by one of two methods. The most accurate method is simply to conduct a triaxial or direct shear test on a loose, reconstituted sample. As discussed in Chapter 2, peak strength for loose sands corresponds closely to the critical state or constant volume friction angle. A second method is to choose ϕ'_{cv} based upon the primary mineral constituent since ϕ'_{cv} has been shown to be principally a function of the mineral to mineral sliding component (ϕ_u).

In addition to the above described material parameters, empirical constants Q and R describing the strength characteristics of the sand are required. In the absence of strength data, Bolton (1986) suggested setting Q and R equal to 10 and 1, respectively. With the exception of the Scoria sand, this approximation was found to be reasonably accurate. It is noted however that further refinement could be made to the predictions by determining a Q and R appropriate to the sand in question. The obvious problem is that strength data is required in order to find Q and R, which defeats the entire purpose of using Bolton's simplified approach. Fortunately, there is some hope that Q and R can be found by other means. This will be discussed briefly in the last section.

It is also noted that the actual failure envelope of the material may be used to make predictions of bearing capacity. In this research, predictions using the failure envelope were used only for comparison purposes, however, if accurate strength data is available, predictions could be made using the procedure outlined in Chapter 4. Using this approach also accounts separately for both material non-linearity and progressive failure effects.

Recommendations for Further Study

In this thesis, a new approach has been presented to estimate the bearing capacity of sands. This approach uses expressions relating dilatancy and strength. There are a number of advantages to using this simplified design procedure. First, the problem of attempting to take intact samples from the field can now be avoided. This has always posed a problem since granular materials tend to fall apart easily, making them difficult to test. The newly proposed design procedure does not require extensive shear strength testing, successfully solving this problem. Secondly, the procedure requires only that a small number of material parameters be defined. As discussed earlier, these parameters may be determined through relatively simple tests. Lastly, it has been shown here that using this simplified approach does not add an unreasonable amount of error to the predictions.

However, this work is simply a starting point for estimating the bearing capacity of sands. Further research should be performed before this technique is used in practice. In particular, future work should investigate the following:

(1) further refining the curve describing the index of progressive failure (I_{PF}).

(2) the use of in-situ tests to better define the empirical constants (Q and R)

used in Bolton's equations.

(3) other methods to determine the level of mean normal effective stress (p') beneath a footing. This should include possibly looking at the use of the equations proposed by Meyerhof (1948) and De Beer (1967) and discussed in Chapter 2.

As seen in Chapter 4, the points describing the curve of progressive failure are rather sparse at low and high values of I_R. In order to better define the curve in these regions, it is recommended that a series of bearing capacity experiments be performed on one or more study sands. These tests should be conducted at a range of footing widths and embedment depths. More importantly, these experiments should also be performed over a range of relative densities. This will provide further data at low and high end values of I_R, allowing the curve of progressive failure to be further refined.

It was mentioned earlier that better predictions of bearing capacity could be made if Q and R were better defined for each sand. At this time, it is possible to correlate data from a cone penetration test (CPT) to an appropriate friction angle. It is therefore conceivable that data from a CPT may be related to appropriate values of Q and R. Research in this area is required to validate this statement.

Further research should also be conducted into appropriate methods to determine the level of mean normal effective stress (p') beneath a footing. In particular, possible consideration may be given to using expressions proposed by Meyerhof (1948) and De Beer (1967). It was maintained in Chapter 2 that little was available on their development and for this reason were not used. However, these expressions may be worth investigating further if better predictions of bearing capacity can be made with their use.

REFERENCES

REFERENCES CITED

Abghari, A. (1987). "Leaning instability of tall structures," Ph.D Thesis, University of California, Davis, CA.

Aiban, S. A. (1991). "Shallow foundations on sands," Ph.D Thesis, University of Colorado, Boulder, CO.

Bolton, M. D. (1986). "The strength and dilatancy of sands," Geotechnique, 36(1), pp. 65-78.

Briaud, J. L. and Gibbens, R. M. (1994). "Predicted and Measured Behavior of Five Spread Footings on Sand," Results Pred. Symp. sponsored by FHWA, Settlement '94 Conf., 41, Texas A&M University.

Chen, W. F. (1975). Limit Analysis and Soil Plasticity, Elsewier Sci. Pub. Co., New York.

Craig, R. F. (1992). Soil Mechanics, 5th edition, Chapman and Hall, London.

Das, B. M. (1990). Principles of Foundation Engineering, 2nd edition, PWS Publishing Company, Boston.

De Beer, E. E. (1963). "The scale effect in the transposition of the results of deepsounding tests on the ultimate bearing capacity of piles and caisson foundations," Geotechnique 13(1), pp. 39-75.

De Beer, E. E. (1967). "Bearing capacity and settlement of shallow foundations on sands," Proc. Symp. On Bearing Capacity and Settlement of Foundations, Duke University, Durham, N.C., pp. 15-33.

De Beer, E. E. (1970). "Experimental determination of the shape factors and bearing capacity factors of sand," Geotechnique, 20(4), pp. 387-411.

Fukushima, S. and Tatsuoka, F. (1984). "Strength and deformation characteristics of saturated sand at extremely low pressures," Soils and Foundations, 24(4), pp. 30-48.

Golder, H. Q. (1941). "The ultimate bearing pressure of rectangular footings," Journal of Institution for Civil Engineers, 17, pp. 161-174.

Gui, D. (1995). "Bearing capacity of shallow foundations on simulated lunar soil," Masters Thesis, Montana State University, Bozeman, MT.

Hansen, J. B. (1970). "A revised and extended formula for bearing capacity," Danish Geotechnical Institute, Bulletin 28, Copenhagen.

Hilf J. W. (1975). Foundation Engineering Handbook, Van Norstrand Reinhold Co.

Kimura, T., Kusakabe, O., and Saitoh, K. (1985). "Geotechnical model tests of bearing capacity problems in a centrifuge," Geotechnique, 35(1), pp. 33-45.

Kimura, T., (1995). Personal Communication.

Kusakabe, O., Yamaguchi, H., and Morikage, A. (1991). "Experiment and analysis on the scale effect of Nγ for circular and rectangular footings," Proc. Int. Conf., Centrifuge '91, A. A. Balkema, Rotterdam, The Netherlands, pp. 179-186.

Kusakabe, O., Maeda, Y., Ohuchi, M. (1992). "Large-scale loading tests of shallow footings in pneumatic caisson," Journal of Geotechnical Engineering, 118(11), pp. 1681-1695.

Kutter, B. L., Aghari, A., and Cheney, J. A. (1988). "Strength parameters for bearing capacity of sand," Journal of Geotechnical Engineering, 114(4), pp. 491-487.

Meyerhof, G. G. (1948). "An investigation of the bearing capacity of shallow foundations on dry sand," Proc. 2nd Int. Conf. Soil Mech. and Foundation Eng.,1, pp. 237-243.

Meyerhof, G. G. (1963). "Some recent research on the bearing capacity of foundations," Canadian Geotechnical Journal, 1(1), pp. 16-26.

Mitchell, J. K. (1976). Fundamentals of Soil Behavior, John Wiley and Sons, New York.

Muhs, E. (1963). "Über die zulässige belastung nichtibindiger böden," Mitteilungen der Deutschen Forschungsgesellshaft Für Bodenmechanik (Degebo), Heft, 16, pp. 102-121.

Perkins, S.W. (1991). "Modeling of regolith structure interaction in extraterrestrial constructed facilities," Ph.D Thesis, University of Colorado, Boulder, CO.

Perkins, S.W. (1995a). "Bearing capacity of highly frictional material," ASTM Geotechnical Testing Journal, 18(4), pp. 450-462.

Perkins, S. W. (1995b). "Non-linear limit analysis for the bearing capacity of highly frictional soils," 2nd Congress on Computing in Civil Engineering, ASCE, New York, N.Y., 1, pp. 629-636.

Perkins, S. W. and Madson, C. R. (1996). "Mechanical and load-settlement characteristics of two lunar soil simulants," Journal of Aerospace Engineering, ASCE, 9(1), pp. 1-9.

Rowe, P. W. (1962). "The stress-dilatancy relation for static equilibrium of an assembly of particles in contact," Proc. of the Royal Society of London, Series A, 269, pp. 500-527.

Schipporeit, T. M. (1988). "Stress-strain and dilatancy behavior of a dense sand at very low effective stresses," Master's Thesis, University of Colorado, Boulder, CO.

Sture, S., Runesson, K., and Macari-Pasqualino, E. J. (1989). "Analysis and calibration of a three-invariant plasticity model for granular materials," Ingenieur-Archiv, 59, pp. 253-266.

Tatsuoka, F., Sakamoto, M., Kawamura, T., and Fukushima, S. (1986). "Strength and deformation characteristics of sand in plane strain compression at extremely low pressures," Soils and Foundations, 26(1), pp. 65-84.

Vesic, A. S. (1973). "Analysis of ultimate loads of shallow foundations," Journal of the Soil Mechanics and Foundations Division, ASCE, 99(1), pp. 45-73.

Willman, B. W., Boles, W. W., McKay, D. S., and Allen, C. C. (1995). "Properties of lunar soil simulant JSC-1," Journal of Aerospace Engineering, ASCE, 8(2), pp. 77-87.

Wroth, C. P. (1984). "The interpretation of in-situ soil tests," 24th Rankine Lecture, Geotechnique, 34(4), pp. 449-489.

Yamaguchi, H., Kimura, T., and Fuji, N. (1976). "On the influence of progressive failure on the bearing capacity of shallow foundations in dense sands," Soils and Foundations, 16(4), pp. 11-22.

APPENDICES

APPENDIX A

CONVENTIONAL TRIAXIAL COMPRESSION AND PLANE STRAIN TEST RESULTS ACCUMULATED FOR THE STUDY SANDS

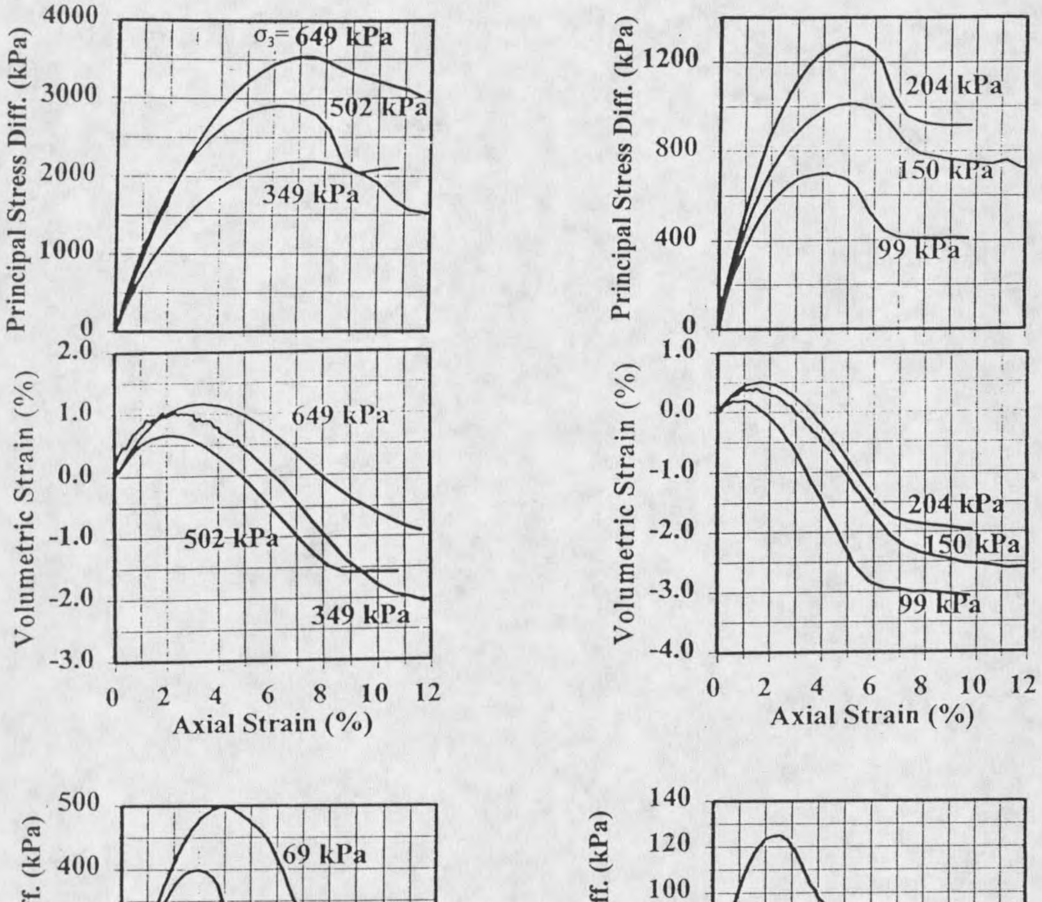

Figure 61. MLS-1 CTC results at 100% relative density, (from Perkins and Madson, 1996).

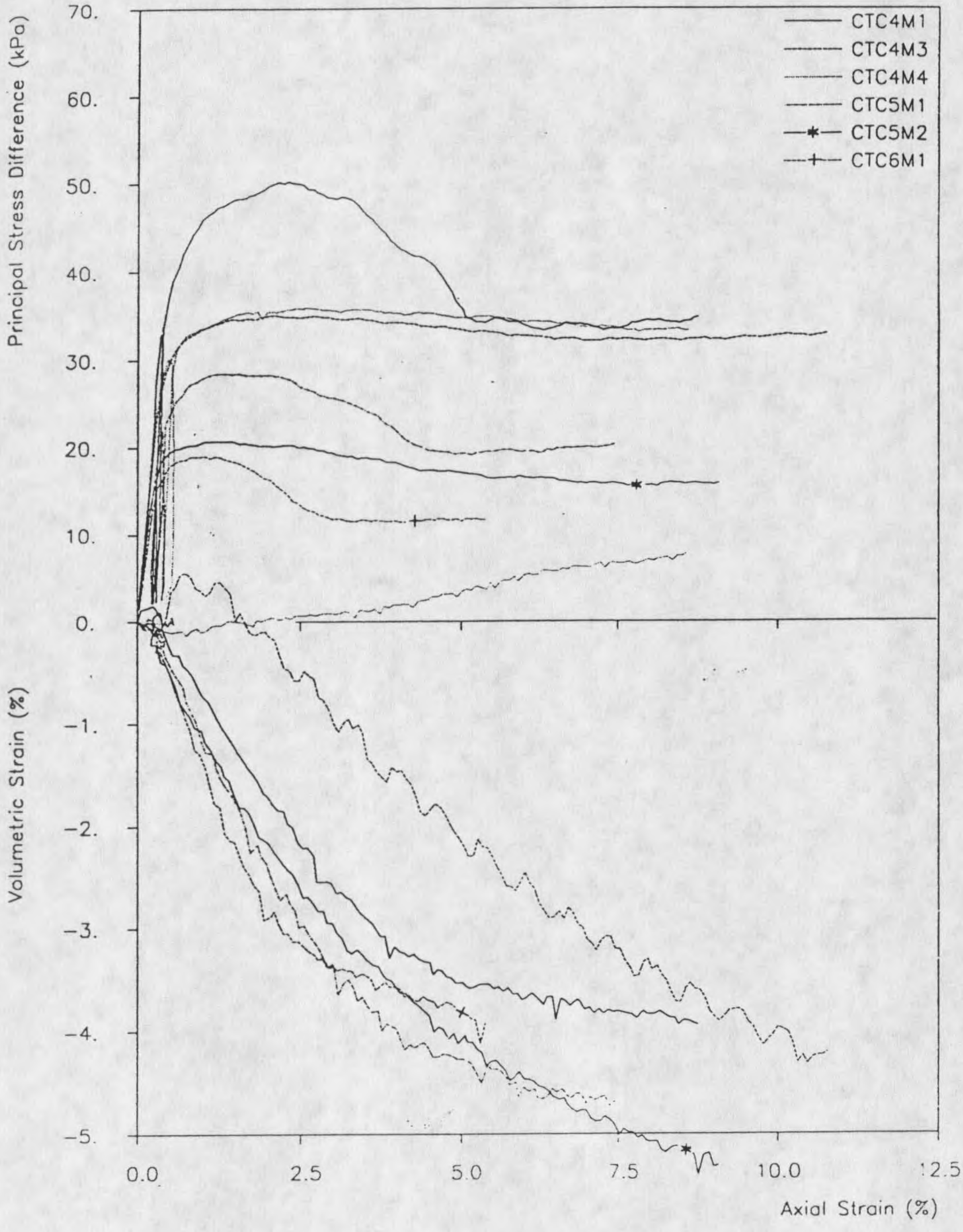

Figure 62. MLS-1 CTC results at σ'_3 = 6.89, 3.44, and 1.72 kPa; 61.5% relative density, (from Perkins, 1991).

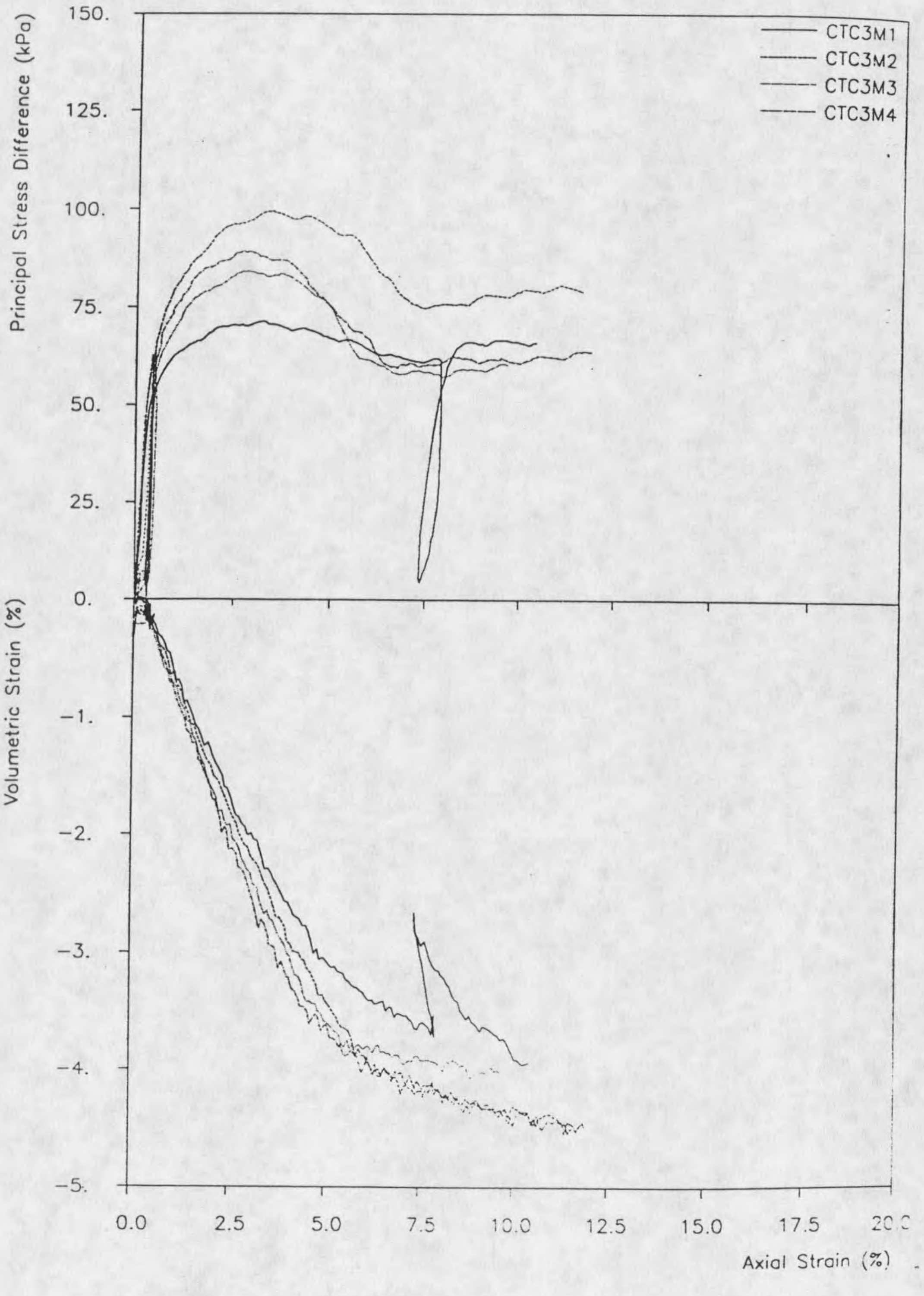

Figure 63. MLS-1 CTC results at $\sigma'_3 = 13.8$ kPa; 61.5% relative density, (from Perkins, 1991).

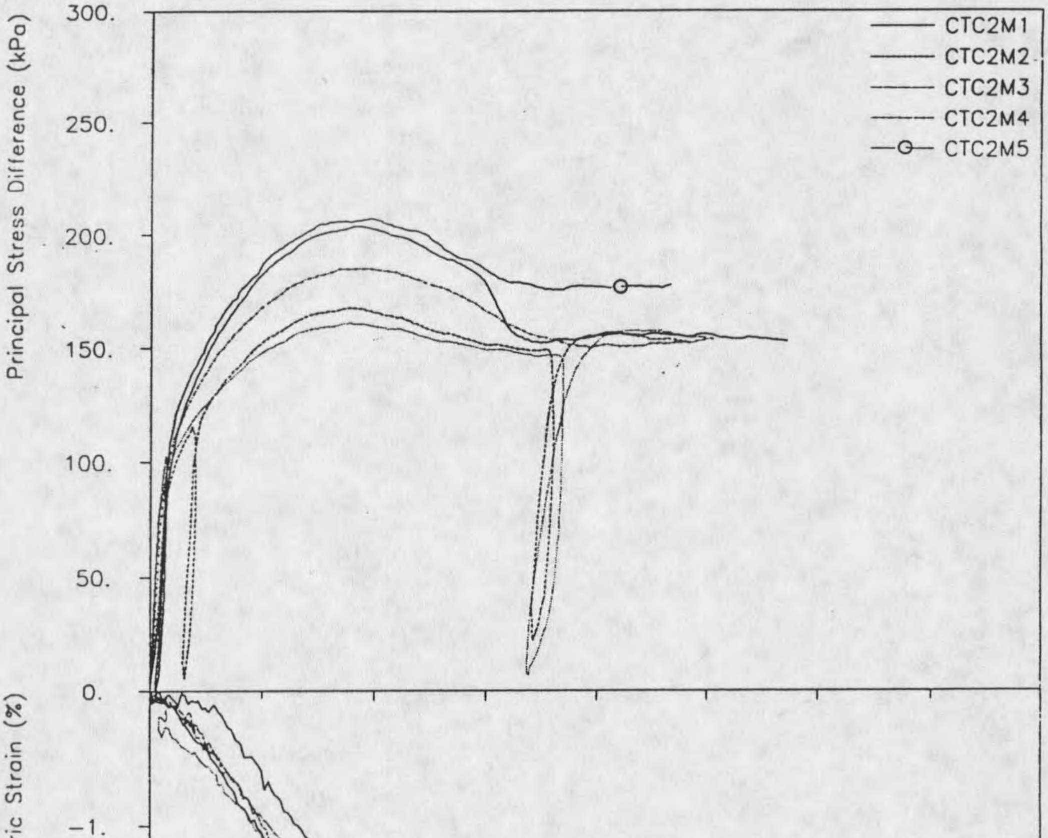

Figure 64. MLS-1 CTC results at $\sigma'_3 = 34.4$ kPa; 61.5% relative density, (from Perkins, 1991).

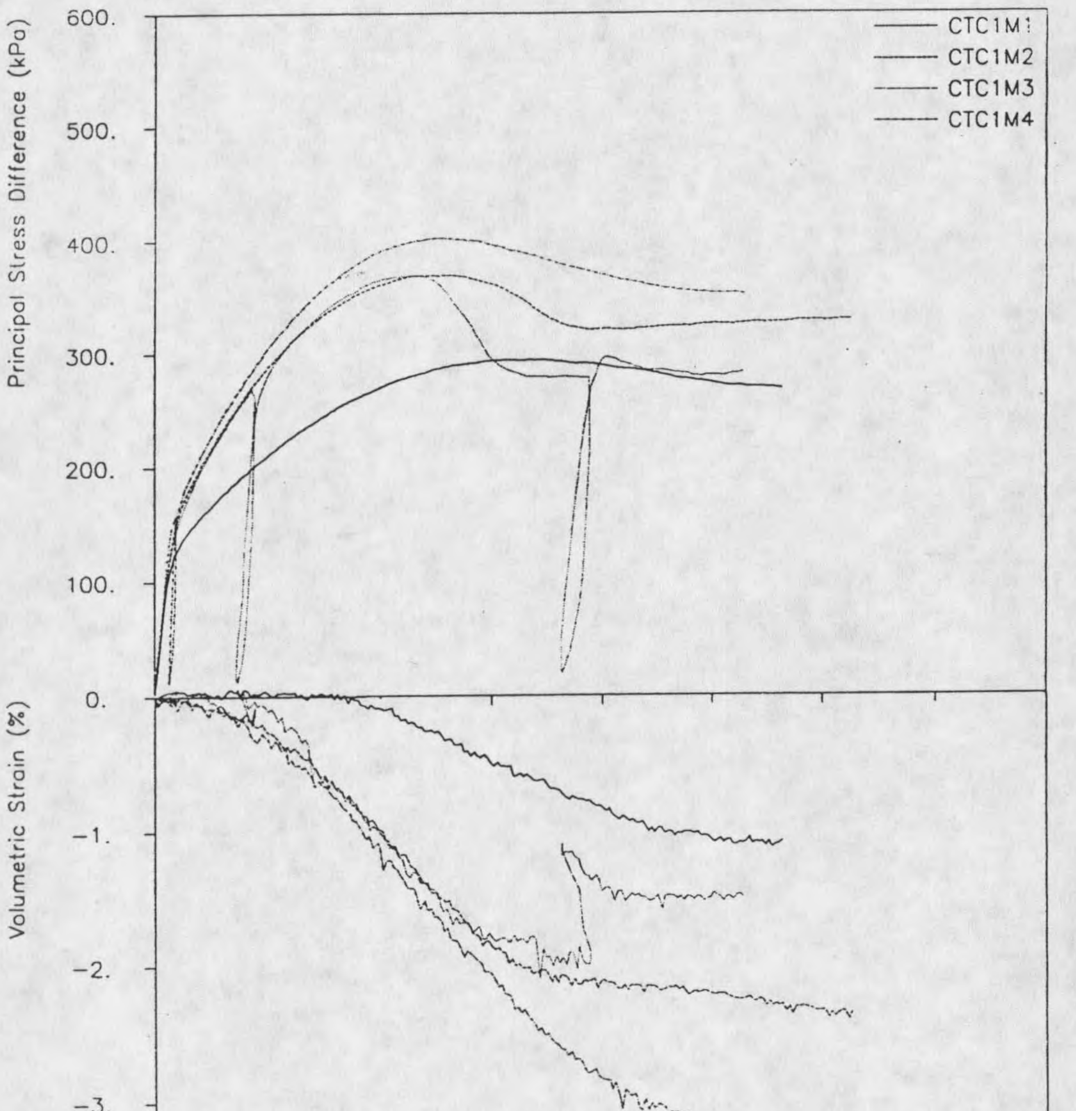

Figure 65. MLS-1 CTC results at $\sigma'_3 = 68.9$ kPa; 61.5% relative density, (from Perkins, 1991).

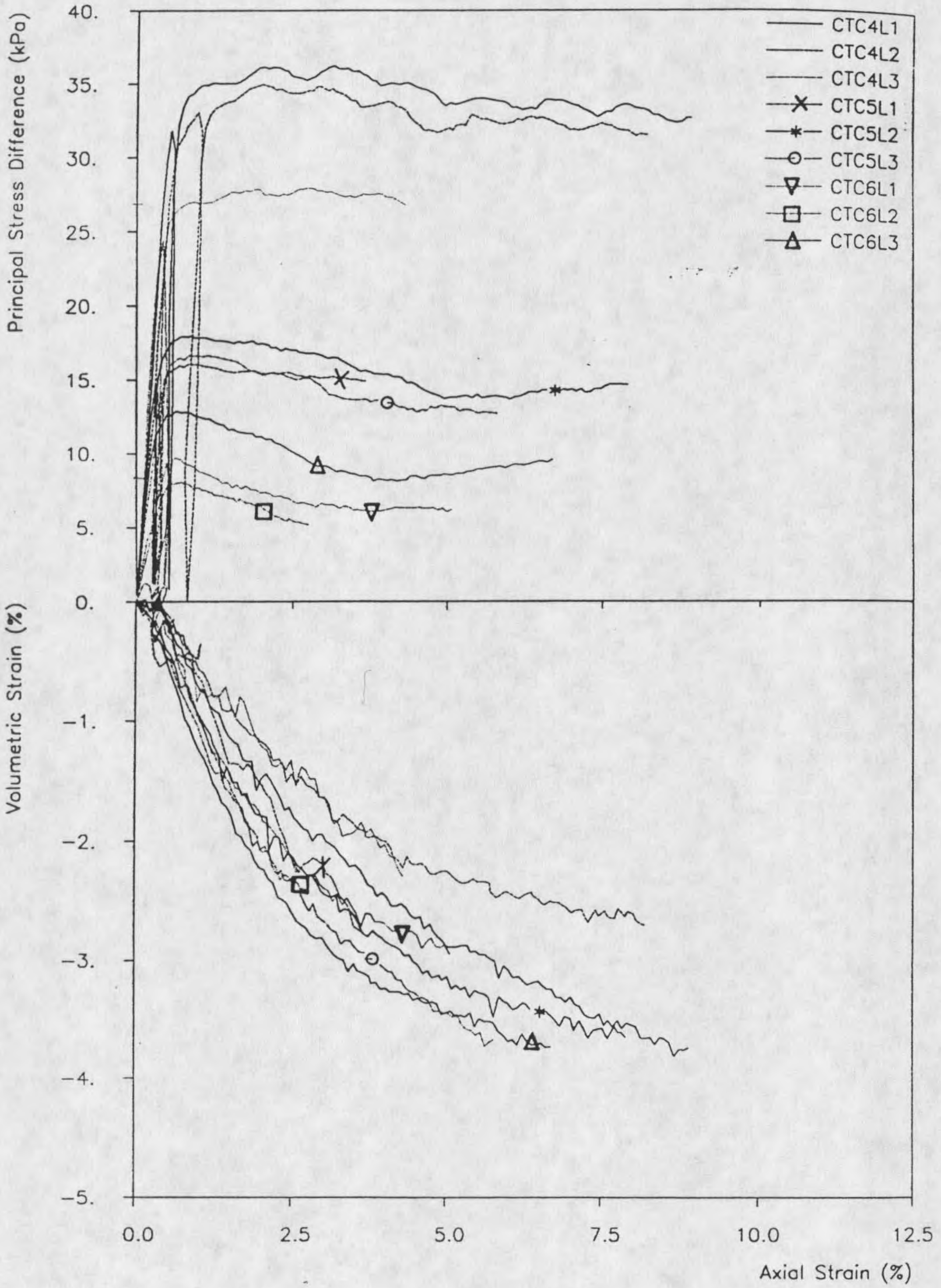

Figure 66. MLS-1 CTC results at $\sigma'_3 = 6.89$, 3.44, and 1.72 kPa; 28% relative density, (from Perkins, 1991).

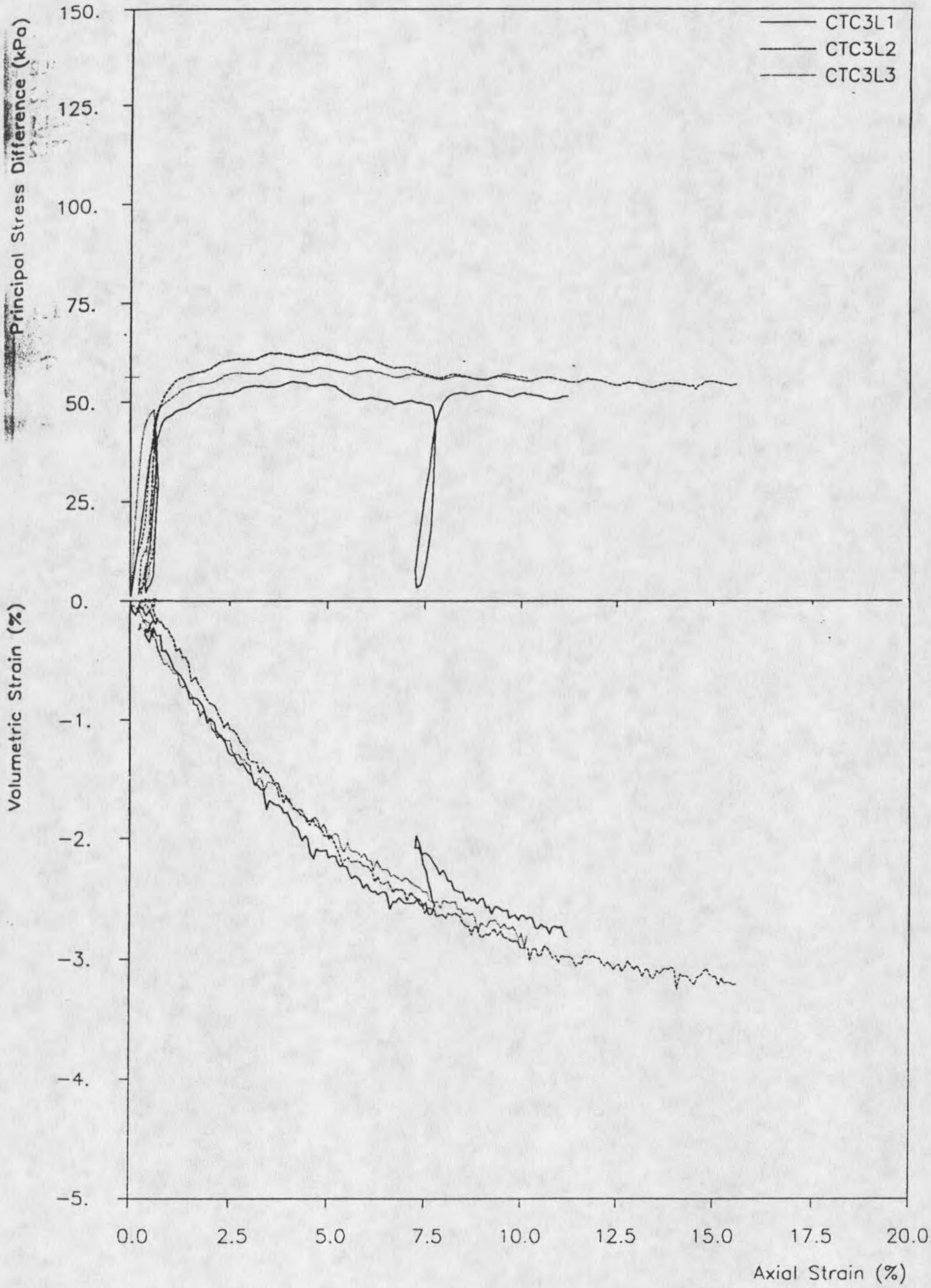

Figure 67. MLS-1 CTC results at $\sigma'_3 = 13.8$ kPa; 28% relative density, (from Perkins, 1991).

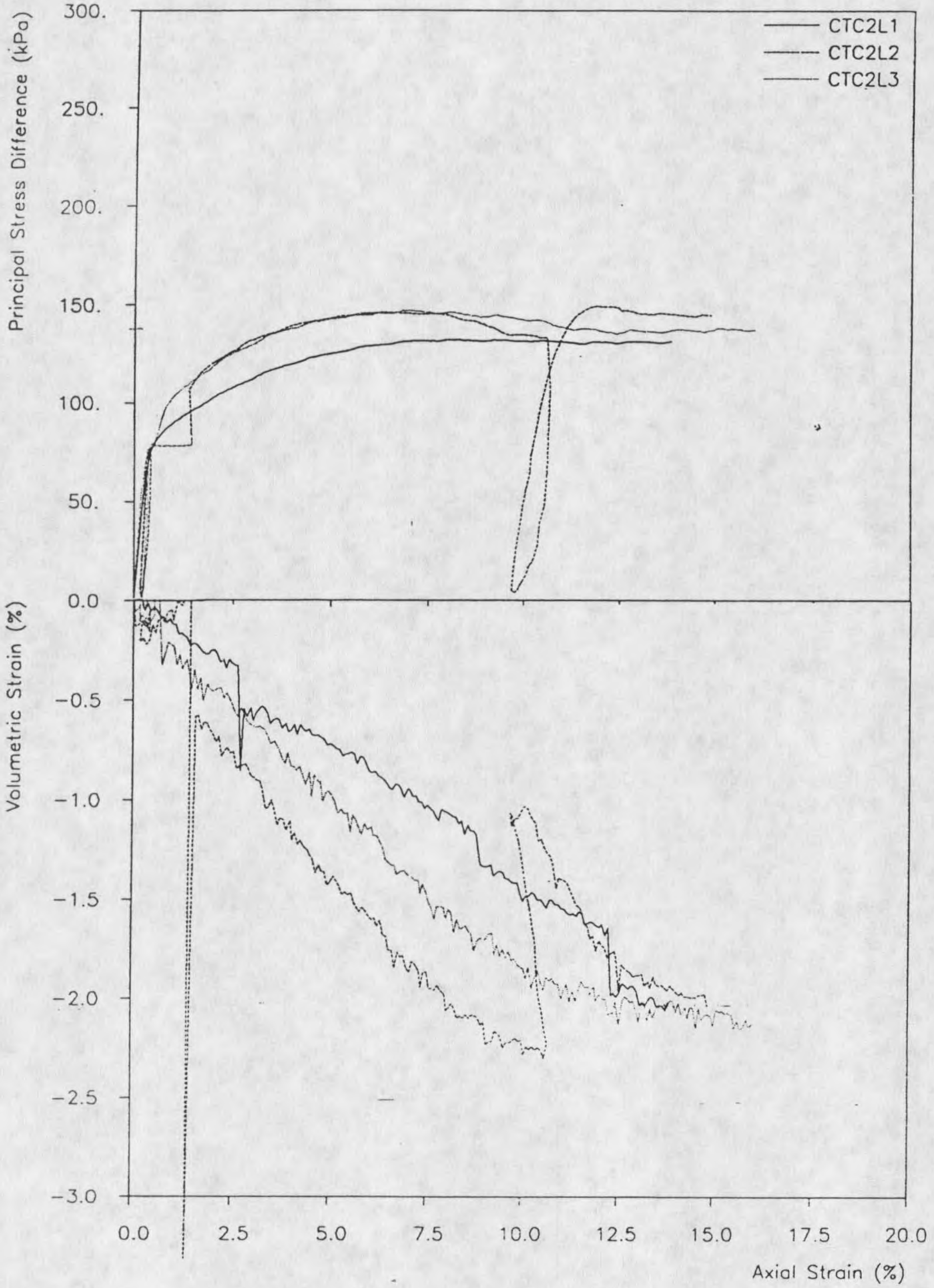

Figure 68. MLS-1 CTC results at σ'_3 = 34.4 kPa; 28% relative density, (from Perkins, 1991).

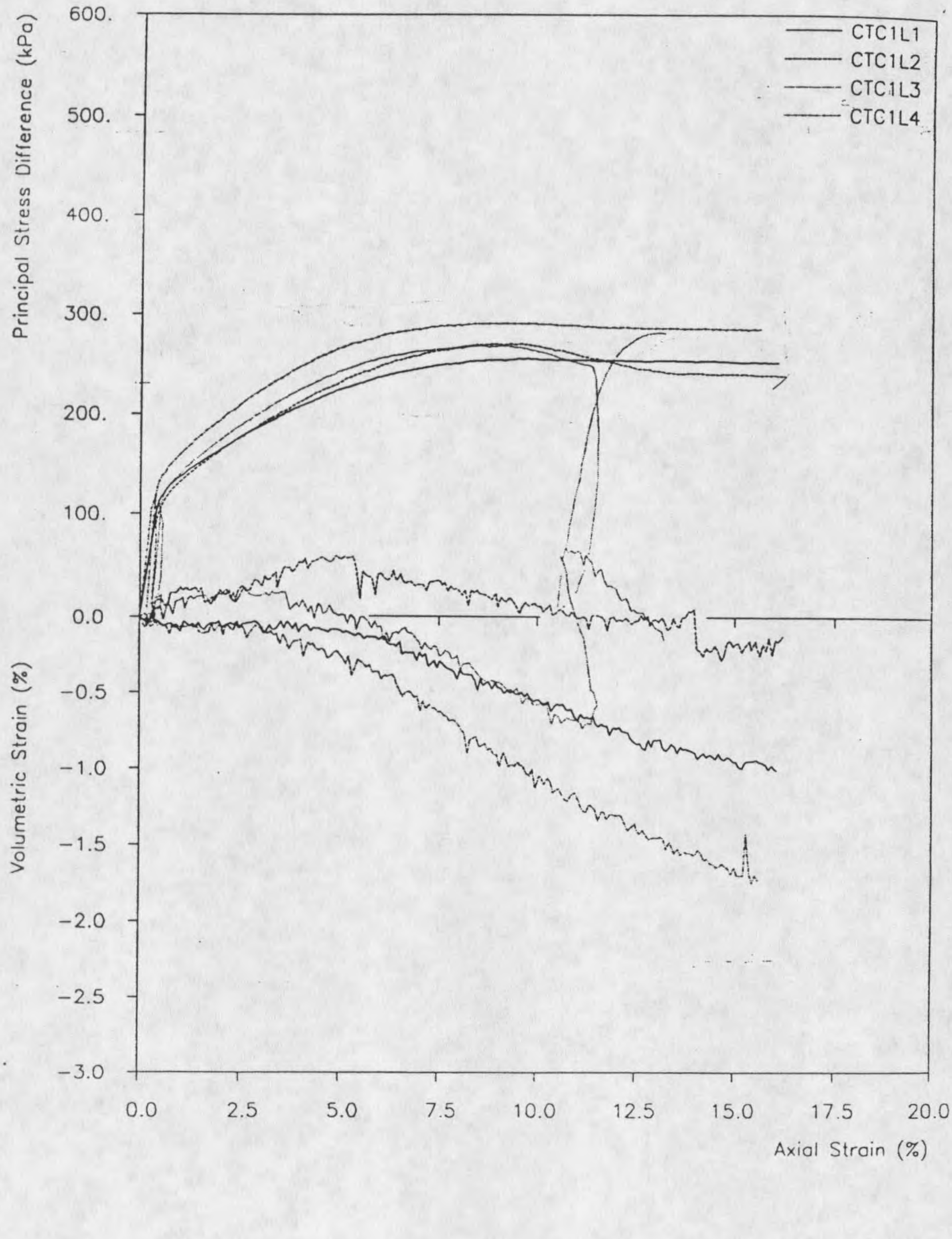

Figure 69. MLS-1 CTC results at $\sigma'_3 = 68.9$ kPa; 28% relative density, (from Perkins, 1991).

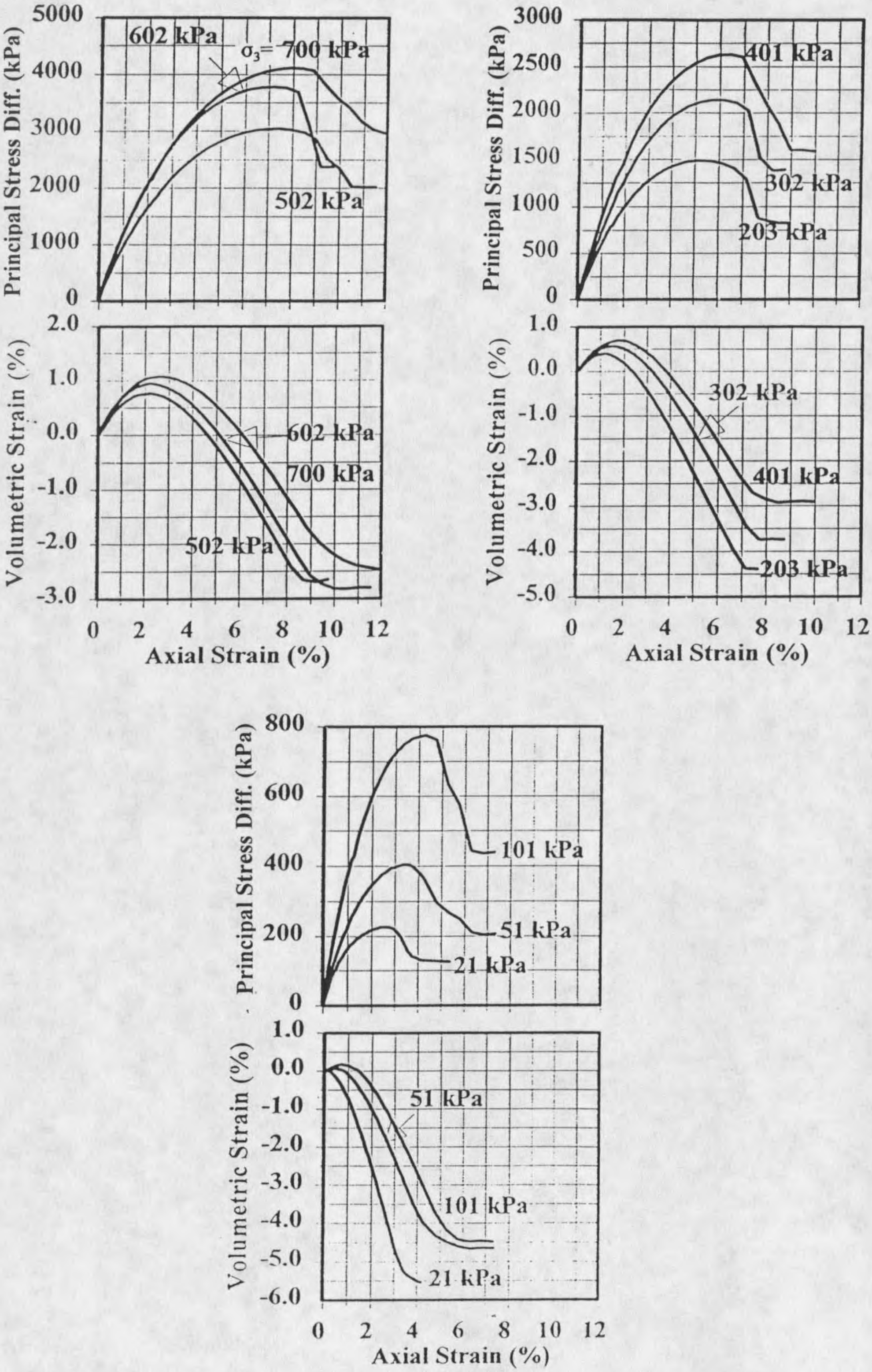

Figure 70. JSC-1 CTC results at 100% relative density, (from Perkins and Madson, 1996).

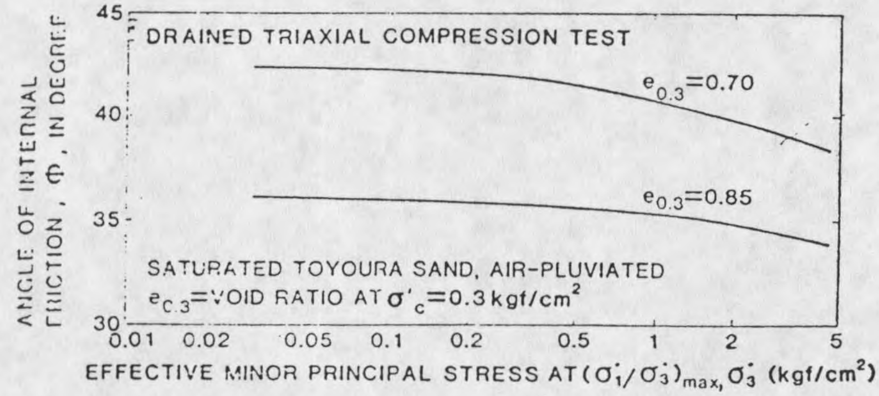

Figure 71. Toyoura sand shear strength data from CTC tests, (from Fukushima and Tatsuoka, 1984).

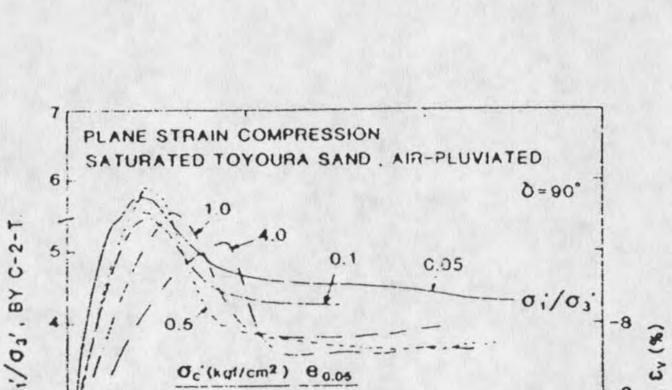

Figure 72. Toyoura sand shear strength data from plane strain tests; 61% relative density, (from Tatsuoka et al., 1986).

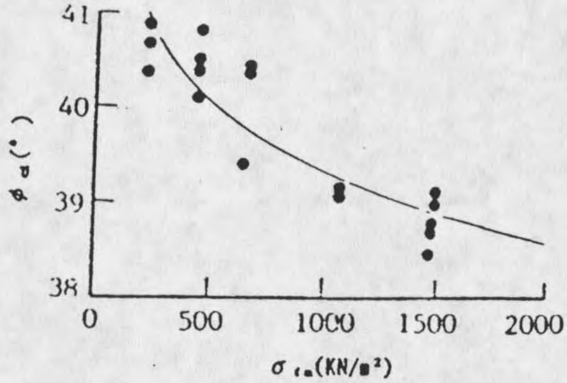

Figure 73. Inagi sand CTC results; approximately 80% relative density (from Kusakabe et al., 1991).

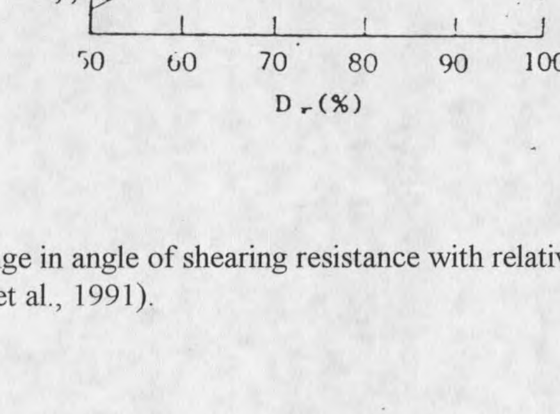

Figure 74. Change in angle of shearing resistance with relative density for Inagi sand (from Kusakabe et al., 1991).

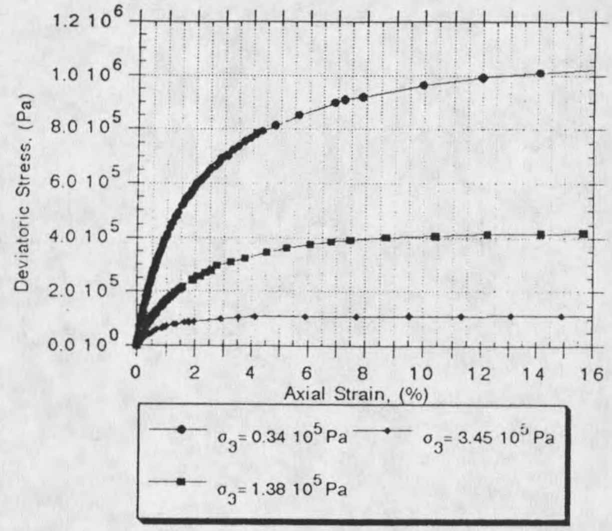

Figure 75. Texas sand - CTC results for samples taken at 0.6 m; approximately 55% relative density (from Briaud and Gibbens, 1994).

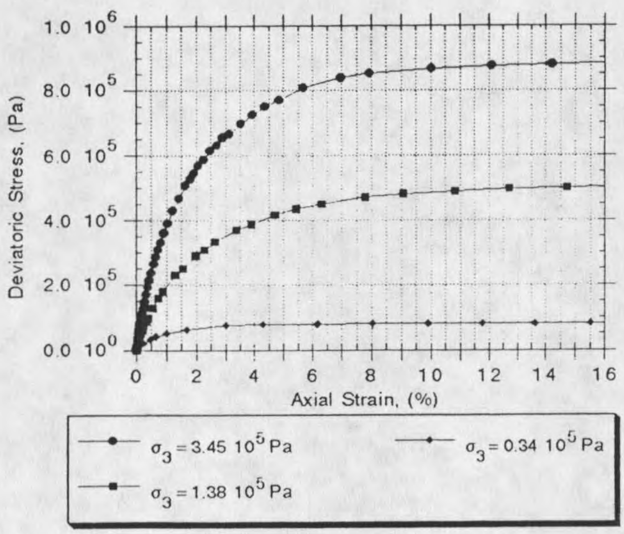

Figure 76. Texas sand - CTC results for samples taken at 3.0 m; approximately 55% relative density (from Briaud and Gibbens, 1994).

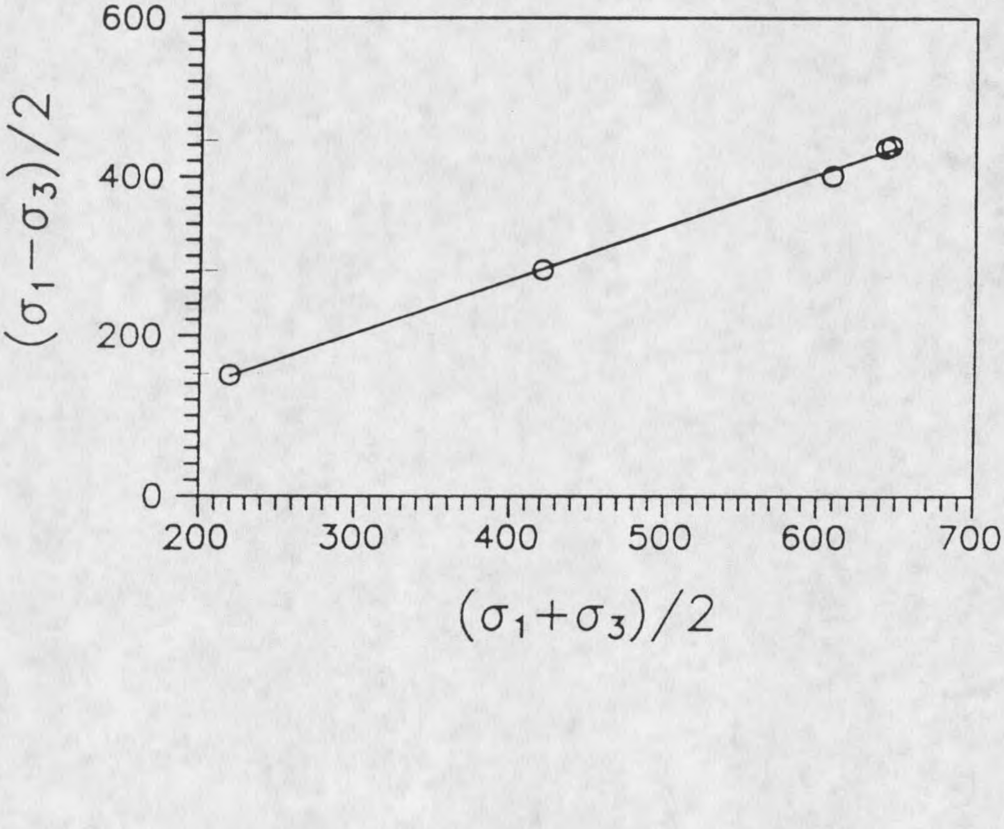

Figure 77. Ottawa sand - CTC results at approximately 88% relative density (from Aiban, 1991).

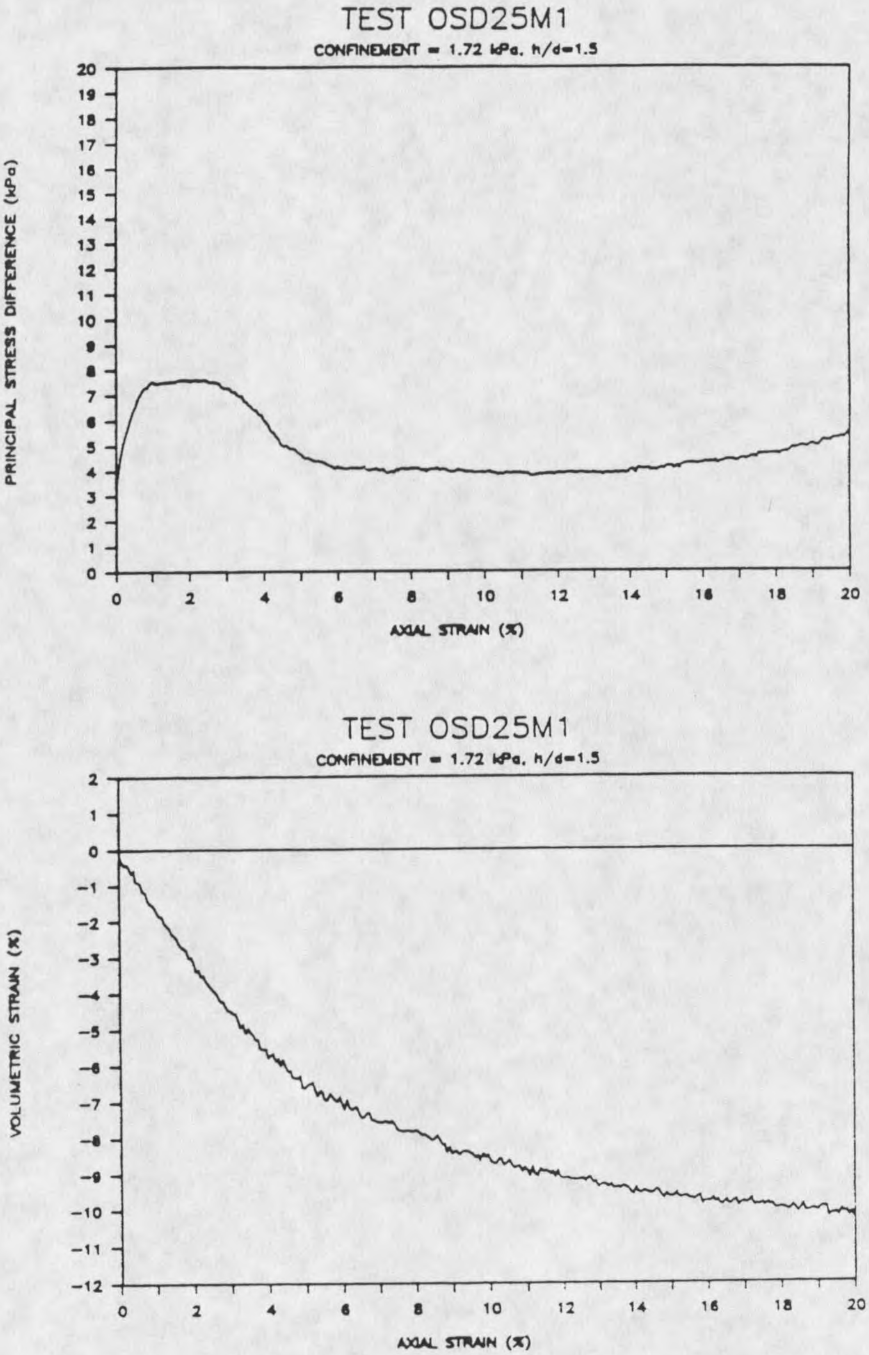

Figure 78. Ottawa sand CTC results at $\sigma'_3 = 1.72$ kPa; approximately 88% relative density, (from Schipporeit, 1988).

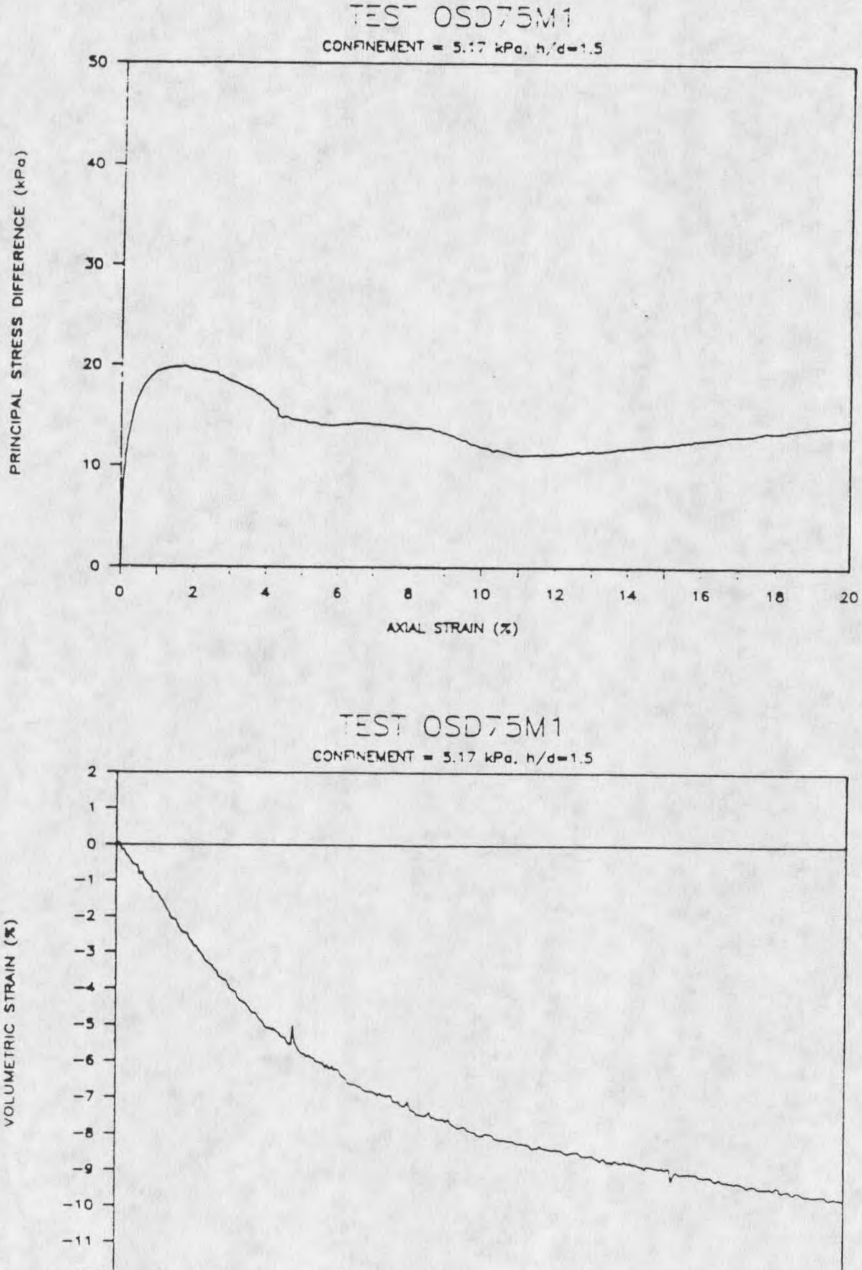

Figure 79. Ottawa sand CTC results at $\sigma'_3 = 5.17$ kPa; approximately 88% relative density, (from Schipporeit, 1988).

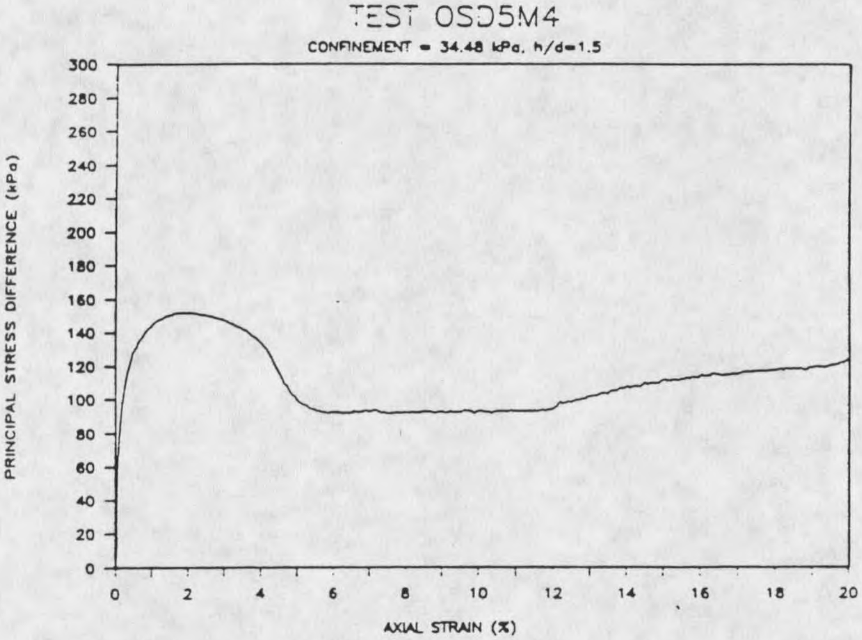

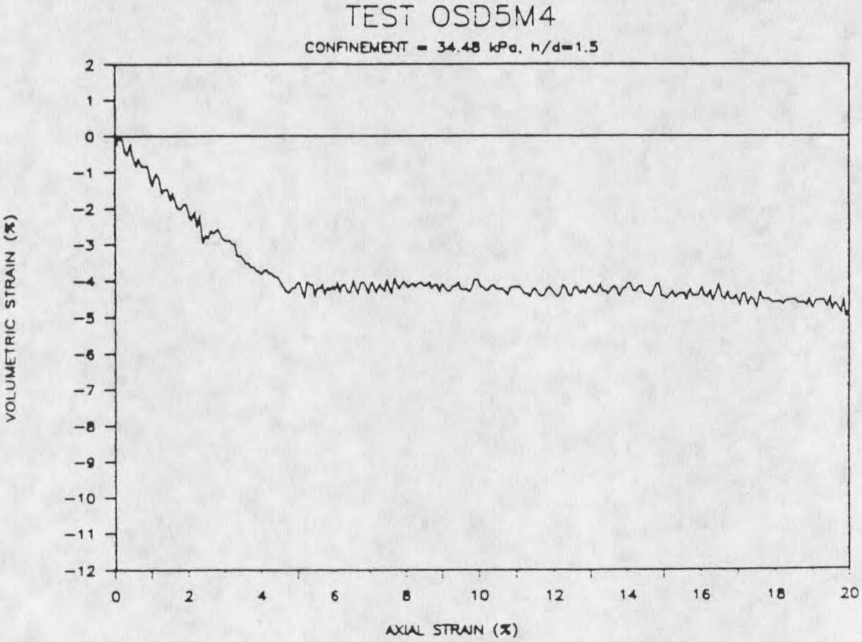

Figure 80. Ottawa sand CTC results at $\sigma'_3 = 34.48$ kPa; approximately 88% relative density, (from Schipporeit, 1988).

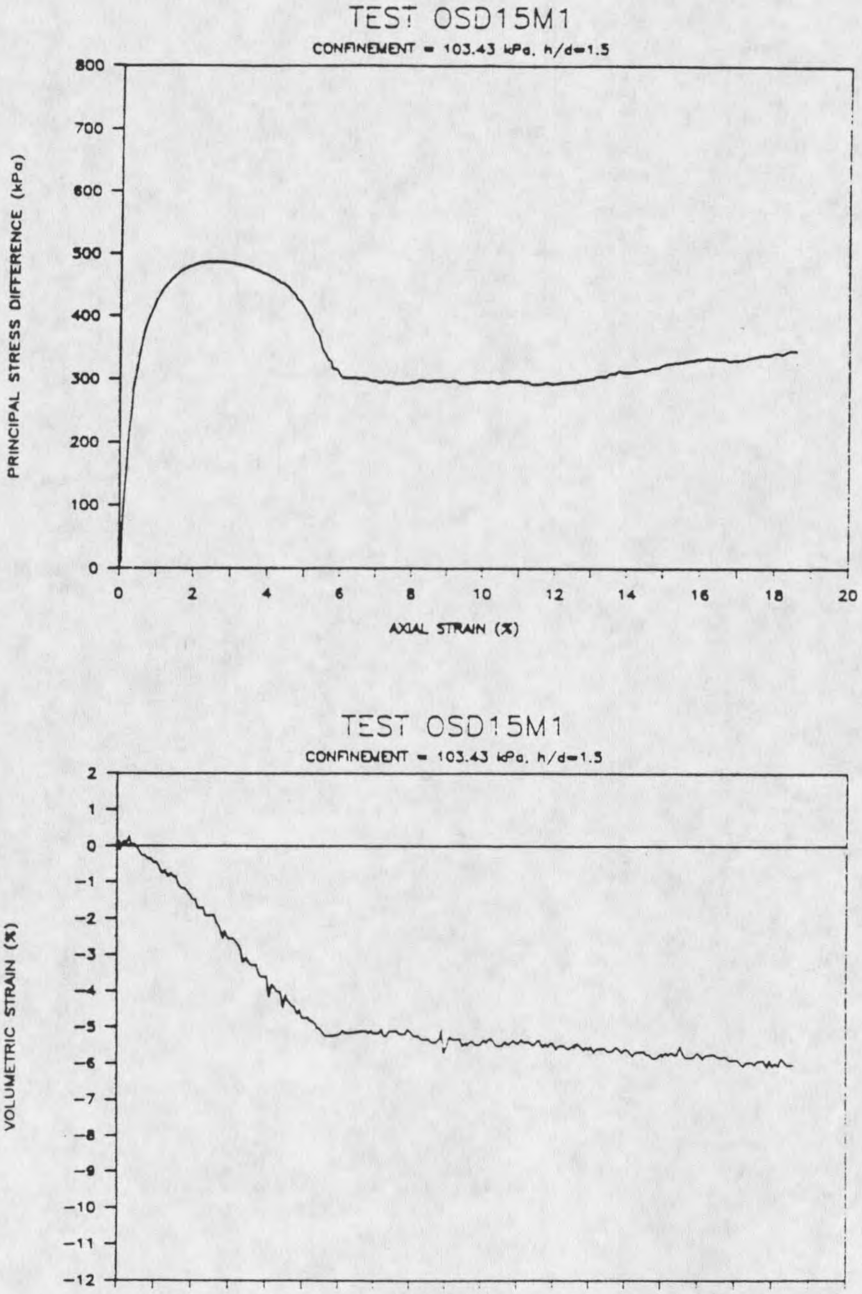

Figure 81. Ottawa sand CTC results at $\sigma'_3 = 103.43$ kPa; approximately 88% relative density, (from Schipporeit, 1988).

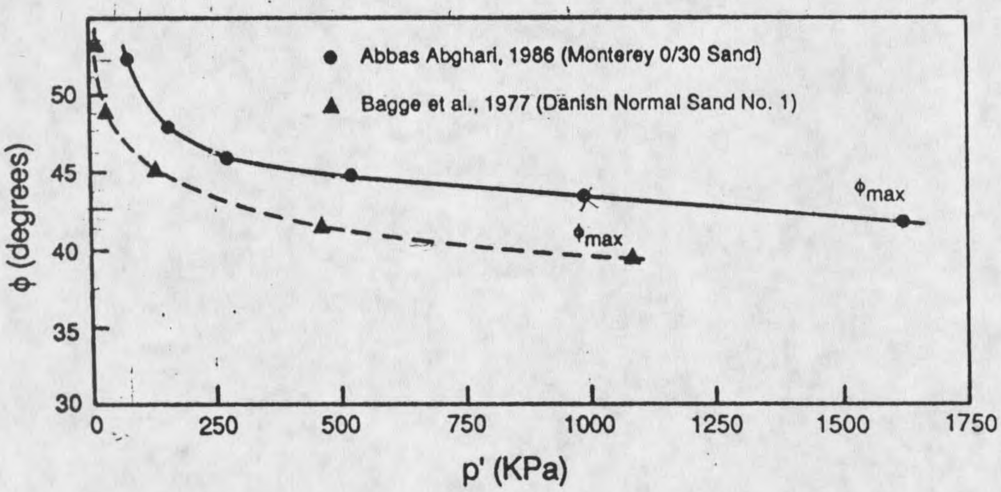

Figure 82. Variation in the peak friction angle with mean normal stress for Monterey sand; approximately 93-95% relative density, (from Kutter et al., 1988).

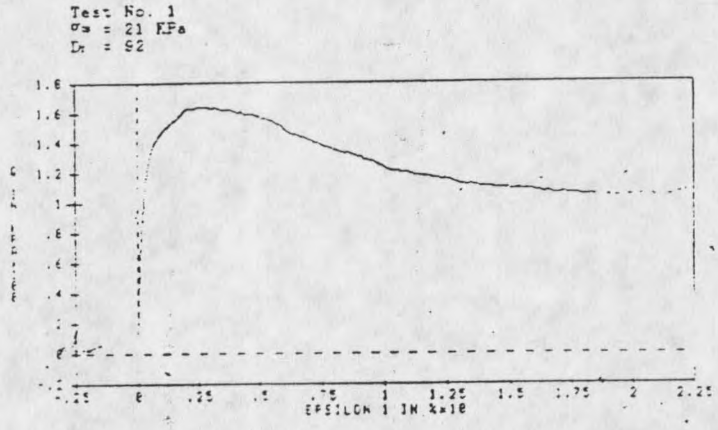

Figure 83. Monterey sand CTC results at $\sigma'_3 = 21$ kPa; approximately 93-95% relative density, (from Abghari, 1987).

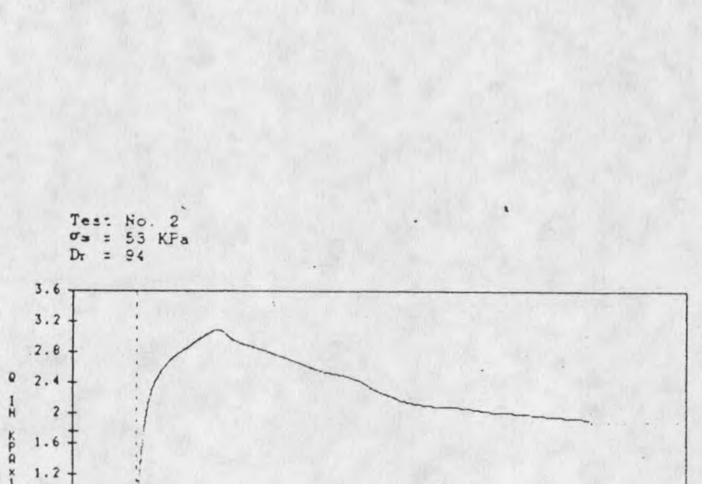

Figure 84. Monterey sand CTC results at $\sigma'_3 = 53$ kPa; approximately 93-95% relative density, (from Abghari, 1987).

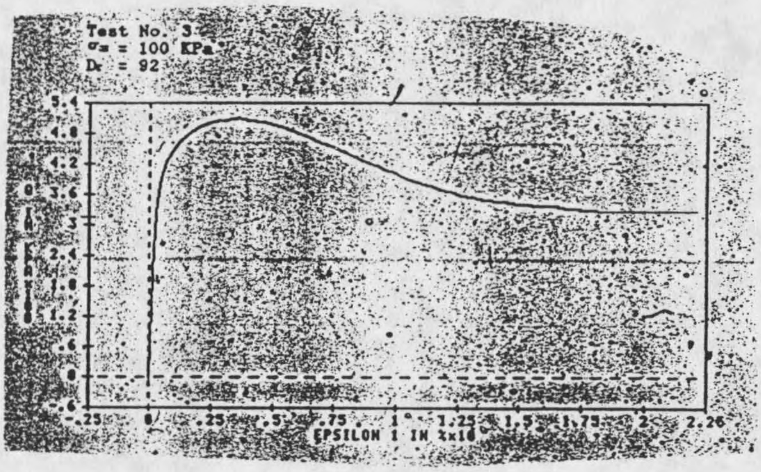

Figure 85. Monterey sand CTC results at $\sigma'_3 = 100$ kPa; approximately 93-95% relative density, (from Abghari, 1987).

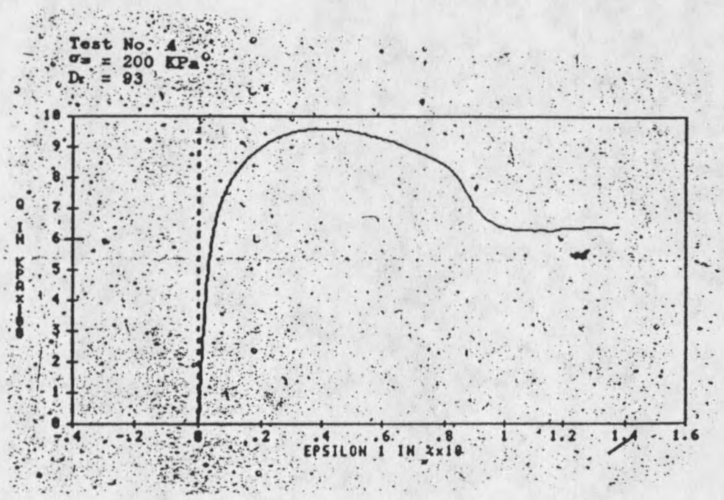

Figure 86. Monterey sand CTC results at $\sigma'_3 = 200$ kPa; approximately 93-95% relative density, (from Abghari, 1987).

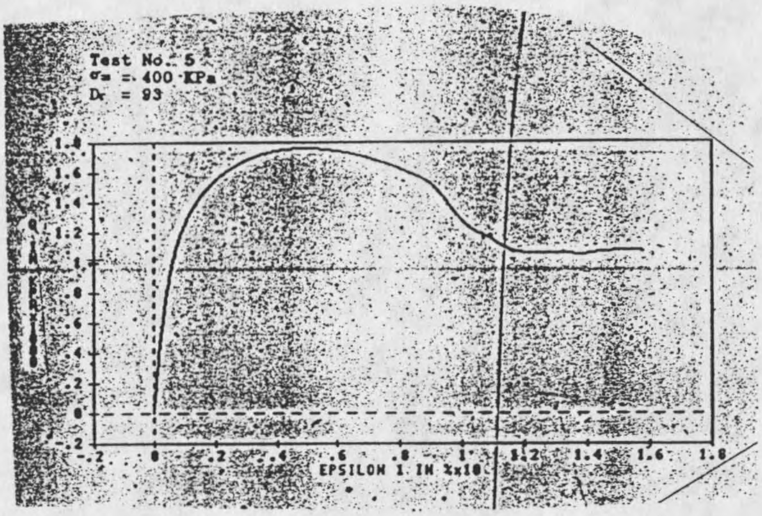

Figure 87. Monterey sand CTC results at σ'_3 = 400 kPa; approximately 93-95% relative density, (from Abghari, 1987).

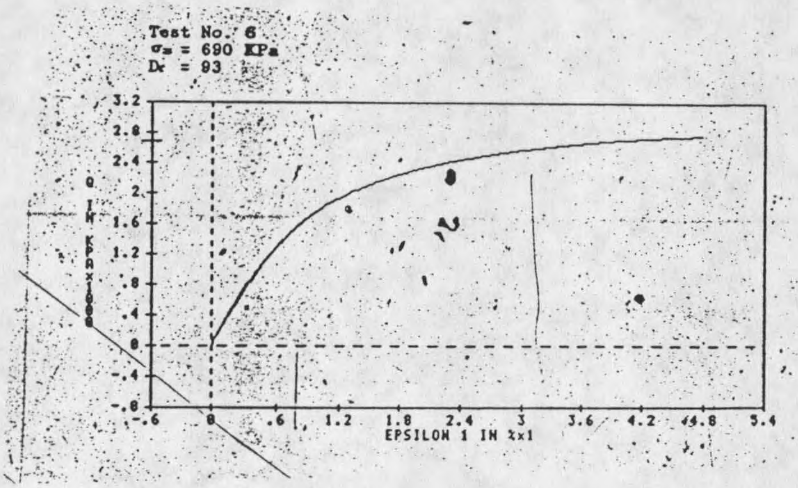

Figure 88. Monterey sand CTC results at σ'_3 = 690 kPa; approximately 93-95% relative density, (from Abghari, 1987).

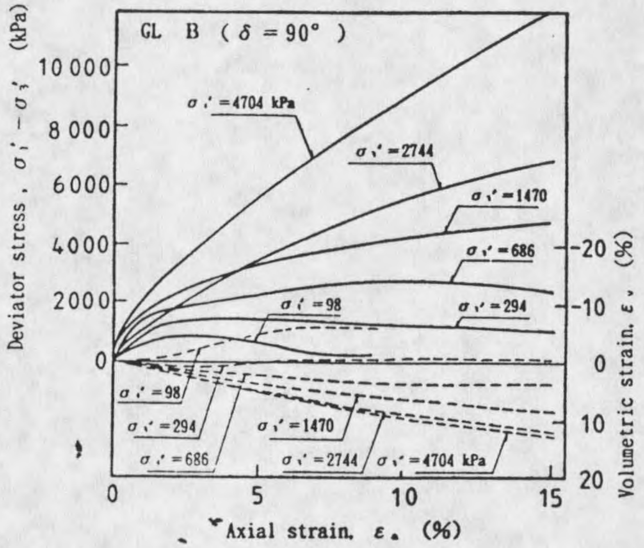

Figure 89. Scoria sand CTC results; approximately 118% relative density, (from Kusakabe et al., 1992).

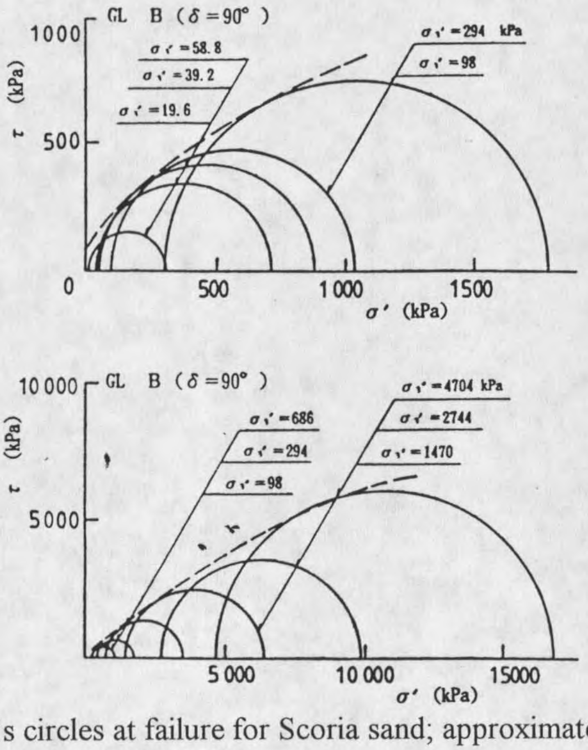

Figure 90. Mohr's circles at failure for Scoria sand; approximately 118% relative density, (from Kusakabe et al., 1992).

APPENDIX B

BEARING CAPACITY RESULTS FOR THE STUDY SANDS

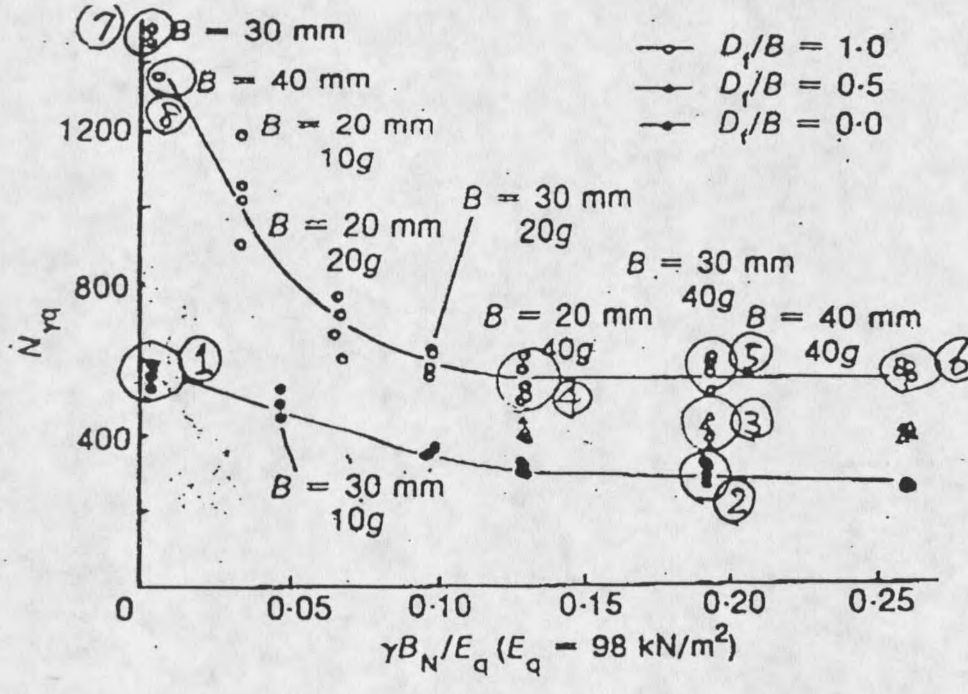

Figure 91. Relationship between $N\gamma_q$ and $\gamma B_N/E_q$ for Toyoura sand, (from Kimura et al., 1985).

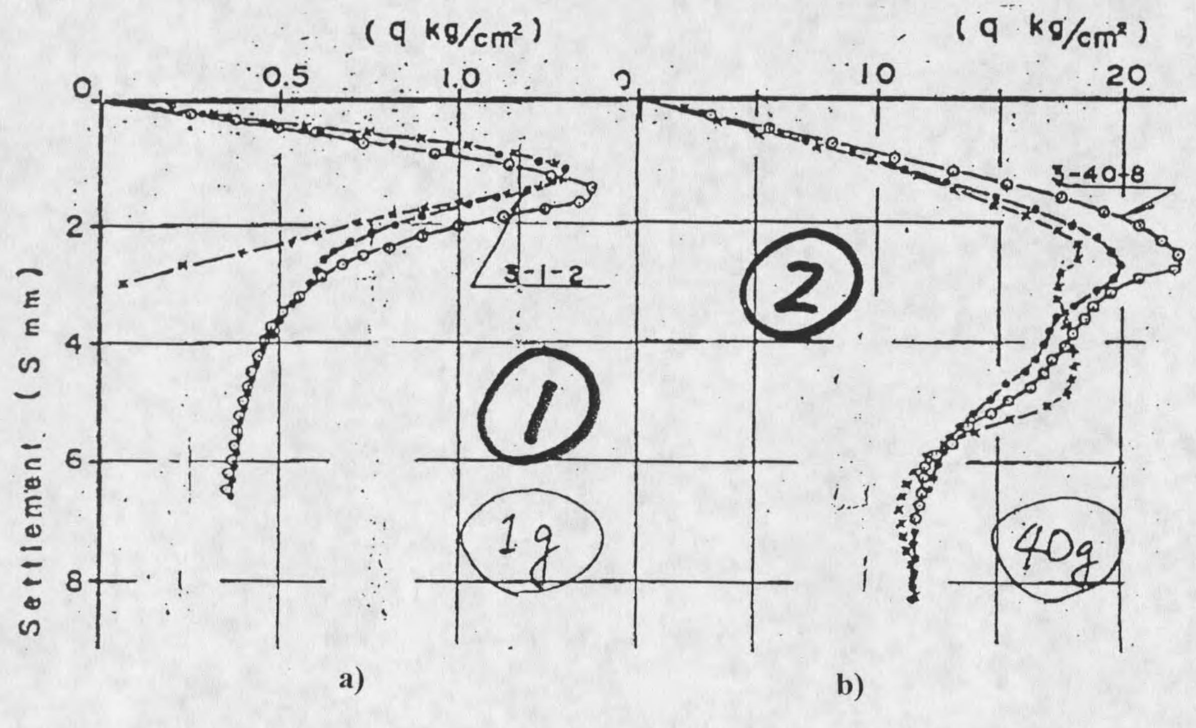

Figure 92. Toyoura sand bearing capacity results for a) B = 3 cm; D/B = 0
b) B = 120 cm; D/B = 0, (from Kimura, 1995).

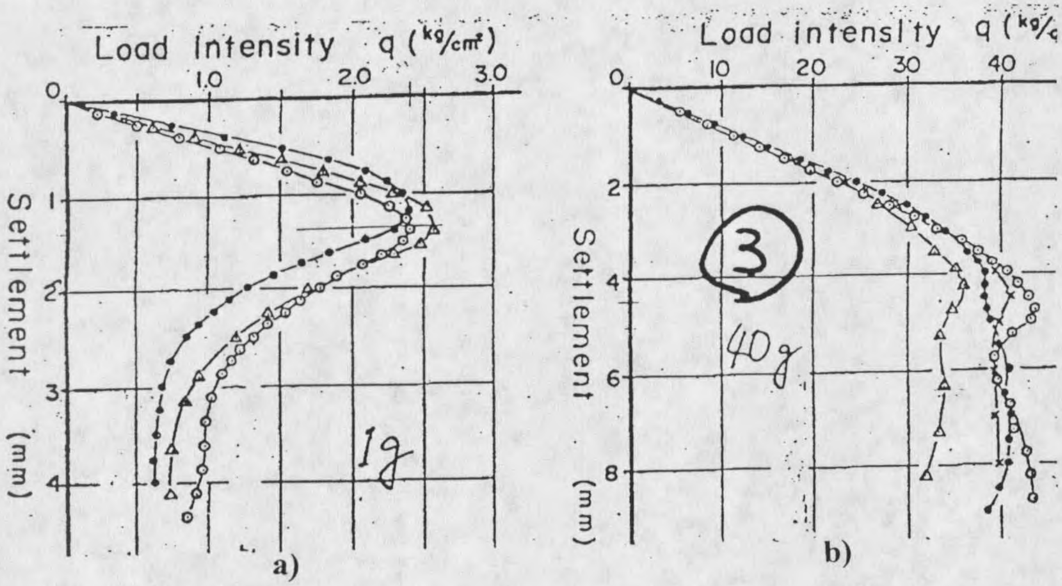

Figure 93. Toyoura sand bearing capacity results for a) B = 3 cm; D/B = 0.5 b) B = 120 cm; D/B = 1.0, (from Kimura, 1995).

Figure 94. Toyoura sand bearing capacity results for a) B = 80 cm; D/B = 1.0 b) B = 120 cm; D/B = 1.0, (from Kimura, 1995).

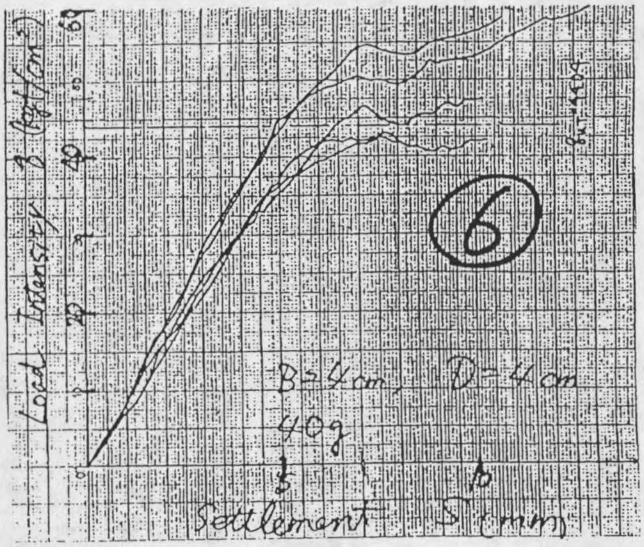

a)

Figure 95. Toyoura sand bearing capacity results for a) B = 160 cm; D/B =1.0, (from Kimura, 1995).

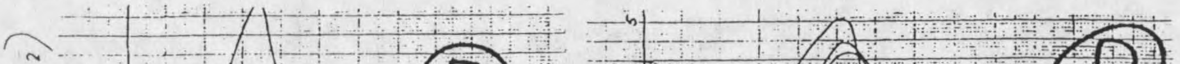

a)

b)

Figure 96. Toyoura sand bearing capacity results for a) B = 3 cm; D/B = 1.0
b) B = 4 cm; D/B = 1.0, (from Kimura, 1995).

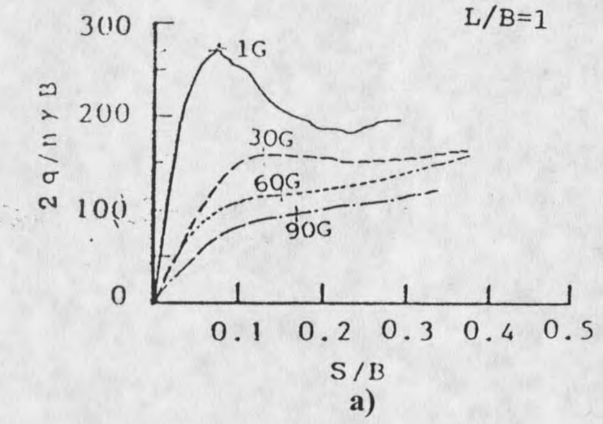

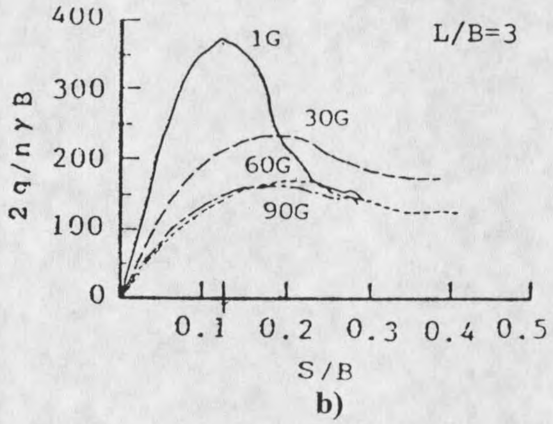

Figure 97. Inagi sand bearing capacity results for a) L/B = 1 b) L/B = 3, (from Kusakabe et al., 1991).

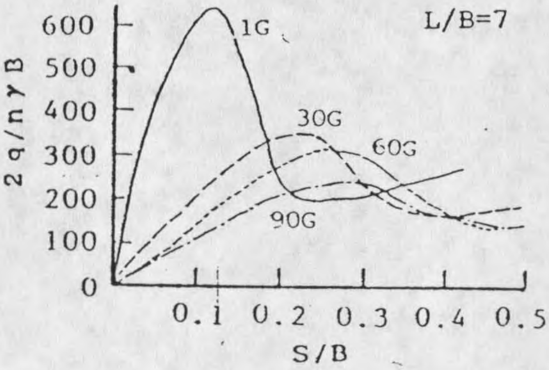

Figure 98. Inagi sand bearing capacity results for an L/B = 7, (from Kusakabe et al., 1991).

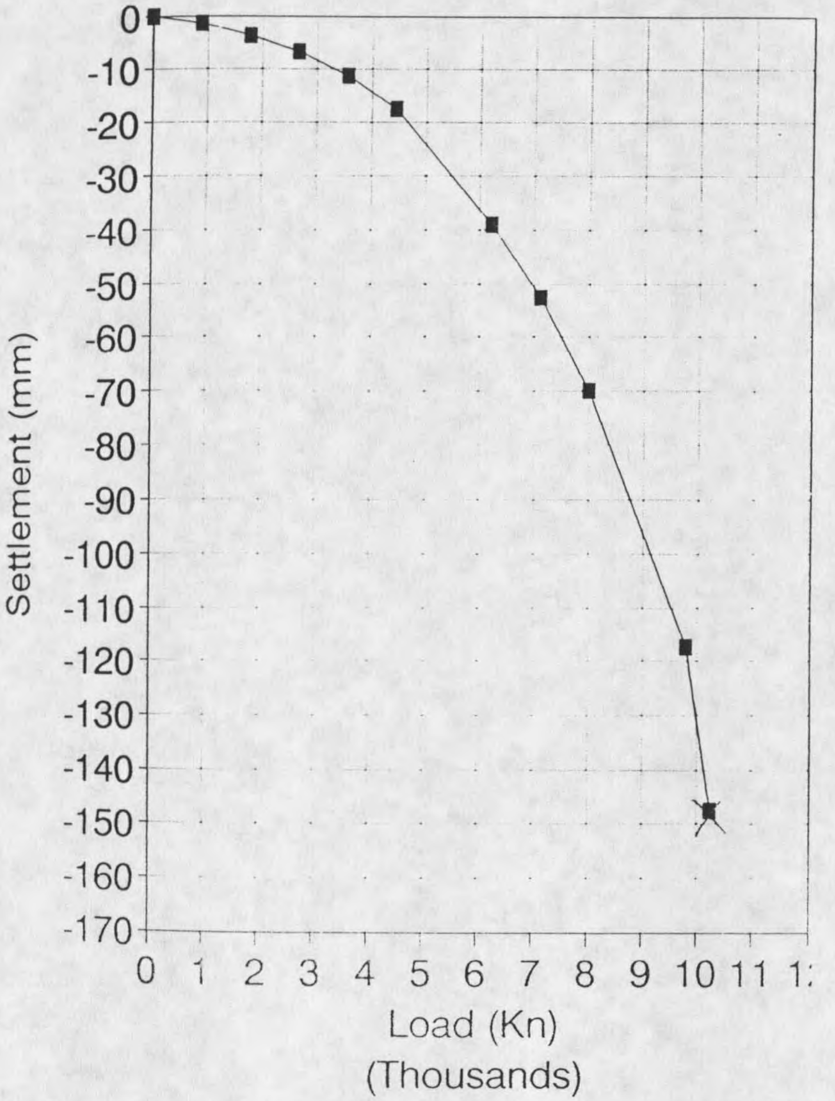

Figure 99. Texas sand bearing capacity results for 3.004 x 3.004 m footing; D/B = 0.25, (from Briaud and Gibbens, 1994).

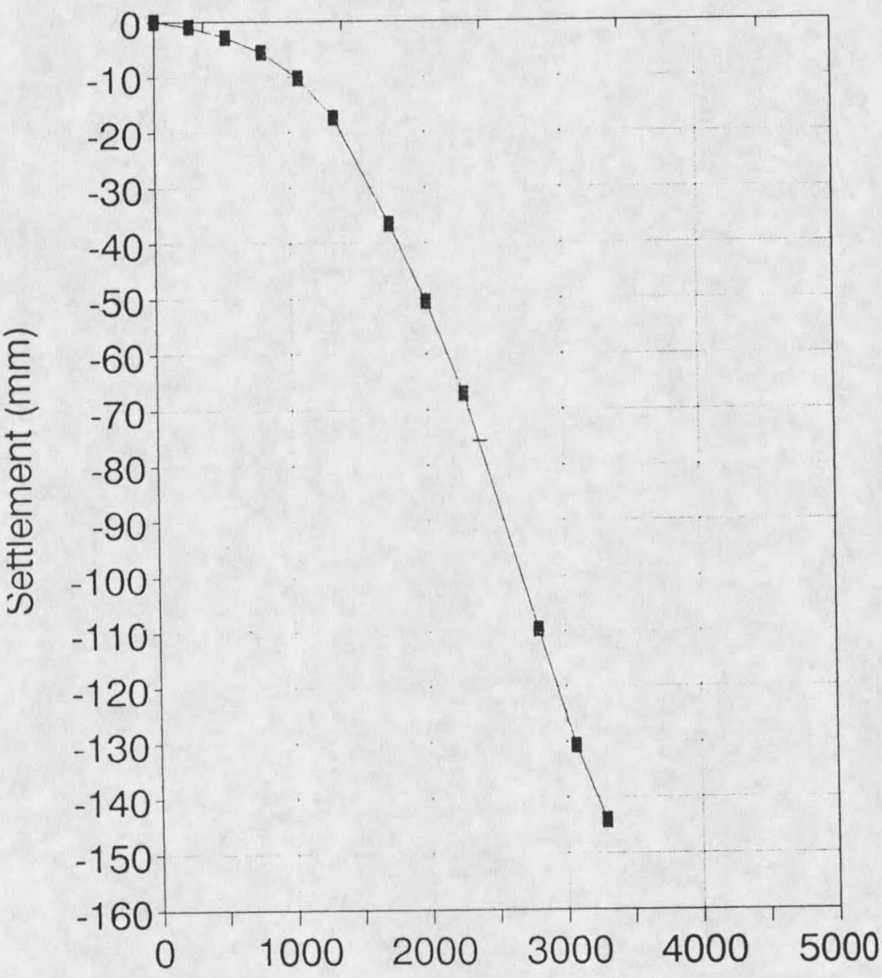

Figure 100. Texas sand bearing capacity results for 1.505 x 1.492 m footing; D/B = 0.51, (from Briaud and Gibbens, 1994).

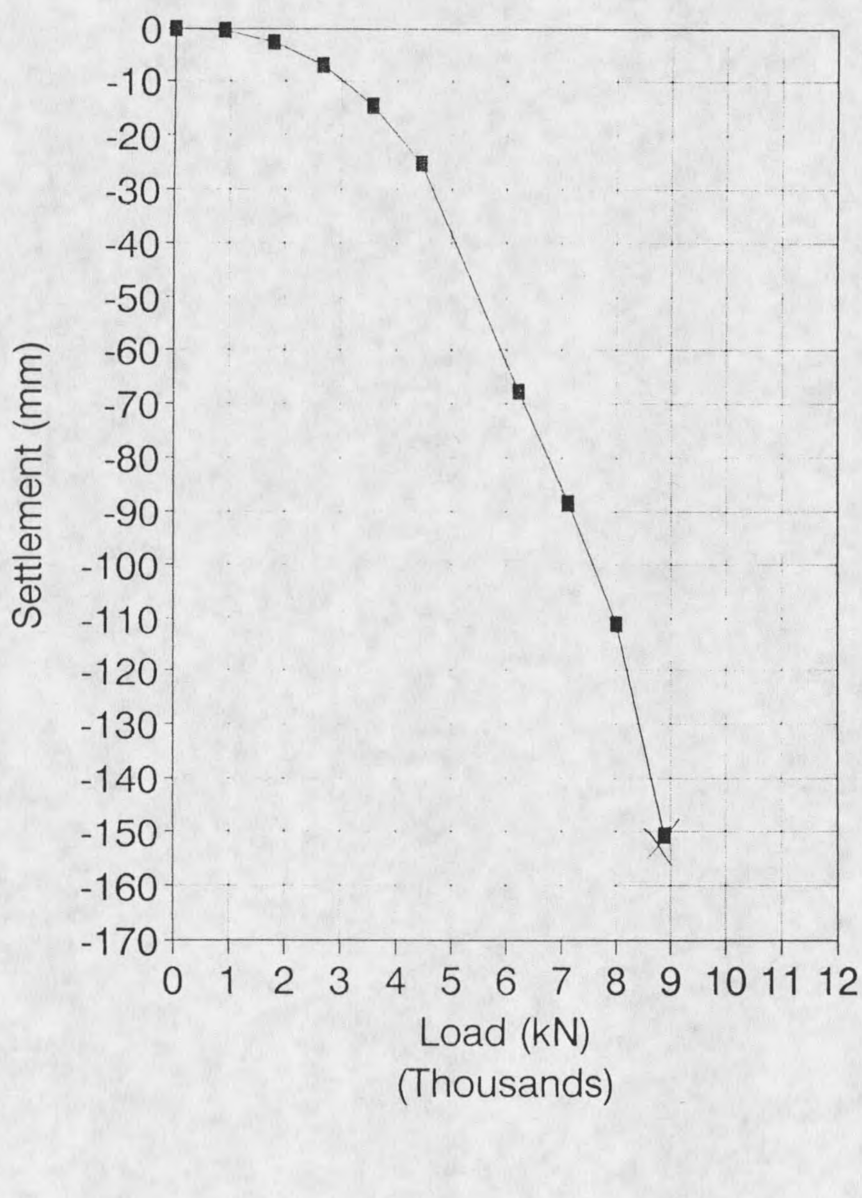

Figure 101. Texas sand bearing capacity results for 3.023 x 3.016 m footing; D/B = 0.29 (from Briaud and Gibbens, 1994).

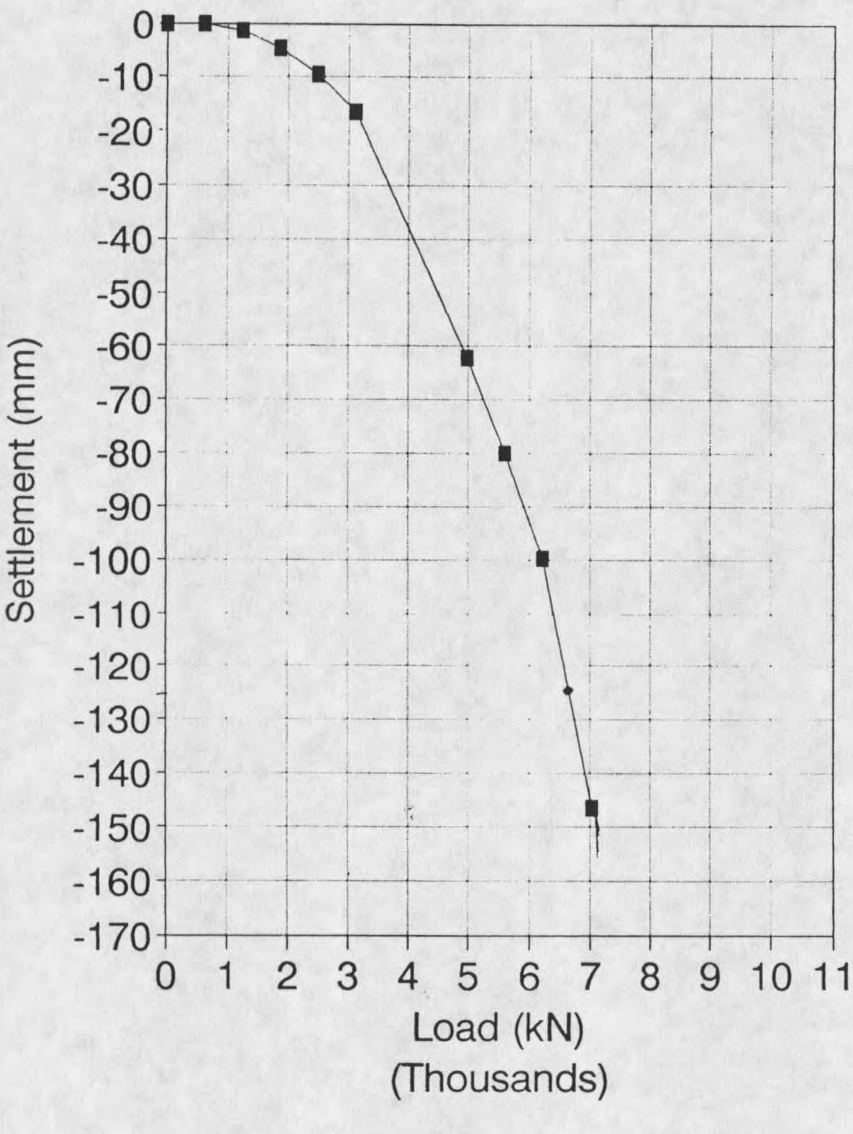

Figure 102. Texas sand bearing capacity results for 2.489 x 2.496 m footing; D/B = 0.31, (from Briaud and Gibbens, 1994).

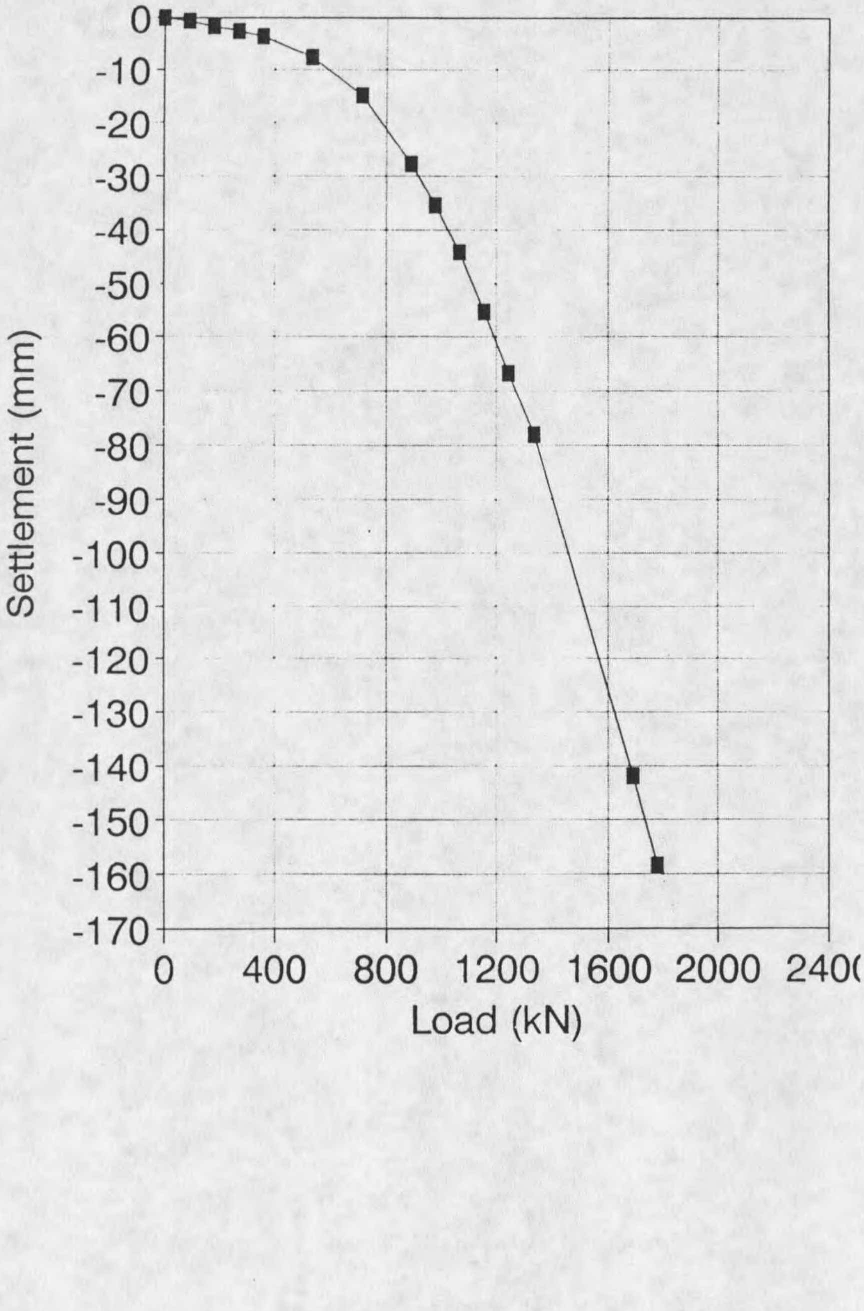

Figure 103. Texas sand bearing capacity results for 0.991 x 0.991 m footing; D/B = 0.72, (from Briaud and Gibbens, 1994).

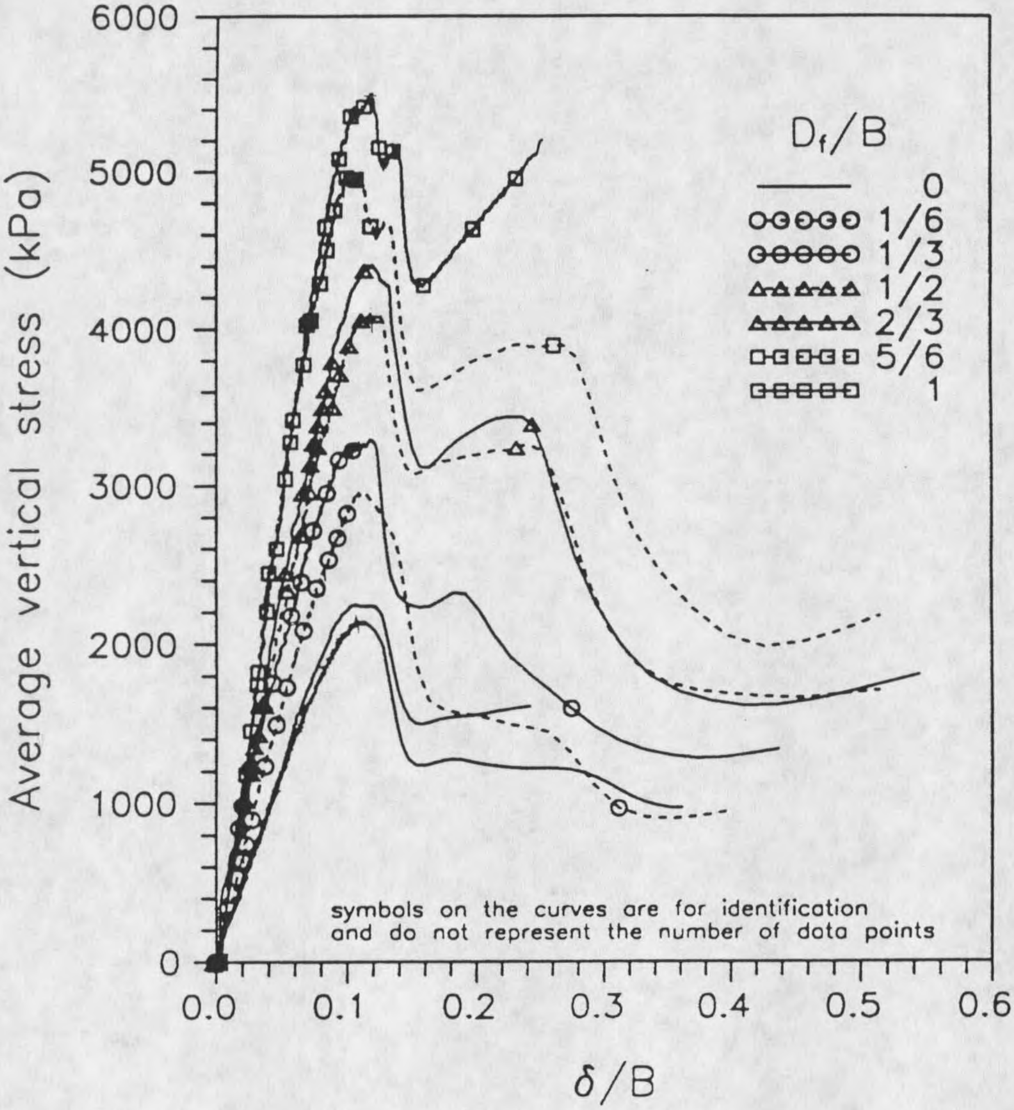

Figure 104. Ottawa sand bearing capacity results for 1.14 m footing; D/B from 0 to 1, (from Aiban, 1991).

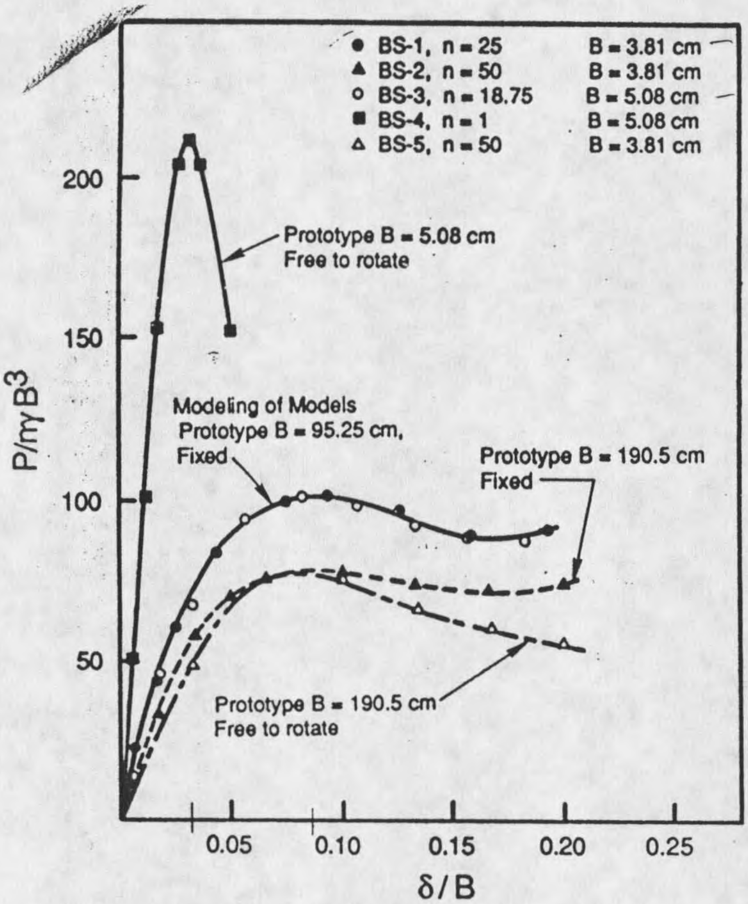

Figure 105. Monterey sand bearing capacity results for circular footings; D/B = 0, (from Kutter et al., 1988).

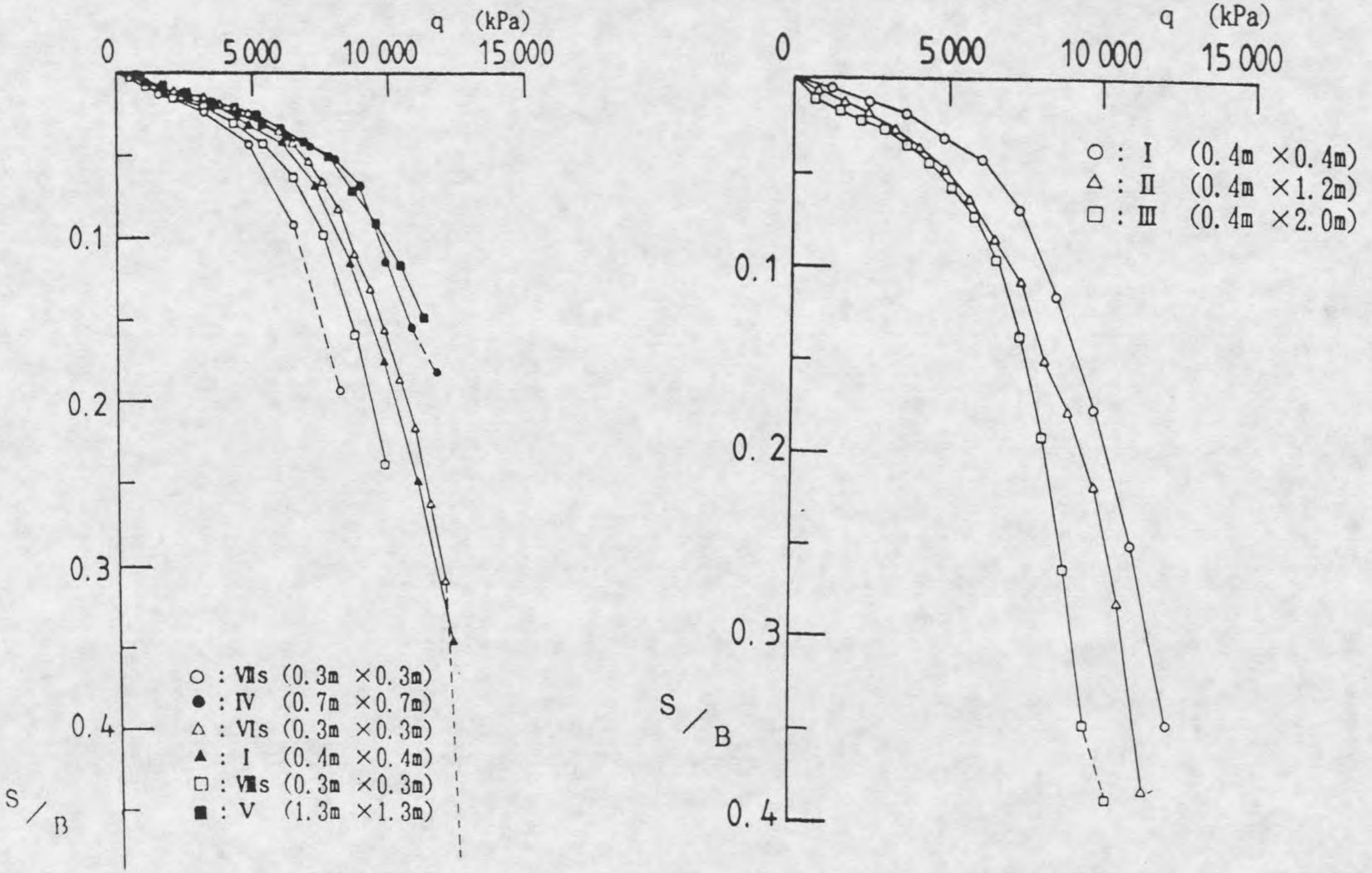

Figure 106. Scoria sand bearing capacity results, (from Kusakabe et al., 1992).

APPENDIX C

COMPARISON OF THE STRENGTH ENVELOPE PREDICTED BY BOLTON WITH RESULTS FROM TRIAXIAL OR PLANE STRAIN DATA FROM EACH OF THE STUDY SANDS

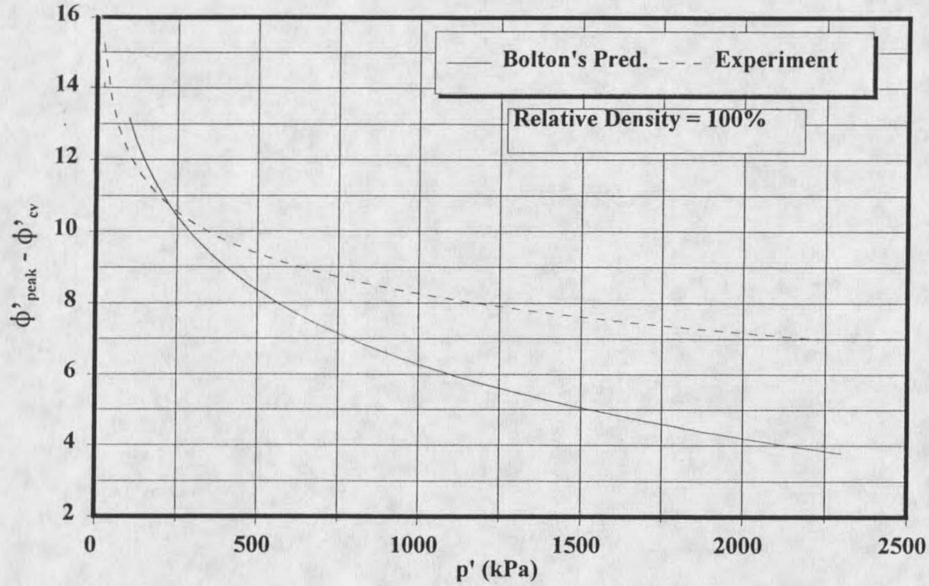

Figure 107. MLS-1- comparison of Bolton's prediction of the strength envelope and the strength envelope developed from CTC results (100% relative density).

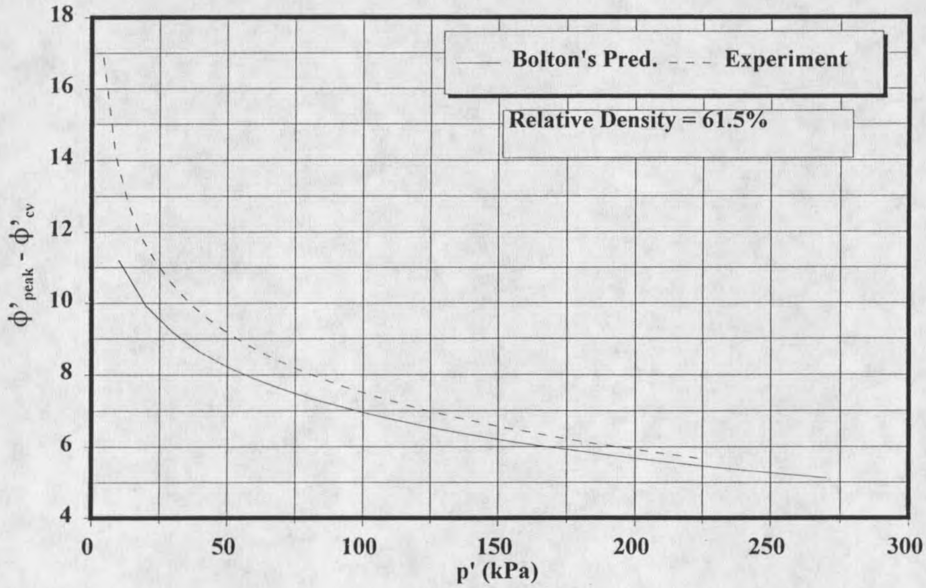

Figure 108. MLS-1 - comparison of Bolton's prediction of the strength envelope and the strength envelope developed from CTC results (61.5% relative density).

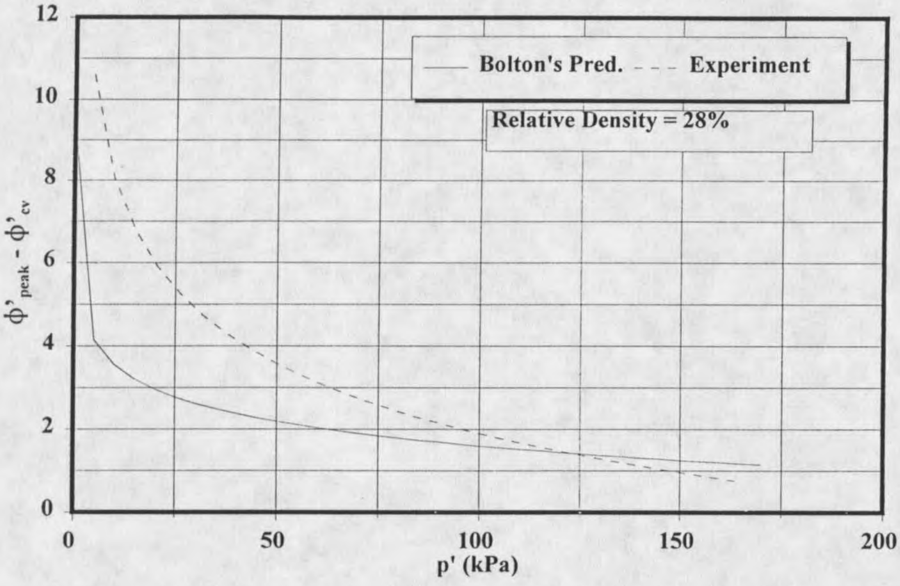

Figure 109. MLS-1- comparison of Bolton's prediction of the strength envelope and the strength envelope developed from CTC results (28% relative density).

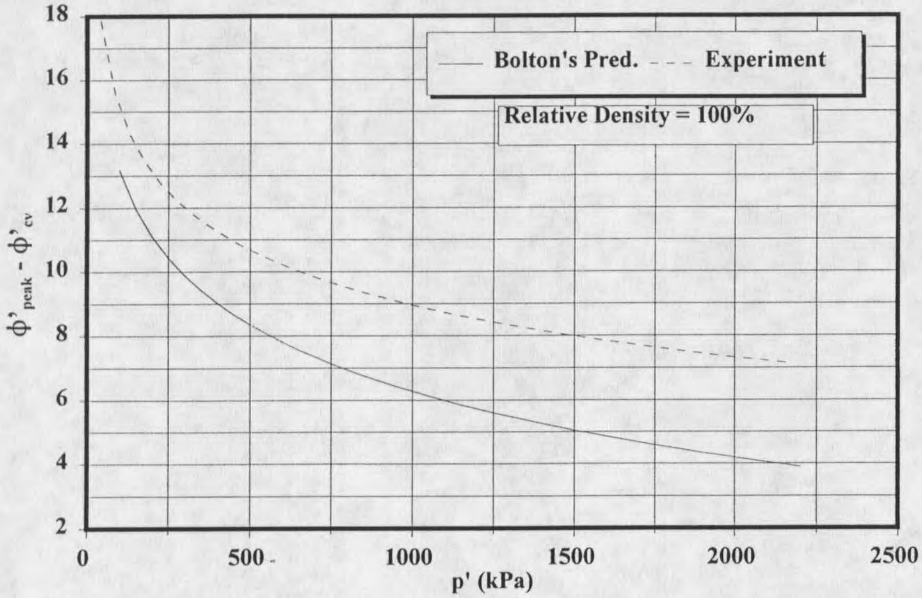

Figure 110. JSC-1 - comparison of Bolton's prediction of the strength envelope and the strength envelope developed from CTC results.

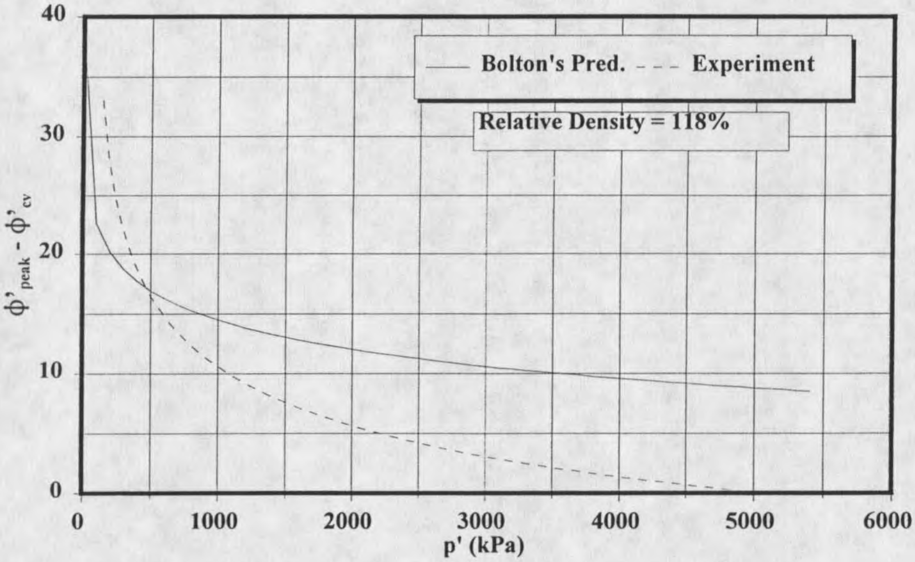

Figure 111. Scoria sand - comparison of Bolton's prediction of the strength envelope and the strength envelope developed from CTC results.

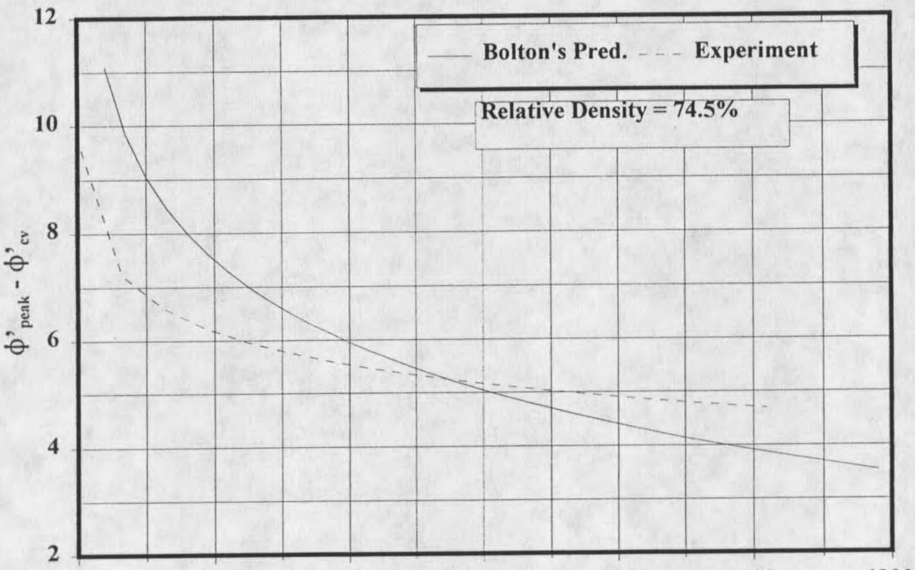

Figure 112. Toyoura sand - comparison of Bolton's prediction of the strength envelope and the strength envelope developed from CTC results (74.5% relative density).

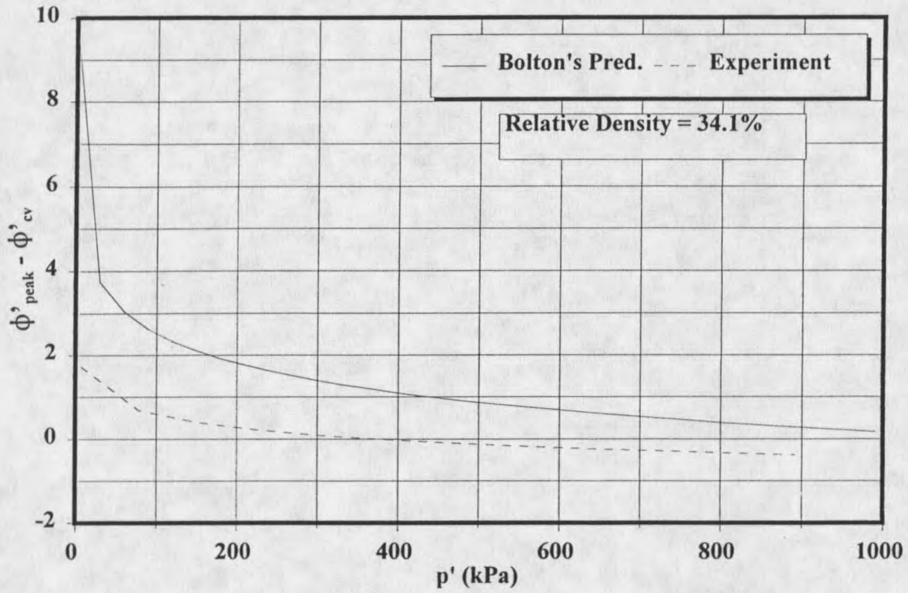

Figure 113. Toyoura sand - comparison of Bolton's prediction of the strength envelope and the strength envelope developed from CTC results (34.1% relative density).

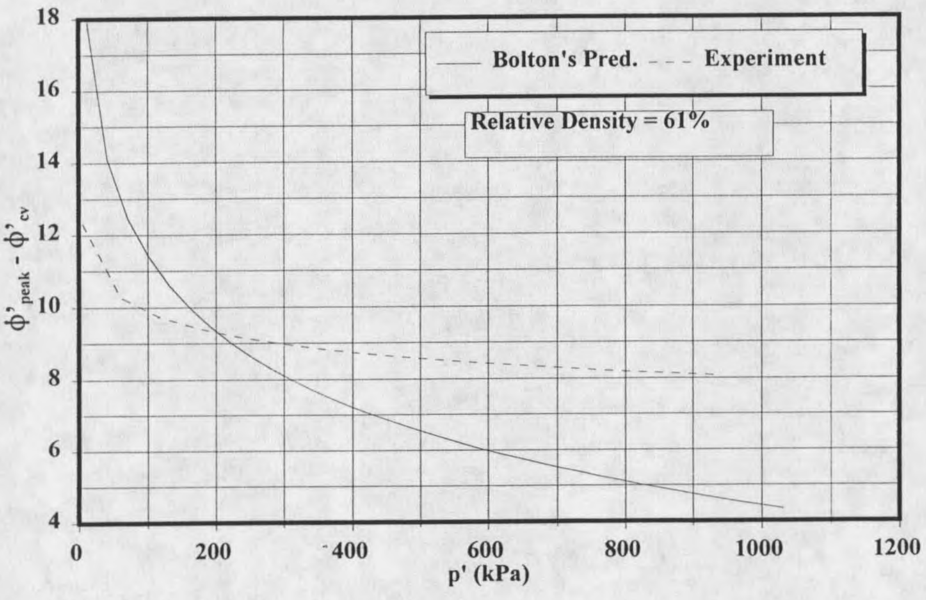

Figure 114. Toyoura sand - comparison of Bolton's prediction of the strength envelope and the strength envelope developed from plane strain tests (61% relative density).

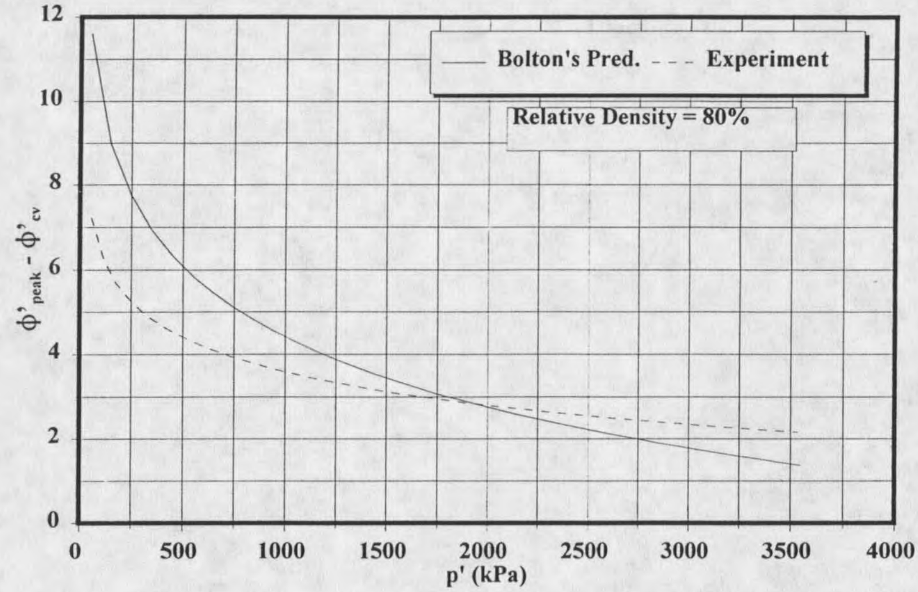

Figure 115. Inagi sand - comparison of Bolton's prediction of the strength envelope and the strength envelope developed from CTC results.

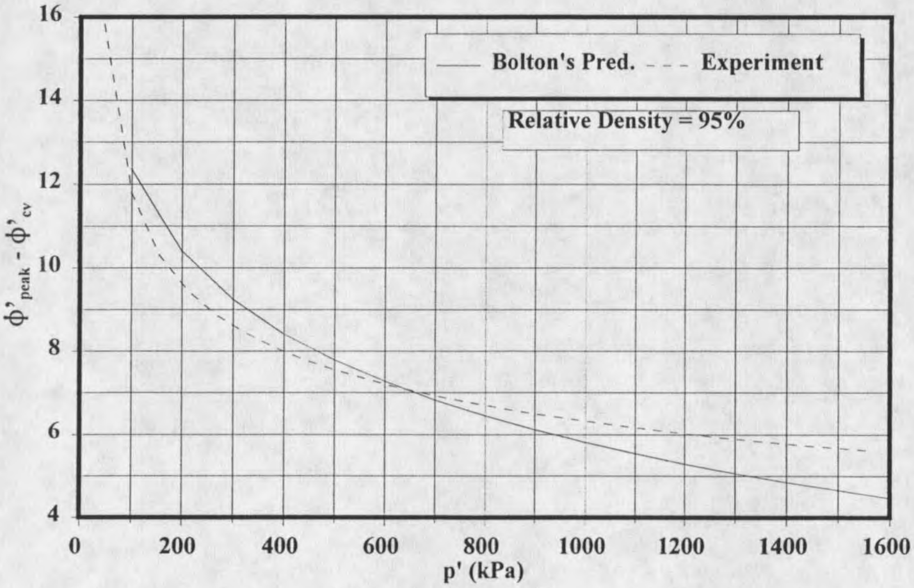

Figure 116. Monterey sand - comparison of Bolton's prediction of the strength envelope and the strength envelope developed from CTC results.

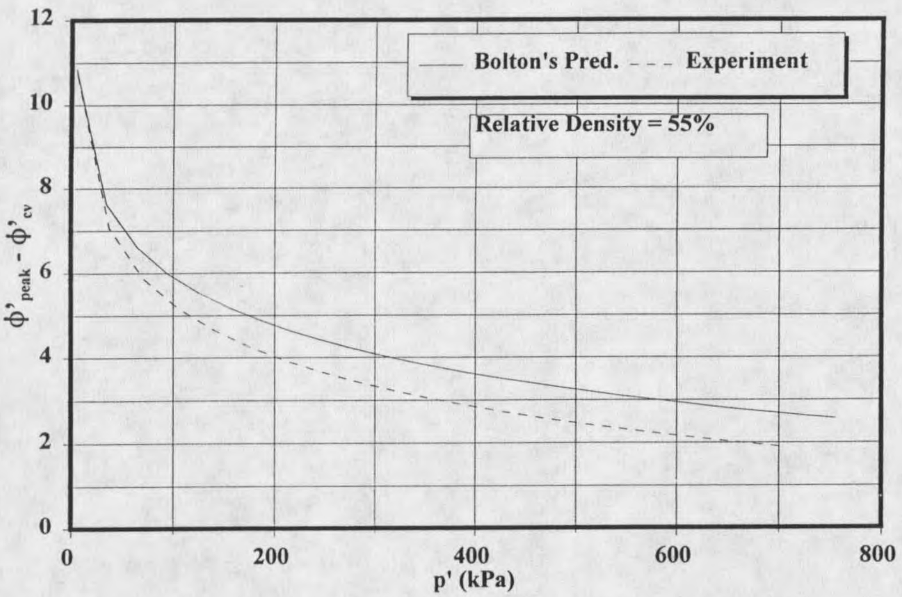

Figure 117. Texas sand - comparison of Bolton's prediction of the strength envelope and the strength envelope developed from CTC results.

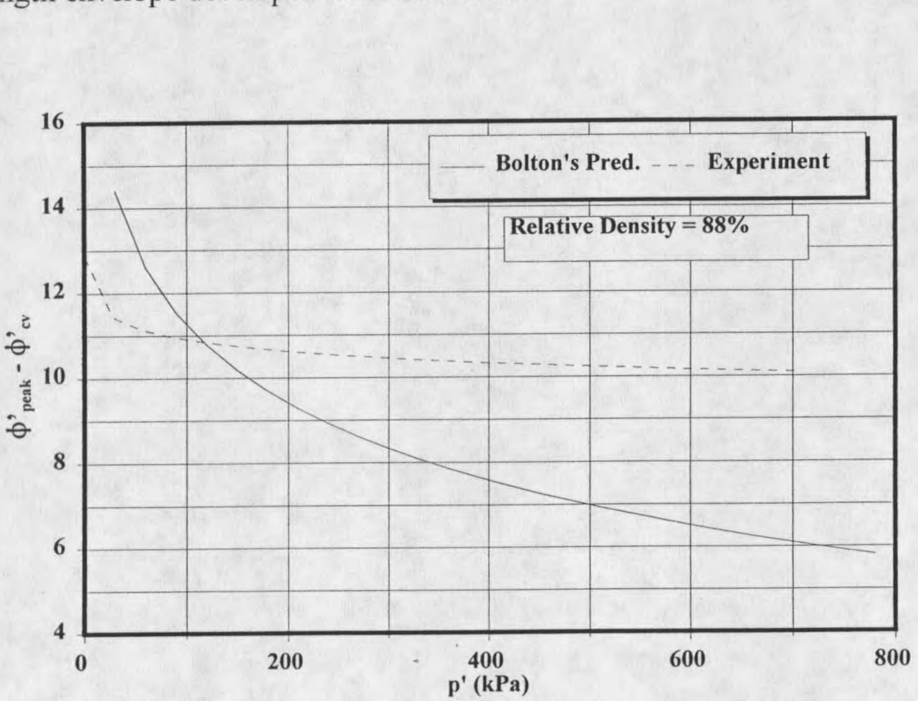

Figure 118. Ottawa sand - comparison of Bolton's prediction of the strength envelope and the strength envelope developed from CTC results.

APPENDIX D

FORTRAN PROGRAMS WRITTEN TO SOLVE FOR THE BEARING CAPACITY OF SHALLOW FOUNDATIONS ON SAND

B.C. Program using Bolton's equations

```
***********************************************************************
*    PROGRAM: BOLT.FOR                                                *
*    ----------------                                                 *
*    BC Solution Using Bolton's Equations and our p/q_ult             *
***********************************************************************
      REAL pi,lb,p,q,r,cv,phro,Id,Ir,d,b,dbf,qultm,rm,ra,ratio,Nq1,
      Ngam1,ng3,ng4,ngm,gammasat
      OPEN(1,FILE='data.txt',STATUS='old')
      OPEN(2,FILE='out.txt',STATUS='unknown')
      pi=3.141592654
      Read(1,*)n
      Do 100 I=1,n
            Read(1,*)b,phro,dbf,qultm,lb,Id,cv,q,r,d,p,gammasat
            depthf=b*(dbf)
            if(d.ge.(b+depthf)) then
                  qsur=depthf*phro*9.81
                  gamma = phro*9.81
            elseif(d.le.depthf) then
                  qsur=(depthf-d)*(gammasat-9.81)+d*phro*9.81
                  gamma=gammasat-9.81
            else
                  qsur=depthf*phro*9.81
                  gamma=(gammasat-9.81)+(d-depthf)/b*(phro*9.81-
                  (gammasat-9.81))
            endif
10    Ir=Id*(Q-log(p))-R
      if(Ir.lt.0.0) then
            Ir=0.0
      endif
      if(LB.ge.7.0) then
            ratio=5.0
      elseif(LB.le.1.0) then
            ratio=3.0
      else
            z=(7.0-LB)/6.0
            ratio=5.0-z*(2.0)
      endif
      phi2sp=(ratio*Ir)+CV
      phis2=phi2sp*pi/180.0
      Nq1=(tan(45.0*pi/180.0+phis2/2.0))**2.0*exp(pi*tan(phis2))
      a=pi/4.0+phis2/2.0
```

```
      term11=0.5*tan(a)*(tan(a)*exp(3.0*pi/2.0*tan(phis2))-1.0)
      term22=3.0*sin(phis2)*cos(phis2)/(2.0*(1.0+8.0*(sin(phis2))
             **2.0)*(1.0-sin(phis2)))
      term33=(tan(a)-1.0/(3.0*tan(phis2)))*exp(3.0*pi/2.0*
      tan(phis2))+tan(a)*1.0/(3.0*tan(phis2))+1.0
      Ngam1=term11+term22*term33
      qult3=Nq1*qsur+0.5*gamma*b*Ngam1
      phi2s=phis2*180.0/pi
      ra=p/qult3*100.0
      rm=310.511*exp(-0.072749*phi2s)
      p=(rm+ra)/2.0/100.0*qult3
      If(abs(rm-ra).gt.0.001) then
             goto 10
      endif
      phis3=CV*pi/180.0
      Nq1=(tan(45.0*pi/180.0+phis3/2.0))**2.0*exp(pi*tan(phis3))
      a=pi/4.0+phis3/2.0
      term11=0.5*tan(a)*(tan(a)*exp(3.0*pi/2.0*tan(phis3))-1.0)
      term22=3.0*sin(phis3)*cos(phis3)/(2.0*(1.0+8.0*(sin(phis3))
             **2.0)*(1.0-sin(phis3)))
      term33=(tan(a)-1.0/(3.0*tan(phis3)))*exp(3.0*pi/2.0*tan(phis3))+tan(a)
             *1.0/(3.0*tan(phis3))+1.0
      Ngam1=term11+term22*term33
      qult4=Nq1*qsur+0.5*gamma*b*Ngam1
      rel=(qultm-qult4)/(qult3-qult4)
      ng3=2.0*qult3/b/9.81/phro
      ngm=2.0*qultm/b/9.81/phro
      ng4=2.0*qult4/b/9.81/phro
      write(2,1000)qult3,qultm,qult4,Ir,rel,ng3,ngm,ng4
1000  format(3(f6.0,2x),f4.2,2x,f4.2,2x,3(f6.0,2x))
100   continue
      STOP
      END
```

B.C. Program using p'-q strength envelopes

```
**********************************************************************
*    PROGRAM: BC.FOR                                                 *
*    -----------------                                               *
*    Using p-q diagram, no Q and R, using our expression for p/q_ult *
**********************************************************************
      REAL pi,lb,p,cv,phro,Ir,d,b,dbf,qultm,rm,ra,ratio,Nq1,
            Ngam1,ng3,ng4,ngm,m,eta,pc,gammasat
      OPEN(1,FILE='data2.txt',STATUS='old')
      OPEN(2,FILE='out.txt',STATUS='unknown')
      pi=3.141592654
      Read(1,*)n
      Do 100 I=1,n
            Read(1,*)b,phro,dbf,qultm,cv,m,eta,pc,lb,gammasat,d,p
            depthf=b*(dbf)
            if(d.ge.(b+depthf)) then
                  qsur=depthf*phro*9.81
                  gamma = phro*9.81
            elseif(d.le.depthf) then
                  qsur=(depthf-d)*(gammasat-9.81)+d*phro*9.81
                  gamma=gammasat-9.81
            else
                  qsur=depthf*phro*9.81
                  gamma=(gammasat-9.81)+(d-depthf)/b*(phro*9.81-
                  (gammasat-9.81))
            endif
10    if(LB.ge.7.0) then
            ratio=5.0
      elseif(LB.le.1.0) then
            ratio=3.0
      else
            z=(7.0-LB)/6.0
            ratio=5.0-z*(2.0)
      endif
      qpeak=p
11    pass=(qpeak*(1.0+qpeak)**m)/eta+pc
      If ((pass-p).ge.0.01) then
            fix=(pass-p)/p
            qpeak=qpeak-qpeak*fix/2.0
            goto 11
      Elseif ((p-pass).ge.0.01) then
            fix=(p-pass)/pass
```

```
            qpeak=qpeak+qpeak*fix/2.0
            goto 11
      Endif
            phitc=asin(qpeak/(2.0*p+qpeak/3.0))*180.0/pi
            Ir=(phitc-cv)/3.0
            phi2sp=phitc*((cv+ratio*Ir)/(cv+3.0*Ir))
            phis2=phi2sp*pi/180.0
            Nq1=(tan(45.0*pi/180.0+phis2/2.0))**2.0*exp(pi*tan(phis2))
            a=pi/4.0+phis2/2.0
            term11=0.5*tan(a)*(tan(a)*exp(3.0*pi/2.0*tan(phis2))-1.0)
            term22=3.0*sin(phis2)*cos(phis2)/(2.0*(1.0+8.0*(sin(phis2))
                  **2.0)*(1.0-sin(phis2)))
            term33=(tan(a)-1.0/(3.0*tan(phis2)))*exp(3.0*pi/2.0*
            tan(phis2))+tan(a)*1.0/(3.0*tan(phis2))+1.0
            Ngam1=term11+term22*term33
            qult3=Nq1*qsur+0.5*gamma*b*Ngam1
            phi2s=phis2*180.0/pi
            ra=p/qult3*100.0
            rm=310.511*exp(-0.072749*phi2s)
            p=(rm+ra)/2.0/100.0*qult3
            If(abs(rm-ra).gt.0.001) then
                  goto 10
            endif
            phis3=CV*pi/180.0
            Nq1=(tan(45.0*pi/180.0+phis3/2.0))**2.0*exp(pi*tan(phis3))
            a=pi/4.0+phis3/2.0
            term11=0.5*tan(a)*(tan(a)*exp(3.0*pi/2.0*tan(phis3))-1.0)
            term22=3.0*sin(phis3)*cos(phis3)/(2.0*(1.0+8.0*(sin(phis3))
                  **2.0)*(1.0-sin(phis3)))
            term33=(tan(a)-1.0/(3.0*tan(phis3)))*exp(3.0*pi/2.0*tan(phis3
                  ))+tan(a)*1.0/(3.0*tan(phis3))+1.0
            Ngam1=term11+term22*term33
            qult4=Nq1*qsur+0.5*gamma*b*Ngam1
            rel=(qultm-qult4)/(qult3-qult4)
            ng3=2.0*qult3/b/9.81/phro
            ngm=2.0*qultm/b/9.81/phro
            ng4=2.0*qult4/b/9.81/phro
            write(2,1000)qult3,qultm,qult4,Ir,rel,ng3,ngm,ng4,p,phitc,phi2s
1000        format(3(f6.0,2x),f4.2,3x,f4.2,2x,4(f6.0,2x),2(f3.0,2x))
100   continue
      STOP
      END
```